UNIVERSITÁ DEGLI STUDI ROMA TRE

Doctorate in Physics – XXXI cycle

Doctor of Philosophy dissertation

Spin dynamics in anisotropic systems in the presence of spin-orbit coupling

Candidate
Iryna Miatka

Supervisor
Prof. Roberto Raimondi

Doctorate courses 2015-2018

"You've got to jump off cliffs and build your wings on the way down."

- Ray Bradbury

Summary

Chapter 1 The first chapter smoothly prepares the reader for the next stages by familiarizing with the main background of the study. The reader will understand the main goal of spintronics and why usage of spin-current has more advantages than the charge current.

Chapter 2 In Chapter 2 the reader can discover the mechanisms of spin-orbit in solid state systems, starting from the Dirac equation and from the energy band interaction in the Kane model.

Chapter 3 In this chapter, we enter in quasi-classical formalism in order to treat the transport problems at a quantum level. It will be derived the Eilenberger equation which is the background for understanding the result of the thesis.

Chapter 4 In this chapter we present our contribution - the result of the interplay of spin-orbit couplings onto the inverse spin-galvanic effect, one of the most relevant phenomena in spintronics that leads to charge-spin tunability. This chapter contains the main study of this work, satisfying the aim presented in the introduction.

Chapter 5 Here we describe how to generate synthetically spin-orbit coupling in a model that is free of disorder but is charge-neutral - ultracold atoms.

Chapter 6 We present the analytical time-dependent exact and approximate solutions to the anisotropic model of cold atoms with spin-orbit coupling and external perturbations. These solutions show a great tunability and a much longer life-time of the spin polarized states comparing to the one of a usual two-dimensional electron gas.

Contents

Chapter 1

Introduction

1.1 Spintronics

Spintronics is a rapidly-developing area of research that in the last decades has investigated exciting effects based on the coupling of electron spin and charge, manipulating them by electro-magnetic fields in solid state systems. The key physical quantity that underlines all the effects is the spin, the internal angular momentum of a particle in quantum mechanics. Electrons possess a charge, as a source of electricity, and a spin, as a source of magnetism. While common electronic devices have been developed by making use of the charge currents, the study of spintronics aims to develop an innovative functionality for high quality devices that operate with spin currents, or flow of spins. The main difficulty that hinder its implementation is hidden in the challenge of driving the spin current in a device. Indeed, only a limited number of proposals exists on how to generate it.

Studying the interaction between charge and spin and their behavior discloses new opportunities for the creation of novel supersensitive devices, such as the spin-exchange-relaxation-free atomic magnetometer (SERF), the most sensitive approach for measuring scanty changes of the Earth's magnetic fields [1]. This device has already found applications in satellites or archeography. Moreover, exploiting the properties of the spin degree of freedom gives a range of advantages with respect to circuits based on charge carriers: smaller size and greater versatility, higher speed and less power consumption. These devices can write and store information through up and down spin orientation and send it along a wire thanks to the long spin relaxation times. The birth of spintronics is considered the observation of giant magnetoresistance in the magnetic multilayers in 1988 [2, 3]. The development of spintronics displayed many other phenomena which are capable of spin current manipulations: spin transfer torque [4], spin Hall effect [5, 6, 7], spin-galvanic effect [8, 9, 10], spintronics in semiconductors and graphene [11].

Carrying out research in spintronics and achieving an understanding in the

interaction between the particle's spin and its solid-state or ultracold atomic environment promises to lead to more performant devices with respect to the classical electronic ones, where the spin-orbit interaction is not able to control spin current and spin polarization through the external fields.

1.1.1 Pseudospintronics

Spin is the key degree of freedom at the core of spintronics. However, as originally observed by Heisenberg [12], any superposition of two-level quantum states can ultimately act as an effective spin. When this happens, we refer to it as pseudospin. As for the case of spin-1/2 particles, pseudospin is conveniently expressed using the set of Pauli matrices $\boldsymbol{\sigma} = (\sigma_x, \sigma_y, \sigma_z)$. Nevertheless, being it not an internal degree of freedom of a particle, pseudospin actually depends on the properties of the physical system. In graphene, for instance, the honeycomb lattice of carbon atoms can be interpreted as a superposition of two triangular sublattices formed by the basis vectors [13]. And the states close to the Fermi energy lie near the K and K' Fermi points at the opposite corners of the Brillouin zone that is a hexagon in momentum space. The twofold degeneracy occurs at the Fermi momentum K and K' of the corners of the Brillouin zone. The wave function is a four-component slowly varying envelope function with the components marked at the Fermi points as pseudospins ± 1 [14]. They contribute to the spectrum of graphene but they have nothing to do with the real spin. In this context, pseudospin is a superposition of the two quantum states on the sublattices and is represented in terms of Pauli matrices.

The analogy between spins and pseudospins is useful only in special circumstances, since pseudospins lifetimes are normally short, and the identified degrees of freedom are often not continuous across sample boundaries. In nuclear physics pseudospin doublets, proposed 50 years ago to describe the near degeneracy of shell-model orbitals with non-relativistic quantum numbers, come from the division of single-particle total angular momentum into pseudo-orbital part and pseudo-spin, which are used to explain the features of deformed nuclei, identical bands and the origins of supersymmetry in the shell-model [15]. The degree of freedom of graphene sublattices can be viewed as a pseudospin and enters the continuum model of the Dirac equation in the same manner that real spin enters Dirac equation for the surface states of topological insulators. In the pseudospin language, the Hamiltonian consists only of a pseudospin-orbit coupling term with an effective magnetic field that is linear in momentum and points in the same direction as momentum. The role of spin in topological-insulator surface states is crucial, and it can be applied equally well to pseudospin in a single-layer graphene. Just as for spin, we can expect that charge currents in single-layer graphene will be accompanied by pseudospin currents. Another example of a two-valued degree of freedom viewed as pseudospin are the two distinct hyperfine states of ultra-cold atoms in external magnetic field. Such system can mimic magnetic systems of spin 1/2 particles [16].

1.1.2 A review of the main effects

Let us start by considering the spin Hall effect. This phenomenon can arise in 2D electron gases as a spin current flowing perpendicularly to the charge current. According to the Onsager reciprocal relations the spin Hall effect has its inverse version, where the spin current driven by electric field creates the charge current in the perpendicular direction. The direct and inverse spin Hall effects are described by spin conductivity, as it was done in the weak disorder limit of impurities in [5]. One can distinguish two mechanisms of spin Hall effect, respectively proposed by D'yakonov and Perel [17] and by Sinova and Murakami independently [7, 18]. The extrinsic spin Hall effect arises due to the scattering of charge carriers by impurities. The intrinsic one is induced by the spin-orbit mechanism in the band structure of the crystal. In the latter case, the electrons accelerate and undergo spin-precession due to the induced electric field, as for Rashba spin-orbit coupling. This kind of spin-orbit coupling was proposed firstly for non-centrosymmetric wurtzite semiconductors [19] and later for 2D electron gases [20]. The ordinary spin-orbit interaction appears as a coupling between the magnetic momentum of a quantum particle and its spin. Spin-orbit interactions comes as a consequence of the corrections to the second order Dirac equation for electron in special relativity. The peculiarity of Rashba spin-orbit interaction is that this kind of interaction is symmetry dependend and exists only in crystals without inversion symmetry. As we describe later, Rashba spin-orbit coupling is related to the surface-induced asymmetry.

Rashba spin-orbit interaction became quite widespread since it was proposed to realize spin transistors by Datta and Das in 1990 [21], whose realization depends on the spin injection from a ferromagnetic electrode in a 2D electron gas and gate controlled precession angle. Since that, Rashba spin-orbit interaction was detected in new materials such as metal surfaces, bulk and interfaces materials of semiconductors [22, 23], heavy metals [24] and topological insulators [25]. Moreover, the effect takes place even in more exotic fields of physics, like with topological states in the insulators and Majorana fermions [26, 27].

Another fundamental effect in spintronics, the Edelstein or inverse spin-galvanic effect, was firstly proposed for gyrotropic crystals [28]. In the absence of external magnetic field, the non-equilibrium generation of a spin polarization is perpendicular to the applied electric field. The Onsager reciprocal of the Edelstein effect, the spin-galvanic effect, can be observed as the charge current perpendicular to the spin polarization injected into a non-magnetic material. In semiconductor materials the Edelstein effect can be traced with the help of time-resolved Kerr rotation or other gyroelectromagnetic effect like Faraday rotation. Both direct and inverse spin-galvanic effects contain a linear coupling of the polar and axial vector, electric current and spin polarization respectively. As we mentioned, in solids the spin-orbit interaction can be extrinsic or intrinsic depending on its origins. In the situation of broken symmetry, when the two splitted spin states appear due to the intrinsic spin-orbit effect, the influence of disorder on the latter may slightly change the spin transport dynamics. Usually, the mechanism of spin relaxation due to disorder effects can be described within the Dyakonov-Perel mechanism. In case of extrinsic

spin-orbit interaction, the spin relaxation mechanism may have the spin-free and spin-dependent contributions, where the latter is referred to as the Elliott-Yafet theory of spin relaxation. The two mechanisms of spin-orbit coupling together show up as interesting non-equilibrium dynamics of spin polarization in the inverse spin-galvanic effect. The generation of spin polarization in non-magnetic materials can be applicable for spin-based information processing or controllability of magnetization.

Both effects, spin Hall effect and Edelstein effect, have been described for "sandwich" materials with the asymmetric interfacial Rashba spin-orbit interaction in [6]. The nonlinear Edelstein effect has been described analytically in the long-time limit for the 2D electron gas with Rashba spin-orbit coupling without including the impurity scattering of the electrons [9]. The inverse Edelstein effect was studied in Ref. [29] and for the two different mechanisms was proposed in Ref. [30]. The experiment for the $In_{0.04}Ga_{0.96}As$ epilayers reported that the magnitude of the current-induced spin polarization is smaller for crystal directions corresponding to larger spin-orbit fields [31] in spite of the theoretical result that gives the opposite image, the larger spin polarization corresponds to the larger spin-orbit fields.

1.1.3 Methods for detection

Usually magneto-optical techniques such as Kerr or Faraday effect, are most commonly used in research for detection spin trasport in semiconductors. These methods allow to characterize the properties of the materials such as magnetic domain structure, spin density of states, dynamics of magnetic phase transitions.

Both effects are the result of the off-diagonal components of the dielectrical tensor. These off-diagonal components give an anisotropic permittivity to the magneto-optic material, meaning that this permittivity differs in different directions.

- *Kerr effect*

  This magneto-optical method describes the changes of light reflected from magnetized surface. The reflected light is characterized by changed polarization and reflected intensity comparing with the initial incident light. There are three types of magneto-optical Kerr effect that are polar, longitudinal and transversal.

  Polar. The effect is called polar when the magnetization vector is perpendicular to the reflection surface and parallel to the plane of incidence. To simplify the analysis in the polar geometry it is usually used near-normal incidence.

  Longitudinal. In the longitudinal effect, the magnetization vector is parallel to both the reflection surface and the plane of incidence.

  Transversal. This configuration is used when the magnetization is perpendicular to the plane of incidence and parallel to the surface. In this case only a change of reflectivity r is measured, and the last is proportional to the

component of magnetization that is perpendicular to the plane of incidence and parallel to the surface. Then depending on where the magnetization component points relatively the incident plane, we may have the intensity of the reflected light as a summing or subtraction of Kerr vector and Fresnel amplitude.

- *Faraday effect*

  This effect describes changes of the transmitted light through a magnetic material. Faraday effect causes a rotation of the plane of polarization which is linearly proportional to the component of the magnetic field in the direction of propagation. It is caused by left and right circularly polarized waves propagating at partly different speeds. As it is known a linear polarization can be decomposed into the superposition of two circularly polarized components of equal amplitude, with opposite handedness and different phase, the phase shift effect rotates the orientation of a wave's linear polarization. The direction of polarization rotation depends on the properties of the material through which the light is shone.

1.1.4 Application

- *Spin transistor*

  The first spintronic device based on Rashba spin-orbit coupling was a spin field-effect transistor proposed by Datta and Das [32]. The implementation of this transistor relies on spin injection from a ferromagnetic electrode into a two-dimentional electron gas and, subsequently, on gate controlled precession angle of the injected electron's spin.

  One advantage over regular transistors is that these spin states can be detected and altered without requiring the application of an electric current. A second advantage of a spin transistor is that the electron spin is semi-permanent and can be used to create cost-effective non-volatile solid state storage that does not require a constant current to operate. It is one of the technologies being explored for Magnetic Random Access Memory (MRAM) [33].

- *Stern-Gerlach spin filter*

  This kind of a filter is based on a spatial gradient of the effective magnetic field caused by Rashba spin-orbit coupling. This spatial gradient created a Stern-Gerlach type of spin separation [34]. Stern-Gerlach spin filter can be used for detection of electrical spin.

- *Spin exchange relaxation-free (SERF) magnetometer*

  It is a type of magnetometer developed at Princeton University in the early 2000s. Spin polarization detection is still done by polarized rotation of the light. And it still remains the most efficient and non-demolition technique. SERF magnetometers measure magnetic fields using lasers and detect the interaction between alkali metal atoms in a vapor and the magnetic field [35].

The sensitivity of SERF magnetometers is improved in comparison with the traditional atomic magnetometers by eliminating the dominant cause of atomic spin decoherence that is created by spin-exchange collisions among the alkali metal atoms. SERF magnetometers are one of the most sensitive magnetic field sensors. Furthermore in some cases, they beat the superconducting quantum interferometric detectors (SQUID) of equivalent size [36]. The magnitude of sensitivity of atomic magnetometers are limited usually by the number of atoms and their spin coherence lifetime.

1.2 Subject of the thesis

1.2.1 The spin-galvanic effect

First of all, let us give our attention to the symmetries that from now on play a key role. In quantum mechanics, any energy state E for half-integer spin systems is degenerate if their Hamiltonian is invariant for reversing of time $t \to -t$, and this is especially relevant for the ground state. This statement was formulated by H.A. Kramers in 1930 [37] and is called the Kramers degeneracy theorem or time-reversal symmetry. Basically, after the time-reversal operation the momentum $\mathbf{p}$ changes its sign, and the same happens to the spin

$$E(\mathbf{p}, \uparrow) = E(-\mathbf{p}, \downarrow).$$

Besides, solids can possess a center of symmetry through which, upon space inversion, the system of the crystalline structure shows the inversion symmetry. In that case, the system is called centrosymmetric and mathematically the eigenenergy E shows that only momentum $\mathbf{p}$ changes the sign, while the spin remains the same

$$E(\mathbf{p}, \uparrow) = E(-\mathbf{p}, \uparrow).$$

When both symmetries, time-reversal and space inversion, are present

$$E(\mathbf{p}, \uparrow) = E(\mathbf{p}, \downarrow)$$

the two electronic energy bands of a system, as for instance in the case of a two-dimension free electron gas, would be degenarate for both spins. In the case when one of the symmetries is absent and

$$E(\mathbf{p}, \uparrow) \neq E(\mathbf{p}, \downarrow),$$

there is no longer spin degeneracy.

When the symmetry is broken we can observe the splitting of the energy bands, and the degeneracy is removed. Usually, it happens when there is some perturbation caused by external field, for instance by the Zeeman or Stark effects. However, working on the two-dimensional electron gas in the wurtzite crystals, Rashba and Bychkov [20] in 1984 showed that the twofold spin degeneracy is removed due to the

perturbational term caused by the interaction between spin and momentum, even in the absence of any external field. This kind of spin-orbit interaction between the electron spin and electron motion linear in momentum, which is strong and caused by the surface-induced asymmetry in the material, is the so-called Rashba interaction.

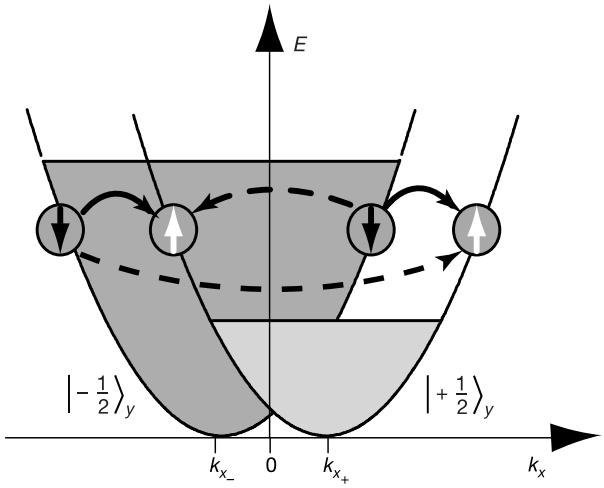

Figure 1.1. Schematic representation of the inverse spin-galvanic effect onto the scheme of splitting of the two energy sub-bands with the spin $|\pm 1/2\rangle_y$ caused by spin-orbit coupling in two-dimensional electron gas. The arrows in the circle are the spin-up and down. With the grey colour is shown the sub-band that contains higher number of electrons, spin-down electrons. The arrows indicate the possible spin-flip scattering. The dashed arrows represent the assymetric distributions of the spin polarization between the two sub-bands. $k_{x_\pm}$ is the wave vector [38].

The lifted spin degeneracy of the two sub-bands with up and down spins for two-dimensional electron gas is shown in Figure 1.1 taken from [38]. In the symmetric case for the two sub-bands when there are equal numbers or spin-up and down, there would not be any current flow. However in non-symmetric case when one of the sub-bands has more spin-down electrons, as we can notice from Figure 1.1, this situation can create an electric current. In other words, a non-equilibrium distribution of a spin polarization on the energy sub-bands creates an electric current, which is the spin-galvanic effect. To make non-equilibrium polarization distribution one can add spin injection using externally driven electric fields, as it was done with the two methods in [38]: from ferromagnetic contacts into the two-dimensional electron gas, using optical orientation in combination with an in-plane magnetic field. This external electric field generated a Zeeman effective magnetic field proportional to the strength of spin-orbit coupling and the shift of the Fermi spheric surface. And the shift caused by the external electric field creates the asymmetry of the occupied states on the two sub-bands. The shift happens in the

direction of motion of electrons perpendicularly to the external electric field.

Spin-galvanic effect and its inverse version mentioned before have been detected in many materials that have a strong spin-orbit splitting. Both effects can be explained with the linear dependence formulas

$$J_i = \sum_j Q_{ij} S_j, \tag{1.1}$$

$$S_i = \sum_j R_{ij} J_j, \tag{1.2}$$

which respectively represent the spin-galvanic effect and the inverse spin-galvanic effect. Here Q_{ij} and R_{ij} are pseudo-tensors. As we notice, the coupling is between the polar and axial vectors, electrical current and spin polarization. In gyroscopic media some components of the polar and axial vectors, that usually have different symmetry properties, have the same symmetry transformation. These components, electrical curent and average spin components, are linearly coupled in gyrotropic point groups where both vectors transform equivalently under symmetry operations, as we can see in Figure 1.2 [39].

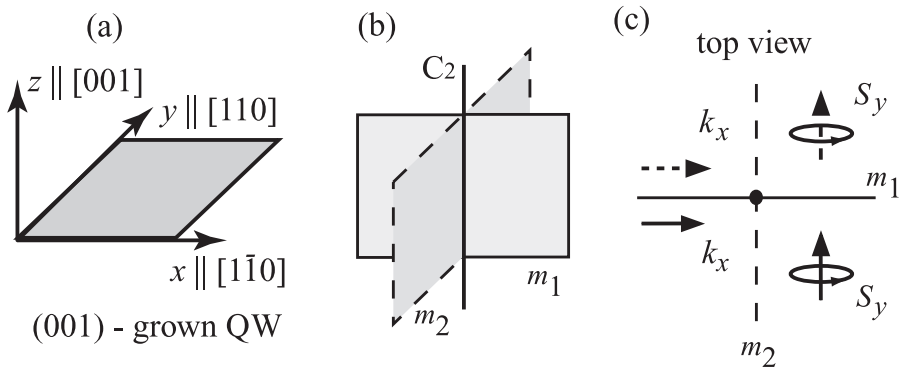

Figure 1.2. (a) Coordinate system used quantum wells(QWs), (b) symmetry elements of the C_{2v} point group. Two mirrow planes, m_1 and m_2 and C_2-axis along z. (c) Arrows indicate the reflection in the mirror plane m_1 and show that it does not change the sign of the polar vector component and the axial vector component, k_x and S_y respectively, which allows the coupling between them under this symmetry operation [39].

In this case, the linear coupling between polar and axial vectors has been proved even experimentally. The two pseudotensors Q_{ij} and R_{ij} can be in fact measured experimentally. They can be decomposed into Rashba spin-orbit coupling and Dresselhaus, similar to the first one but occurring in the bulk of the material, and measured experimentally as it was done in [39].

1.2.2 The spin-galvanic effect in quantum wells

The effect was firstly proposed by Ivchenko and Pikus in Ref. [28] in 1978. Later it was theoretically explained by Edelstein [40] for a two-dimensional electron gas with Rashba spin-orbit coupling and in [30]. The first experimental measurements of the inverse spin-galvanic effect were carried out in the semiconductor heterostructures as it was done in [41] by observing the change in the rotation rate of the plane of light polarization in Te crystal. Besides, the experiments with the spin-galvanic effect in quantum wells were carried out by Ganichev in Ref. [38, 42], where they used optical spin orientation perpendicular to a quantum well and showed that homogeneous non-equlibrium spin-polarization in semiconductor heterostructures results in an electric current. In practice the results can be measured by optical methods like Faraday or Kerr methods as we mentioned in subsection (1.1.3).

The spin-pumping technique for measuring the effects at interfaces was used for Bi/Ag Rashba interface to inject a spin current from a $NiFe$ layer into a Bi/Ag bilayer [43]. The pump-probe technique in semiconductor epilayers was used in [31, 44], where the inverse spin-galvanic effect and the spin-orbit splitting along the crystallographic axes [1, 1] and [1, −1] were measured . The results on the bulk epilayers [44] show a negative differential relationship between the magnitude of the inverse spin-galvanic effect and that of spin-orbit splitting, whereas the theoretical results explains qualitatively such effect only in two-dimensional electron gas [45]. Also, in [31] the authors measured the magnitude and direction of the inverse spin-galvanic effect and of the spin-orbit splitting in $InGaAs$, as a function of the in-plane electric and magnetic fields in the experiment with the cross patterns and four electrical contacts on the $GaAs$ substrate (see Figure 1.3). By varying the external magnetic field also the internal one was found to change, while remaining in extrema along [1, 1] and [1, −1]. The experimental results showed that the inverse spin-galvanic effect in $InGaAs$ epilayers is stronger when the internal spin-orbit coupling field is smaller and vice versa, in contrast to common understanding.

After this unexpected result, we desire to explain these recent fundings concerning the inverse spin-galvanic effect in $InGaAs$ epilayers. To this purpose we consider various forms of the frequency-dependent inverse spin galvanic effect in semiconductor quantum wells and epilayers. We take into account, besides the linear spin-orbit coupling, also the cubic term in the electron momentum spin-orbit coupling in the Rashba and Dresselhaus forms, concentrating on the inverse spin-galvanic effect.

1.2.3 The spin-galvanic effect in cold gases

Another possibility for studying the spin-galvanic effect are ultracold atomic systems, that are the "clean" systems and avoid problem with disorder. However, for an atomic system the spin-orbit interaction does not exist naturally as it was in the 2D electron gas. Hence, the first problem that we are facing is how to create Rashba spin-orbit interaction for cold atomic systems. Experimentally, the difficulty is in achieving a temperature as low as 0.1-10 μK. The first solution to synthesize a

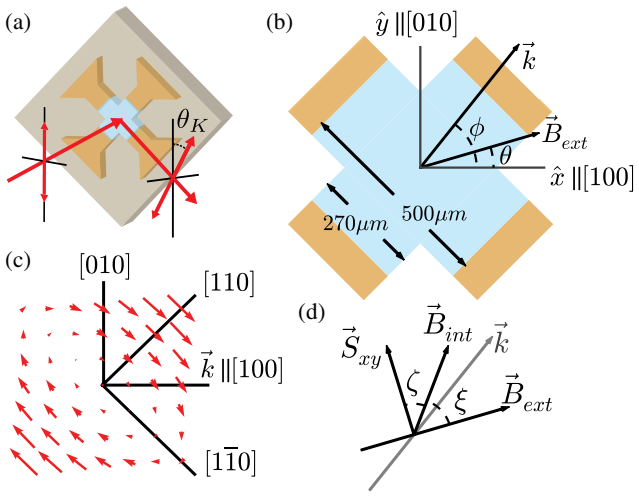

Figure 1.3. (a) InGaAs epilayer (blue) is etched into cross patterns with four electrical contacts (orange) on the GaAs substrate (gray). Kerr rotation measures the component of spin polarization along the laser axis $\mathbf{e_z}$. (b) Voltages applied to the contacts determine the electron drift momentum $\vec{k}$ at angle ϕ with respect to the [100] crystal direction. B_{ext} is oriented at angle θ by rotating the cryostat. (c) Total spin-orbit field as a function of $\vec{k}$ from structure and bulk inversion asymmetries components with relative strength $\alpha/\beta = 2$ and $\alpha > 0$. (d) The spin-orbit field B_{int} makes an angle ξ with respect to the external magnetic field B_{ext}. The steady-state in-plane spin polarization S_{xy} is shifted from B_{int} by angle ζ. The measured inverse spin-galvanic effect is maximized when $\xi + \zeta = \pi/2$. The figure is taken from [31]

magnetic field for neutral atoms was experimentally demonstrated in [46]. Such light-matter interaction can change the phase of the atomic wave function similarly to the Aharonov-Bohm effect, as for a charged particle in the presence of a magnetic field. So, by inducing artificially gauge potential with different symmetry, we are able to create a synthetic magnetic field [47, 48]. Creation of artificial gauge fields in quantum gases gives a series of advantages. First, these gauge fields can be controlled externally, so that they depend on coupling parameters between atoms and light. Moreover a real field cannot influence the synthetic one in any way since the last does not have dynamical degrees of freedom.

Recently it was proposed to create Rashba spin-orbit interaction via lasers of Rabi frequencies as Raman coupling, experimentally with neutral atomic Bose-Einstein condensate [49] and theoretically [50] with two-dimensional Fermi atomic gas [51, 52, 53]. The coupling is provided between the motion of the atom and its hyperfine spin states. In cold atoms these two hyperfine spin states form the two 1/2 pseudospin states. Here, pseudospin is described in terms of Pauli matrixes for 1/2 spin and stands out as a coherent superposition of two quantum states.

The spin Hall effect has been already investigated theoretically [54] and experimentally in cold atomic system [55, 49], where atoms show the spin-dependent

trajectory separation. This separation leads to a spin current in the direction perpendicular to the effective electric field and gauge field. Nonetheless, the inverse-spin galvanic effect was not considered yet in the literature.

Thus, in this thesis we build on very recent results by Vignale and Tokatly [9], on non-linear effects in inverse SGE, to discuss the applicability with anisotropic spin-orbit couplings with a Zeeman field. We demonstrate that adding this additional term still allows for an analytical solution of the model, and its phenomenology can be fully analyzed. In particular, we investigate the dynamics of the spins in the adiabatic regime with Rashba spin-orbit coupling. To investigate the spin-dependent evolution we directly solve the Schrödinger equation in terms of spinors and present the analytical solutions. In addition, we describe the average non-equilibrium spin polarization and tunability of the system for different values of the two Rashba coefficients. And then we compare the result with the adiabatically-approximated spin polarization.

Chapter 2

Spin-orbit coupling in solid state systems

In the general case of semiconductors the inversion and time-reversal symmetries lead to the spin degeneracy of electron and hole states. This fact implies a twofold degeneracy of single-particle energies. However, in materials with broken inversion symmetry the spin-degeneracy is removed and we obtain the two branches of energy dispersion. In some materials like heterostructures and quasi-2D quantum wells in the absence of magnetic field the spin splitting can be a result of bulk and structure inversion asymmetry and low microscopic symmetry at the interface. Structure inversion asymmetry, considered a reason for Rashba effect, contributes to a spin splitting in the presence of macroscopic and microscopic electric field from the atoms, while bulk inversion asymmetry is due to the microscopic spin-orbit interaction.

Below we show the two main types of spin-orbit interaction in solid systems, where they exist and the mechanisms that cause the interaction.

Table 2.1. BIA: Bulk-Induced-Assymetry; SIA: Surface-Induced-Asymmetry.

Symmentry-	Exists in crystals	Mechanism
-independent	of all types	stem from SOI in atomic orbitals
-dependent	no inversion symmetry	Dresselhaus interaction in bulk (BIA) Bychkov-Rashba on surface (SIA)

Symmetry-dependent spin-orbit interaction often can be observed in non-centrosymmetric crystals, as it was done in Ref. [20].

2.1 Derivation from Dirac equation

In solids spin-orbit coupling leads to the well-known spin-splitting of electron states. Here, spin-orbit interaction plays a key role since it strongly affects the atomic spectra [56]. It appears in the Hamiltonian from the non-relativistic approximation in the Dirac equation with an additional term that represents the spin-orbit interaction [57]. To make the wave equation satisfy the postulates of both quantum mechanics and relativistic theory it is required to take the root of the Hamiltonian

$$H = \sqrt{\mathbf{p}^2\, c^2 + m^2\, c^4}, \tag{2.1}$$

where c is the speed of light, m is the effective mass of the quantum particle, and the root must be linear in momentum $\mathbf{p}$. This feature will preserve the symmetries in time and space in the equations [58]. Dirac proposed in 1928 the following equation

$$H = (\alpha\, \mathbf{p})c + mc^2\, \beta, \tag{2.2}$$

where the unknown quantities β and α must be found from the condition

$$\mathbf{p}^2c^2 + m^2c^4 = ((\alpha\, \mathbf{p})c + \beta mc^2)^2$$

or

$$\mathbf{p}^2\, c^2 + m^2\, c^4 = (\alpha\, \mathbf{p})^2\, c^2 + \beta^2\, m^2\, c^4 + (\alpha\, \beta + \beta\, \alpha)\, \mathbf{p}\, mc^3.$$

Since this must hold true for any $\mathbf{p}$,

$$\begin{aligned} \mathbf{p}^2 &= (\alpha\, \mathbf{p})^2, \\ \beta^2 &= 1, \\ \alpha\, \beta + \beta\, \alpha &= 0. \end{aligned}$$

It follows that the α and β must be operators, i.e. matrices. Eventually the Dirac equation looks like the Schrödinger equation and, specifically, it is invariant under Lorenz transformations

$$i\, \hbar \frac{\partial \psi}{\partial t} = ((\hat{\alpha}\hat{\mathbf{p}})\, c + \hat{\beta}\, m\, c^2)\, \psi. \tag{2.3}$$

Then we choose the matrix $\hat{\gamma}^\mu$ ($\mu = 0,\ 1,\ 2,\ 3$) with the components $\hat{\gamma}^0 = \hat{\beta}$ and $\hat{\gamma}^i = \hat{\beta}\hat{\alpha}_i$ ($i = 1,2,3$) and coefficients

$$\hat{\beta} = \begin{pmatrix} 1 & 0 \\ 0 & -1 \end{pmatrix}, \qquad \hat{\alpha} = \begin{pmatrix} 0 & \sigma \\ \sigma & 0 \end{pmatrix}, \tag{2.4}$$

where σ denotes Pauli matrices.

Now let us consider a particle with charge e in electromagnetic field and potential $\mathbf{A}$ and V, and make the expansion for $1/c^2$

$$\left((\hat{\alpha}, \hat{\mathbf{p}} - e\mathbf{A}/c)\, c + e\, V + \hat{\beta}\, m\, c^2\right)\, \psi = E\psi, \tag{2.5}$$

with

$$\psi = \begin{pmatrix} \phi \\ \chi \end{pmatrix}, \qquad \int (\phi^\dagger \, \phi + \chi^\dagger \, \chi) = 1. \tag{2.6}$$

After the expansion we have

$$\left(\frac{\hat{p} - e\mathbf{A}/c}{2m} + e\,V + \Delta_1 \, \hat{H} + \Delta_2 \, \hat{H} \right) \psi = E^{'} \psi, \tag{2.7}$$

where $\Delta_1 \, \hat{H}$ is the correction of the first-order expansion and $\Delta_2 \, \hat{H}$ is the correction of the second-order expansion

$$\Delta_2 \, \hat{H} = -\frac{(\hat{\sigma}\hat{\mathbf{p}})}{2m} \, \frac{E^{'} - eV}{2m\,c^2} (\hat{\sigma}\hat{\mathbf{p}}) + \frac{e}{8m^2c^2} (\hat{\mathbf{p}}^2 V - V\hat{\mathbf{p}}^2).$$

After the action of the operator $\hat{\mathbf{p}}$ we have

$$\Delta_2 \, \hat{H} = -\frac{i\hbar}{4m^2c^2} e(\hat{\sigma}\nabla V) \, (\hat{\sigma}\hat{\mathbf{p}}) - \frac{E^{'} - eV}{2m\,c^2} \frac{(\hat{\sigma}\hat{\mathbf{p}})^2}{2m} - \frac{e\hbar^2}{8m^2c^2} \nabla^2 V - \frac{i\,e\,\hbar}{4m^2\,c^2} (\nabla \, V \, \hat{\mathbf{p}}).$$

Then we can make the substitution

$$(E^{'} - e\,V)\hat{\mathbf{p}}^2 = \frac{\hat{\mathbf{p}}^4}{2m} - e\hbar^2 \nabla^2 \, V - 2ie\hbar \, (\nabla \, V \hat{\mathbf{p}}).$$

Finaly, the second correction to the Dirac equation is

$$\Delta_2 \, \hat{H} = -\frac{\hat{\mathbf{p}}^4}{8m^3c^2} + \frac{\hbar\,e}{4m^2c^2} (\hat{\sigma}[\nabla \, V \hat{\mathbf{p}}]) + \frac{e\hbar^2}{8m^2c^2} \nabla^2 \, V.$$

The first term in this expression is a correction to the dependence of the velocity on the mass of a particle. The second term corresponds to the spin-orbit coupling, that describes the interaction between the internal orbital momentum of an electron with the magnetic field, generated by the core which is moving around it in this reference system

$$H_{SO} = -\frac{\hbar}{4m_0^2c^2} \boldsymbol{\sigma} \cdot \boldsymbol{p} \times (\nabla V_0), \tag{2.8}$$

being $\hbar$ the Planck's constant, m_0 the mass of a free electron, c the speed of light, $\boldsymbol{p} = -i\hbar\nabla$ the momentum operator, V_0 the Coulomb potential of the atomic core and $\boldsymbol{\sigma} = (\sigma_x, \sigma_y, \sigma_z)$ the vector of Pauli matrices. In solid-state physics of crystals the motion of electrons is described by energy bands $E_n(\boldsymbol{k})$, with band index n and wave vector $(\boldsymbol{k})$. In such systems the spin-orbit coupling affects the energy band structure $E_n(\boldsymbol{k})$ as well.

2.2 Kane model

In solids, when one wants to describe the motion of charge carriers taking into account impurities due to disorder, external fields and spin-orbit interaction, the $\mathbf{k}\cdot\mathbf{p}$ method for the 8×8 Kane model described in [59] satisfies the requirements. In this case the p-like bands are partially split by spin-orbit coupling into four degenerate levels: the light and heavy hole bands and two split-off levels. For materials with large energy gaps between the valence and the conduction bands, the effective Hamiltonian reduces to a 2×2 matrix and the solution is a conduction band spinor. This model explains explicitly how the spin-orbit coupling appears in solids.

All semiconductors with inversion-asymmetric zinc blende structure can be described within the extended Kane model with up to 14×14 matrix Hamiltonian using the second order perturbation theory. In this model the term with linear order in momentum in the conduction band and structure inversion asymmetry is presented by the Rashba term. The Rashba model with such spin splitting of 2D electron states in conduction band can be solved fully analytically by the Lowding partitioning [60] for the quasi-bulk Hamiltoninan and for the subband Hamiltonian. The same model in valence band is more complicated due to the fourfold degeneracy, and it has been evaluated numerically in the Luttinger model. The third mechanism for spin splitting in semiconductors, interface contributions, has been studied for the heterointerfaces in quasi-2D systems.

2.3 Effective spin-orbit coupling in Kane model

The $\mathbf{k}\cdot\mathbf{p}$ model gives the most accurate description of electronic band structure. In Ref. [61] this method was used for III-V semiconductors from 40-band tight-binding model.

The derivation of the $\mathbf{k}\cdot\mathbf{p}$ model starts with the Schödinder equation for the Bloch functions in the microscopic lattice-periodic crystal potential $V_0(r)$ [60]

$$\left[\frac{p^2}{2m_0}+V_0(r)\right] e^{i\mathbf{k}\cdot\mathbf{r}}\,U_{\nu\mathbf{k}}(r)=E_\nu(\mathbf{k})e^{i\mathbf{k}\cdot\mathbf{r}}\,U_{\nu\mathbf{k}}(r), \tag{2.9}$$

where m_0 is the free-electron mass and ν is the band index. The Bloch functions are $e^{i\mathbf{k}\cdot\mathbf{r}}\,U_{\nu\mathbf{k}}(r)=e^{i\mathbf{k}\cdot\mathbf{r}}\langle r|\nu k\rangle$, where $U_{\nu\mathbf{k}}(r)$ is the periodic function of the lattice. Including the effect of the kinetic-energy on the plane wave part of the Bloch functions and spin-orbit interaction derived from the Dirac equation, we have that the lattice-periodic parts of the Bloch functions become the two-component spinors $|n\mathbf{k}\rangle$. In this case the modified Schrödinger equation is

$$H_{eff}\,|n\mathbf{k}\rangle=\left[\frac{p^2}{2m_0}+V_0(r)+\frac{\hbar^2k^2}{2m_0}+\frac{\hbar}{m_0}\mathbf{k}\cdot\pi+\frac{\hbar}{4m_0^2c^2}\mathbf{p}\cdot\sigma\times(\nabla V_0)\right]\,|n\mathbf{k}\rangle=E_n(\mathbf{k})\,|n\mathbf{k}\rangle, \tag{2.10}$$

where

$$\pi = p + \frac{\hbar}{4m_0c^2}\sigma \times \nabla V_0$$

with Pauli matrices $\sigma = (\sigma_x, \sigma_y, \sigma_z)$. If we fix the wave vector k_0, the set of functions $|n\,k_0\rangle$ forms a complete orthonormal basis for the Eqs. (2.10) and we can expand $|n\,k\rangle$ in terms of band Bloch functions as

$$|n\,k\rangle = \sum_{\nu',\,\sigma'=\uparrow,\downarrow} c_{n\,\nu'\,\sigma'}(\mathbf{k})\,|\nu'\,\sigma'\rangle, \tag{2.11}$$

where

$$|\nu'\,\sigma'\rangle = |\nu'\,\mathbf{0}\rangle \otimes |\sigma'\rangle,$$

and the set of fuctions $|\nu'\mathbf{0}\rangle$ form the complete and orthonormal basis similar to Eq. (2.10), but without spin-orbit terms from the Dirac equation. This set was chosen as a basis for the eigenvectors of the Hamiltonian without spin-orbit terms since spin-orbit interactions can be treated as small perturbations [60].

Multiplying Eq. (2.10) by $\langle\nu\sigma|$, and using the eigenvalue equation for $|\nu\sigma\rangle$, we get the equation for the dispersion $E_n(\mathbf{k})$

$$\sum_{\nu',\sigma'}\left([E_{\nu'}(0) + \frac{\hbar^2k^2}{2m_0}]\,\delta_{\nu\nu'}\delta_{\sigma\sigma'} + \frac{\hbar}{m_0}\mathbf{k}\cdot\mathbf{P}_{\substack{\nu\nu'\\ \sigma\sigma'}} + \Delta^{\nu\nu'}_{\sigma\sigma'}\right) c_{n\,\nu'\sigma'}(\mathbf{k}) = E_n(\mathbf{k})\,c_{n\,\nu\sigma}(\mathbf{k}), \tag{2.12}$$

where

$$\mathbf{P}_{\substack{\nu\nu'\\ \sigma\sigma'}} = \langle\nu\sigma|\pi|\nu'\sigma'\rangle,$$
$$\Delta^{\nu\nu'}_{\sigma\sigma'} = \frac{\hbar}{4m_0^2c^2}\langle\nu\sigma|[\mathbf{p}\cdot\sigma\times(\nabla V_0)]|\nu'\sigma'\rangle.$$

In the dispersion relation in Eq. (2.12) the off-diagonal terms $\frac{\hbar}{m_0}\mathbf{k}\cdot\mathbf{P}_{\substack{\nu\nu'\\ \sigma\sigma'}}$ represent the mixing of the band edge states $|\nu\,\mathbf{0}\rangle$, which become stronger if the wave vector $\mathbf{k}$ increases and the band edges $E_\nu(0)$ get closer in energy [60]. The matrix elements of $\Delta^{\nu\nu'}_{\sigma\sigma'}$ represent a splitting of the degenerate energy levels $E_\nu(\mathbf{k})$, also when $\mathbf{k} = \mathbf{0}$.

The $\mathbf{k}\cdot\mathbf{p}$ method and the spin-orbit interaction are more carefully taken into account when we consider N bands. In this case, the Hamiltonian contains some additional terms with higher-order wave vector $\mathbf{k}$. In principle the extended Kane model takes into account the spin-orbit interactions between the bands Γ_8^c, Γ_7^c, Γ_6^c, Γ_8^v and Γ_7^v, while interactions with the other bands are described in a second-order perturbation theory (see Figure 2.1).

The Hamiltonian of the extended Kane model is a 14×14 matrix composed in

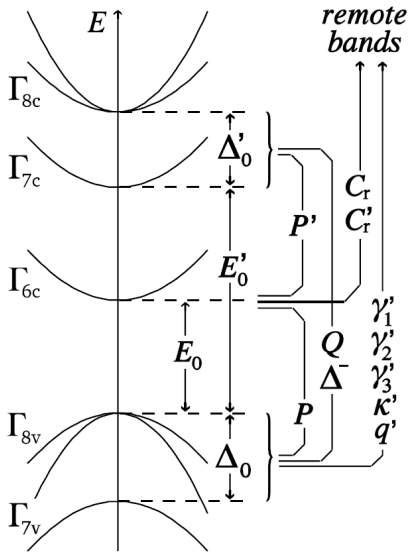

Figure 2.1. Schematic band structure for the 14×14 extended Kane model [60].

blocks

$$\mathcal{H}_{14\times14} = \begin{pmatrix} \mathcal{H}_{8c8c} & \mathcal{H}_{8c7c} & \mathcal{H}_{8c6c} & \mathcal{H}_{8c8v} & \mathcal{H}_{8c7v} \\ \mathcal{H}_{7c8c} & \mathcal{H}_{7c7c} & \mathcal{H}_{7c6c} & \mathcal{H}_{7c8v} & \mathcal{H}_{7c7v} \\ \mathcal{H}_{6c8c} & \mathcal{H}_{6c7c} & \mathcal{H}_{6c6c} & \mathcal{H}_{6c8v} & \mathcal{H}_{6c7v} \\ \mathcal{H}_{8v8c} & \mathcal{H}_{8v7c} & \mathcal{H}_{8v6c} & \mathcal{H}_{8v8v} & \mathcal{H}_{8v7v} \\ \mathcal{H}_{7v8c} & \mathcal{H}_{7v7c} & \mathcal{H}_{7v6c} & \mathcal{H}_{7v8v} & \mathcal{H}_{7v7v} \end{pmatrix} \tag{2.13}$$

The matrix elements of the momentum and spin-orbit interaction that are also shown in Figure 2.1, are

$$P = \frac{\hbar}{m_0} \langle S \left| p_x \right| X \rangle , \tag{2.14}$$

$$P' = \frac{\hbar}{m_0} \langle S \left| p_x \right| X' \rangle , \tag{2.15}$$

$$Q = \frac{\hbar}{m_0} \langle X \left| p_y \right| Z' \rangle , \tag{2.16}$$

$$\Delta_0 = -\frac{3i\hbar}{4m_0^2c^2} \left\langle X \left| [(\nabla V_0) \times p]_y \right| Z \right\rangle , \tag{2.17}$$

$$\Delta_0' = -\frac{3i\hbar}{4m_0^2c^2} \left\langle X' \left| [(\nabla V_0) \times p]_y \right| Z \right\rangle , \tag{2.18}$$

$$\Delta^- = -\frac{3i\hbar}{4m_0^2c^2} \left\langle X \left| [(\nabla V_0) \times p]_y \right| Z' \right\rangle , \tag{2.19}$$

where (X, Y, Z) correspond to the topmost bonding p-like valence band states and the $(X', Y',$ and $Z')$ states are the antibonding s-like and p-like states in the lowest conduction bands [60]. Besides, the real matrix elements are P, Q, Δ_0, Δ_0', the other two elements P' and Δ^- are imaginary. The elements Δ_0 and Δ_0' can be considered as spin-orbit splitting between bands Γ_8^v and Γ_7^v, Γ_8^c and Γ_7^c, respectively.

Summary

In this chapter I considered the various types of spin-orbit coupling in solid-state systems. In particular, I derived the spin-orbit coupling in the Dirac equation as a correction to the second-order expansion. Besides, I described the effective spin-orbit coupling in Kane's model. The results of this chapter will be used for further calculations in the next chapters.

Chapter 3

Quasi-classical formalism

In 2D electron gases with spin-orbit coupling, a spin current and spin polarization can be evaluated as a response to the external field. To calculate the response of a system to an external perturbation we can use the Green's function to derive the Kubo formula for various spin transport coefficients and, finally, to use the impurity diagrammatic technique for disordered electron systems [6]. There is however another way to obtain information about the spin polarization dynamics, i.e. the quasi-classical formalism in the Keldysh representation [8, 45, 62], which simplifies the complex non-equilibrium problem to the standard equilibrium problems with perturbative techniques. The Keldysh formalism is a general method for describing the system and its quantum mechanical evolution when the system is in a non-equilibrium state due to the presence of time varying fields [10, 63].

In this chapter I will consider a two-dimensional electron gas, one of the most studied systems in spintronics, to study in particular the inverse-spin galvanic effect. To this aim, I will briefly derive the Eilenberger equation using the Keldysh Green's function technique. The next chapter, where I am going to present my original contribution, will start from the results of the current chapter.

3.1 Keldysh formalism

The non-equilibrium Green's functions are the perfect tool to study perturbations in non-equilibrium systems through closed time path diagrams. Since we would like to have physical quantities in real time, below we will discuss an approach that is specifically tailored for a real-time formalism. In the general case, the non-equilibrium Green's function can be defined as

$$G_{\sigma\sigma'}(x_1, x_2) = -i \left\langle T_t \psi_\sigma(x_1) \psi^\dagger_{\sigma'}(x_2) \right\rangle . \tag{3.1}$$

Here the times t_1 and t_2 correspond to the different parts of the contour in (Figure 3.1), i.e. the upper and lower ones. The indices of the Green's functions are

related to the specific contour times: G_{12} means that t_1 belongs to the upper contour and t_2 to the lower one, while G_{11} or G_{22} mean that both times belong to the same contour, whether upper or lower. Hence, the Green's functions define the 2×2 configuration matrix

$$\hat{G} = \begin{pmatrix} \hat{G}_{11} & \hat{G}_{12} \\ \hat{G}_{21} & \hat{G}_{22} \end{pmatrix}. \tag{3.2}$$

Now let us define the generalized Green's functions as

$$\begin{aligned} \hat{G}_{11} &= -i\left\{\theta\left(t_1 - t_2\right)\left\langle\psi\left(x_1\right)\psi^{\dagger}\left(x_2\right)\right\rangle - \theta\left(t_2 - t_1\right)\left\langle\psi^{\dagger}\left(x_2\right)\psi\left(x_1\right)\right\rangle\right\}, \\ \hat{G}_{12} &= i\left\langle\psi^{\dagger}\left(x_2\right)\psi\left(x_1\right)\right\rangle, \\ \hat{G}_{21} &= -i\left\langle\psi\left(x_1\right)\psi^{\dagger}\left(x_2\right)\right\rangle, \\ \hat{G}_{22} &= -i\left\{\theta\left(t_2 - t_1\right)\left\langle\psi\left(x_1\right)\psi^{\dagger}\left(x_2\right)\right\rangle - \theta\left(t_1 - t_2\right)\left\langle\psi^{\dagger}\left(x_2\right)\psi\left(x_1\right)\right\rangle\right\}. \end{aligned} \tag{3.3}$$

where $\psi\left(x_1\right) = \psi\left(\mathbf{r}_1, t_1\right)$ and $\psi\left(x_2\right) = \psi\left(\mathbf{r}_2, t_2\right)$, and ψ is the Heisenberg representation of the wave vector. Performing the Keldysh rotation

$$\hat{G} \rightarrow \frac{1}{\sqrt{2}}\left[\hat{\sigma}_0 - i\hat{\sigma}_2\right]\hat{\sigma}_3\ \hat{G}\frac{1}{\sqrt{2}}\left[\hat{\sigma}_0 + i\hat{\sigma}_2\right], \tag{3.4}$$

the Keldysh Green's function becomes

$$\hat{G} = \frac{1}{2}\begin{pmatrix} \hat{G}_{11} - \hat{G}_{12} + \hat{G}_{21} - \hat{G}_{22} & \hat{G}_{11} + \hat{G}_{12} + \hat{G}_{21} + \hat{G}_{22} \\ \hat{G}_{11} - \hat{G}_{12} - \hat{G}_{21} + \hat{G}_{22} & \hat{G}_{11} + \hat{G}_{12} - \hat{G}_{21} - \hat{G}_{22} \end{pmatrix}. \tag{3.5}$$

The components of the Green's function are connected through the relation

$$\hat{G}_{11} + \hat{G}_{22} = \hat{G}_{12} - \hat{G}_{21}, \tag{3.6}$$

so that only three components are independent and we can rewrite Eq. (3.5) as

$$\hat{G} = \begin{pmatrix} \hat{G}_{11} - \hat{G}_{12} & \hat{G}_{12} + \hat{G}_{21} \\ 0 & \hat{G}_{11} - \hat{G}_{21} \end{pmatrix} = \begin{pmatrix} \hat{G}^R & \hat{G}^K \\ 0 & \hat{G}^A \end{pmatrix}, \tag{3.7}$$

with

$$\begin{aligned} \hat{G}^R(1,2) &= -i\theta\left(t_1 - t_2\right)\left\langle\left\{\psi\left(x_1\right), \psi^{\dagger}\left(x_2\right)\right\}\right\rangle, \\ \hat{G}^A(1,2) &= i\theta\left(t_2 - t_1\right)\left\langle\left\{\psi\left(x_1\right), \psi^{\dagger}\left(x_2\right)\right\}\right\rangle, \\ \hat{G}^K(1,2) &= i\left\langle\left[\psi\left(x_1\right), \psi^{\dagger}\left(x_2\right)\right]\right\rangle. \end{aligned} \tag{3.8}$$

Here, the last component $\hat{G}^K$ is the Keldysh component, while the first two $\hat{G}^R$, $\hat{G}^A$ are, respectively, the retarded and advanced components.

In order to illustrate the method, we apply it briefly to the case of the Fermi gas, whose field operator is described by

$$\psi_\sigma(x) = \frac{1}{\sqrt{V}} \sum_{\mathbf{k}} e^{i\mathbf{k}\cdot\mathbf{r}} e^{-i\epsilon(\mathbf{k})t} c_{\mathbf{k}\sigma}, \tag{3.9}$$

where $c_{\mathbf{k}\sigma}$ and $c^\dagger_{\mathbf{k}\sigma}$ are the creation and annihilation operators for the spin σ, respectively, we can write the anticommutator as

$$\begin{aligned}\left\langle \left\{ \psi(x_1), \psi^\dagger(x_2) \right\} \right\rangle &= \frac{1}{V} \sum_{\mathbf{k}_1\mathbf{k}_2} e^{i\mathbf{k}_1\cdot\mathbf{r}_1 - i\mathbf{k}_2\cdot\mathbf{r}_2} e^{-i\epsilon(\mathbf{k}_1)t_1 - i\epsilon(\mathbf{k}_2)t_2} \left\langle \left\{ c_{\mathbf{k}_1\sigma_1}, c^\dagger_{\mathbf{k}_2\sigma_2} \right\} \right\rangle \\ &= \frac{1}{V} \sum_{\mathbf{k}\sigma} e^{i\mathbf{k}\cdot(\mathbf{r}_1 - \mathbf{r}_2)} e^{-i\epsilon(\mathbf{k})(t_1 - t_2)}\end{aligned} \tag{3.10}$$

Now let us make a Fourier transform in space and time as

$$G(\mathbf{r}_1 - \mathbf{r}_2, t_1 - t_2) = \frac{1}{V} \sum_{\mathbf{k}} e^{i\mathbf{k}\cdot(\mathbf{r}_1 - \mathbf{r}_2)} \int_{-\infty}^{\infty} \frac{d\omega}{2\pi} e^{-i\omega(t_1 - t_2)} G(\mathbf{k}, \omega), \tag{3.11}$$

$$\frac{1}{V} \sum_k \equiv \int \frac{d\mathbf{k}}{(2\pi\hbar)^d} \tag{3.12}$$

so we find the retarded and advanced Green's functions for the Fermi gas as

$$G^{R/A}(\mathrm{k}, \omega) = \frac{1}{\hbar\omega - \epsilon(\mathrm{k}) \pm i0^+} \tag{3.13}$$

For the component G^K making the same steps we have

$$\left\langle \left[\psi(1), \psi^\dagger(2) \right] \right\rangle = \delta_{\sigma_1\sigma_2} \delta_{\mathbf{k}_1\mathbf{k}_2} (1 - 2f(\epsilon(\mathbf{k}))). \tag{3.14}$$

And after Fourier transform for Keldysh Green function we have

$$G^K(\mathbf{k}, \omega) = \left[G^R(\mathbf{k}, \omega) - G^A(\mathbf{k}, \omega) \right] (1 - 2f(\epsilon(\mathbf{k}))) \tag{3.15}$$

$$= -2\pi i \delta(\omega - \epsilon(\mathbf{k}))(1 - 2f(\epsilon(\mathbf{k}))), \tag{3.16}$$

where $f(\epsilon(\mathbf{k})) = \tanh \frac{\epsilon(\mathbf{k})}{2T}$. It is worth to say that the retarded and advanced Green functions carry an information about the spectrum of the excitations and the Keldysh Green function can tell about statistical occupation.

3.2 Eilenberger equation

Here we provide the derivation of the Eilenberger equation following Ref. [63]. To derive the quantum kinetic equation let us write the left-right subtracted Dyson

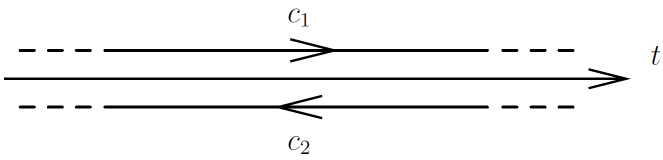

Figure 3.1. Closed real-time contour [60].

equation as

$$\left[G_0^{-1} - \Sigma \overset{\otimes}{,} G\right]_- = 0, \tag{3.17}$$

where self-energy Σ is

$$\Sigma = \begin{pmatrix} \Sigma^{\mathrm{R}} & \Sigma^{\mathrm{K}} \\ 0 & \Sigma^{\mathrm{A}} \end{pmatrix} \tag{3.18}$$

The matrix multiplication is

$$[A \overset{\otimes}{,} B]_- = A \otimes B - B \otimes A, \qquad [A \overset{\otimes}{,} B]_+ = A \otimes B + B \otimes A. \tag{3.19}$$

Then we find the kinetic equation for a general case from Eq. (3.17)

$$\left[G_0^{-1} - \Re e\Sigma \overset{\otimes}{,} G^{\mathrm{K}}\right]_- \left[\Sigma^K \overset{\otimes}{,} \Re e G\right]_- = \frac{i}{2}\left[\Sigma^K \overset{\otimes}{,} A\right]_+ - \frac{i}{2}\left[\Gamma \overset{\otimes}{,} G^K\right]_+, \tag{3.20}$$

where the spectral weight functions for the Green function and self-energy are

$$\begin{aligned} A\left(1,1'\right) &\equiv i\left(G^{\mathrm{R}}\left(1,1'\right) - G^{\mathrm{A}}\left(1,1'\right)\right), \\ \Re e\, G\left(1,1'\right) &\equiv \frac{1}{2}\left(G^{\mathrm{R}}\left(1,1'\right) + G^{\mathrm{A}}\left(1,1'\right)\right), \\ \Gamma\left(1,1'\right) &\equiv i\left(\Sigma^{\mathrm{R}}\left(1,1'\right) - \Sigma^{\mathrm{A}}\left(1,1'\right)\right), \\ \Re e\, \Sigma\left(1,1'\right) &\equiv \frac{1}{2}\left(\Sigma^{\mathrm{R}}\left(1,1'\right) + \Sigma^{\mathrm{A}}\left(1,1'\right)\right). \end{aligned} \tag{3.21}$$

To have a form of quantum kinetic equation that will be similar to the form of classic kinetic equation let us introduce the Wigner coordinates as follows

$$\mathbf{R} = \frac{\mathbf{x}_1 + \mathbf{x}_{1'}}{2} \quad , \quad \mathbf{r} = \mathbf{x}_1 - \mathbf{x}_{1'}, \tag{3.22}$$

and time variables

$$T = \frac{t_1 + t_{1'}}{2} \quad , \quad t = t_1 - t_{1'}. \tag{3.23}$$

And the Dyson equation becomes

$$(i\hbar\partial_T + \frac{\hbar^2}{m}\partial_{\mathbf{r}}\partial_{\mathbf{R}})\, G(\mathbf{R},T;\mathbf{r},t) - [\Sigma(\mathbf{R},T;\mathbf{r},t), G(\mathbf{R},T;\mathbf{r},t)] = 0. \tag{3.24}$$

Here the pair of variables $(\mathbf{r},t)$ describes the microscopic scale properties coming from the characteristics of the system, the other pair of variables $(\mathbf{R},T)$ describes the macroscopic scale properties that come from the non-equilibrium characteristics of the state in the presense of external fields. Then for a Green function we introduce the Fourier transform with respect to the relative coordinates as

$$G(X,p) \equiv \int dx\, e^{-ipx} G(X + x/2,\, X - x/2), \tag{3.25}$$

where we used X, x as

$$X = (T,\mathbf{R}) \quad , \quad x = (t,\mathbf{r}), \tag{3.26}$$

and p, xp as

$$p = (E,\mathbf{p}) \quad , \quad xp = -Et + \mathbf{p}\cdot\mathbf{r}. \tag{3.27}$$

Now the convolution $C = A \otimes B$ in the Wigner coordinates becomes

$$(A\otimes B)(X,p) = e^{\frac{i}{2}\left(\partial_X^A \partial_p^B - \partial_p^A \partial_X^B\right)} A(X,p)B(X,p), \tag{3.28}$$

where

$$\partial_X^A = (-\partial_T, \nabla_{\mathbf{R}}) \quad , \quad \partial_p^A = (-\partial_E, \nabla_{\mathbf{p}}) \tag{3.29}$$

and

$$\partial_X^A \partial_p^B \equiv -\frac{\partial^A}{\partial T}\frac{\partial^B}{\partial E} + \frac{\partial^A}{\partial \mathbf{R}}\cdot\frac{\partial^B}{\partial \mathbf{p}}. \tag{3.30}$$

The quantities with Wigner coordinates will be denoted as $\tilde{C}(X,x) \equiv C(X + x/2, X - x/2) = C\left(x_1, x_{1'}\right)$. And we write the convolution as

$$C\left(x_1, x_{1'}\right) \equiv \int dx_2 A\left(x_1, x_2\right) B\left(x_2, x_{1'}\right), \tag{3.31}$$

putting it in the Wigner coordinates as

$$\begin{aligned} \tilde{C}(X,x) &\equiv \int dx_2 A\left(X + x/2, x_2\right) B\left(x_2, X - x/2\right) \\ &= \int dx_2 \tilde{A}\left(\frac{1}{2}\left(X + x/2 + x_2\right), X + x/2 - x_2\right) \\ &\times \tilde{B}\left(\frac{1}{2}\left(x_2 + X - x/2\right), x_2 - (X - x/2)\right). \end{aligned} \tag{3.32}$$

Then setting $x_2 \to x_2 - (X - x/2)$ we rewrite the previous equation as

$$\tilde{C}(X,x) = \int dx_2 \tilde{A}\left(X + x_2/2, x - x_2\right) \tilde{B}\left(X - x/2 + x_2/2, x_2\right), \tag{3.33}$$

and then in the Wigner coordinates we have

$$\begin{aligned} C(X,p) &= \int dx e^{-ixp} \int dx_2 \tilde{A}\left(X + x_2/2, x - x_2\right) \tilde{B}\left(X - x/2 + x_2/2, x_2\right) \\ &= \int dx e^{-ixp} \int dx_2 \int \frac{dp'}{(2\pi)^4} e^{-ip'(x-x_2)} A\left(X + x_2/2, p'\right) \\ &\times \int \frac{dp''}{(2\pi)^4} e^{-ip''x_2} B\left(X - x/2 + x_2/2, p''\right). \end{aligned} \tag{3.34}$$

Then we can make an expansion and partial integration and we have

$$\begin{aligned} (A \otimes B)(X,p) = A(X,p)B(X,p) + \frac{i}{2}\left(\partial_X A(X,p)\right)\partial_p B(X,p) \\ - \frac{i}{2}\left(\partial_p A(X,p)\right)\partial_X B(X,p), \end{aligned} \tag{3.35}$$

that is what we needed, the computed Eq. (3.28). Then the G_0^{-1} from Eq. (3.17) becomes

$$G_0^{-1}(E, \mathbf{p}, \mathbf{R}, T) = E - \xi - V(\mathbf{R}, T), \tag{3.36}$$

with the applied potential $V(\mathbf{R}, T)$, the single-particle energy $\xi = \epsilon - \mu$ with the chemical potential μ and dispersion $\epsilon = \mathrm{p}^2/2\mathrm{m}$. Now we define the quasi-classical Green's function making the ξ-integration [63]

$$\breve{g}\left(\mathbf{R}, \hat{\mathbf{p}}, t_1, t_{1'}\right) = \frac{i}{\pi} \int d\xi \breve{G}\left(\mathbf{R}, \mathbf{p}, t_1, t_{1'}\right). \tag{3.37}$$

This ξ-integration can be explained with the following scheme with the deforming integration countour as in Figure 3.2. According to Figure 3.2 the ξ-integration becomes

$$\int_{-\infty}^{+\infty} d\xi \cdots = \frac{1}{2} \int_{C_{low}} d\xi \cdots + \frac{1}{2} \int_{C_{high}} d\xi \ldots \tag{3.38}$$

As we can notice the ξ-integration is separated into two contours, low and high energy contribution. The one with low energy contribution is crucial for the kinetic equation, because the upper one represents the high energy contribution which do not contribute. The latter does not depend on the non-equilibrium state and is constant. Thus, the high energy contribution vanishes from the left-right substracted Dyson equation

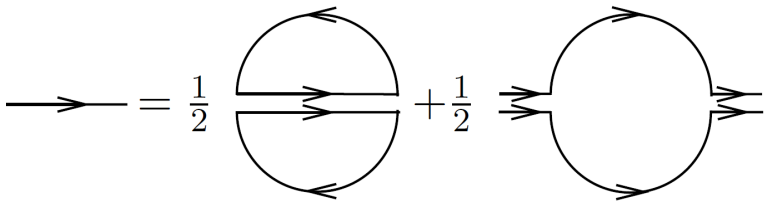

Figure 3.2. Splitting in high- and low-energy contributions [63].

$$i(\partial_{t_1} + \partial_{t_{1'}} + \frac{\mathbf{p}}{m} \cdot \nabla_{\mathbf{R}})\, G(\mathbf{R}, \mathbf{p}; t_1, t_{1'}) = \int dt_2 \left[\Sigma(\mathbf{R}, \mathbf{p}; t_1, t_2)\, G(\mathbf{R}, \mathbf{p}; t_2, t_{1'}) - G(\mathbf{R}, \mathbf{p}; t_1, t_2)\, \Sigma(\mathbf{R}, \mathbf{p}; t_2, t_{1'})\right] \quad (3.39)$$

and we can present physical quantities in terms of the quasi-classical Green's fuction $g^K(\mathbf{R}, \hat{\mathbf{p}}, t_1, t_{1'})$ as

$$\left[\tilde{\partial}_{t_1} + \tilde{\partial}_{t_{1'}} + v_F \hat{\mathbf{p}} \cdot \tilde{\partial}_{\mathbf{R}}\right]\, \check{g}(\mathbf{R}, \hat{\mathbf{p}}, t_1, t_{1'}) = -i \left[\check{\Sigma}(\mathbf{R}, \hat{\mathbf{p}}, t_1, t_{1'}), \check{g}(\mathbf{R}, \hat{\mathbf{p}}, t_1, t_{1'})\right], \quad (3.40)$$

where $\tilde{\partial}_\mu \hat{g} = \partial_\mu \hat{g} + i\,[eA_\mu, \hat{g}]$ is the covariant derivatives.

As it will be shown in Chapter 4 the spin-density in the presence of spin-orbit couplings can be computed through the Keldysh component of the quasi-classical Green's function as

$$S^i = -\frac{n_0}{4} \int d\epsilon \left\langle g_i^K \right\rangle, \quad (3.41)$$

where $n_0 = m/2\pi$ is the density of states for a two-dimensional electron gas with quadratic dispersion and having set $\hbar = 1$. Then, the cut-off energy of the semi-circles E_c is chosen to be much greater than the Fermi energy.

Chapter 4

Spin-orbit coupling in quantum wells

This chapter focuses on our contribution in explaining theoretically the result of the experiment in Ref. [44, 31] mentioned in Chapter 1, which observes a greater inverse spin-galvanic effect when the spin-orbit coupling is smaller.

We start here from the Dyson equation derived in Chapter 3 for the case with no disorder, but now an impurity potential is added. We take into account the bulk level of the material, considering the Dresselhaus spin-orbit coupling contribution up to the third power of the electron momentum besides the linear Rashba-Dresselhaus spin-orbit couplings, which gave completely opposite result than the experiment [40, 30]. Let us recall that when the electron system is confined in one direction the Dresselhaus spin-orbit coupling remains only linear in momentum, and the spin-polarization depends on the frequency of the driving electric field. Thus, by varying the contributions of the linear and cubic Rashba-Dresselhaus spin-orbit couplings, we estimate whose influence is the most significant along the direction and magnitude of the inverse spin-galvanic effect. The combination of these two spin-orbit couplings displays a situation with the inverse spin-galvanic effect along the two crystallographic axes $[1, -1, 0]$ and $[1, 1, 0]$ where there are also the minimum and maximum values of the internal magnetic field along these axes. The effect depends on the strength of these two types of spin-orbit couplings. Besides, we consider two regimes: diffusive and beyond diffusive. The latter corresponds to the case when the spin precession rate caused by the spin-orbit coupling is of the same order as impurity-determined scattering rate. The result of our theoretical study can be found in Ref. [64].

Considering a semiconductor heterostructure as quantum well, the electrons are confined in a two-dimensionl plane XY in the presence of impurity scattering. Such model in the presence of a generic intrinsic spin-orbit coupling can be described by the following Hamiltonian (for the sake of simplicity units are chosen so that

$\hbar = 1$)

$$H = \frac{p^2}{2m} + \mathbf{b}\cdot\boldsymbol{\sigma} + V(\mathbf{r}), \tag{4.1}$$

where $V(\mathbf{r})$ and $\mathbf{p} = (p_x, p_y)$ represent the impurity potential and the vector of momentum, respectively. The random potential has zero average and

$$\langle V(\mathbf{r})V(\mathbf{r}')\rangle = \delta(\mathbf{r}-\mathbf{r}')n_i v_0^2,$$

being v_0 the single-impurity scattering amplitude and n_i the impurity concentration. The effective magnetic field $\mathbf{b}$ contains the combination of Rashba and Dresselhaus spin-orbit couplings.

As we mentioned, in the following we will use the result derived in Chapter 3. By adopting the Wigner coordinates and by making a Fourier transform of the relative and center of mass coordinates, we obtain the following left-right subtracted Dyson equation for the Keldysh Green function

$$\partial_t \check{G} + \frac{1}{2}\Big\{\frac{\mathbf{p}}{m} + \frac{\partial}{\partial\mathbf{p}}(\mathbf{b}\cdot\boldsymbol{\sigma}), \frac{\partial}{\partial\mathbf{x}}\check{G}\Big\} + i[\mathbf{b}\cdot\boldsymbol{\sigma}, \check{G}] = -i[\check{\Sigma}, \check{G}], \tag{4.2}$$

where the self-energy $\check{\Sigma}$ includes disorder effects, while the curly brackets denote the anticommutator. The quasi-classical Green function is defined as

$$\check{g} = \frac{i}{\pi}\int d\xi \check{G}, \tag{4.3}$$

where the energy, with respect to the chemical potential in the absence of spin-orbit coupling, is $\xi = p^2/2 - \mu$. Now let us suppose the ansatz for the Green function as for the spin Hall effect in Ref. [65]

$$\check{G} = \begin{bmatrix} G^R & G^K \\ 0 & G^A \end{bmatrix} = \frac{1}{2}\left\{ \begin{bmatrix} G_0^R & 0 \\ 0 & -G_0^A \end{bmatrix}, \begin{bmatrix} \tilde{g}^R & \tilde{g}^K \\ 0 & \tilde{g}^A \end{bmatrix} \right\}, \tag{4.4}$$

with G_0^R and G_0^A being, respectively, the retarded and advanced Green functions in the absence of external perturbations

$$G_0^{R(A)} = \frac{1}{(\epsilon-\xi)\sigma^0 - \mathbf{b}\cdot\boldsymbol{\sigma} - \Sigma^{R(A)}} \tag{4.5}$$

with the self-energy $\Sigma^{R(A)}$ due to the impurity potential, which will be devired later. When the system is in equilibrium, considering the ansatz in Eq. (4.4) we have

$$\check{\tilde{g}} = \begin{bmatrix} 1 & 2\tanh(\epsilon/2T) \\ 0 & -1 \end{bmatrix} \otimes \sigma^0, \tag{4.6}$$

where the identity matrix σ^0 accounts for the spin structure. Then, let us expand the effective magnetic field $\mathbf{b}$ around the small values of the energy ξ and, observing that $|\xi| \ll \mu$, we find that

$$b \equiv |\mathbf{b}| \approx b_0 + \xi \frac{\partial b_0}{\partial \xi}, \tag{4.7}$$

$$|p_\pm| \approx p_F \mp \frac{|b_0|}{v_F}, \tag{4.8}$$

where b_0 is the value taken at the Fermi surface and $p_\pm$ refers to the Fermi momentum in the $\pm$-band. The limit is taken for small $\mathbf{b}$ comparing to the Fermi energy. For the two subbands we have the two projection operators

$$\mathcal{P}_\pm = \frac{1}{2}\left(\sigma^0 \pm \mathbf{b}_0 \cdot \boldsymbol{\sigma}\right), \qquad \mathbf{b}_0 = \mathbf{b}/b. \tag{4.9}$$

Now let us rewrite the quasi-classical Green function $\check{g}$ as

$$\begin{aligned} \check{g} &= \sum_{\nu=\pm} (1 - \nu \partial_\xi b_0) \frac{1}{2} \left\{ \mathcal{P}_\nu, \check{\tilde{g}} \right\} \equiv \sum_{\nu=\pm} (1 - \nu \partial_\xi b_0) \check{\tilde{g}}_\nu \\ &= \frac{1}{2} \{\sigma^0 - \partial_\xi \mathbf{b}_0 \cdot \boldsymbol{\sigma}, \check{\tilde{g}}\}. \end{aligned} \tag{4.10}$$

The last expression allows us to find

$$\check{\tilde{g}} = \check{g} + \frac{1}{2} \{\partial_\xi \mathbf{b}_0 \cdot \boldsymbol{\sigma}, \check{g}\}. \tag{4.11}$$

from which, using Eq. (4.10), we can see that

$$\check{g}_\nu = \frac{1}{2} \{\mathcal{P}_\nu, \check{g}\}, \quad \check{g} = \sum_{\nu=\pm} \check{g}_\nu, \tag{4.12}$$

and the expression for any function of momentum becomes as

$$\frac{i}{\pi} \int d\xi f(p) \check{G} = \sum_{\nu=\pm} f(p_\nu) \check{g}_\nu. \tag{4.13}$$

Hence, we can integrate the last equation and Eq. (4.3) over the energy ξ and obtain the Eilenberger equation as

$$\begin{aligned} &\sum_{\nu=\pm} \left[\partial_t \check{g}_\nu + \frac{1}{2} \left\{ \frac{p_\nu}{m} + \frac{\partial}{\partial \mathbf{p}} (\mathbf{b} \cdot \boldsymbol{\sigma}), \frac{\partial}{\partial \mathbf{x}} \check{g}_\nu \right\} + i[\mathbf{b} \cdot \boldsymbol{\sigma}, \check{g}_\nu] \right] \\ &= -i[\check{\Sigma}, \check{g}], \end{aligned} \tag{4.14}$$

where the self-energy in the Born approximation limit is

$$\check{\Sigma} = -\frac{i}{2\tau} \langle \check{g} \rangle, \qquad \frac{1}{\tau} = 2\pi n_0 n_i v_0^2 \tag{4.15}$$

with τ the elastic scattering time at the Fermi level and $n_0 = m/2\pi$ the density of states in the absence of spin-orbit coupling. The right-hand side of Eq. (4.14) describes the spin-independent scattering by disorder, and it is a collision integral. The quasi-classical Green function in Eq. (4.15) is taken as the angular average over the momentum directions.

Since the retarded and advanced quasi-classical Green functions do not contain information about spin, they are simply constant

$$\check{g}^R = 1, \qquad \check{g}^A = -1$$

and $g^R = \sigma^0 - \partial_\xi (\mathbf{b}_0 \cdot \sigma)$. At the equilibrium we have that

$$\begin{aligned} g^K &= \tanh\left(\frac{\epsilon}{2T}\right)\left(g^R - g^A\right) = \\ &2\tanh\left(\frac{\epsilon}{2T}\right)\left(\sigma^0 - \partial_\xi(\mathbf{b}_0\cdot\boldsymbol{\sigma})\right) \equiv g_{eq}\left[\sigma^0 - \partial_\xi(\mathbf{b}_0\cdot\boldsymbol{\sigma})\right], \end{aligned} \tag{4.16}$$

which defines g_{eq}. We can write the Keldysh component of the collision integral as

$$[\check{\Sigma}, \check{g}]^K = \Sigma^R g^K + \Sigma^K g^A - g^R \Sigma^K - g^K \Sigma^A. \tag{4.17}$$

while that of the Eilenberger equation, according to Eq. (4.14), has the form

$$(M_0 + M_1) g^K = (N_0 + N_1)\left\langle g^K \right\rangle, \tag{4.18}$$

where

$$M_0 = g^K + \tau\partial_t g^K + v_F \tau \hat{\mathbf{p}}\cdot\partial_{\mathbf{x}} g^K + i\tau[\mathbf{b}_0\cdot\boldsymbol{\sigma}, g^K], \tag{4.19}$$

$$\begin{aligned} \frac{1}{\tau}M_1 = &-\frac{1}{2}\left\{\frac{\mathbf{b}_0\cdot\boldsymbol{\sigma}}{p_F}\hat{\mathbf{p}} - \partial_{\mathbf{p}}(\mathbf{b}_0\cdot\boldsymbol{\sigma}), \partial_{\mathbf{x}} g^K\right\} \\ &- i\left[\partial_\xi(\mathbf{b}_0\cdot\boldsymbol{\sigma}), \left\{\mathbf{b}_0\cdot\boldsymbol{\sigma}, g^K\right\}\right] \\ &- \frac{1}{2\tau}\left\{\partial_\xi(\mathbf{b}_0\cdot\boldsymbol{\sigma}), g^K\right\}, \end{aligned} \tag{4.20}$$

$$N_0\left\langle g^K\right\rangle = \left\langle g^K\right\rangle,$$

$$N_1\left\langle g^K\right\rangle = \left\{\partial_\xi(\mathbf{b}_0\cdot\boldsymbol{\sigma}), g^K\right\}, \tag{4.21}$$

and $\hat{\mathbf{p}} = \mathbf{p}/|\mathbf{p}|$. The matrix expressions of the linear operators in Eqs. (4.21) and (4.29) are

$$M_0 = \begin{bmatrix} L & 0 & 0 & 0 \\ 0 & L & 0 & -2\tau b_0 \hat{b}_y \\ 0 & 0 & L & 2\tau b_0 \hat{b}_x \\ 0 & 2\tau b_0 \hat{b}_y & -2\tau b_0 \hat{b}_x & L \end{bmatrix}, \tag{4.22}$$

$$N_0 + N_1 = \begin{bmatrix} 1 & -c\hat{b}_x & -c\hat{b}_y & 0 \\ -c\hat{b}_x & 1 & 0 & 0 \\ -c\hat{b}_y & 0 & 1 & 0 \\ 0 & 0 & 0 & 1 \end{bmatrix}. \tag{4.23}$$

We can rewrite the angular average $\langle g^K \rangle$ in the presence of spin-orbit coupling as a system of four equations according to the spin structure of the quasi-classical Green function as

$$g^K = g_0^K \sigma^0 + g_i^K \sigma^i, \qquad i = x, y, z. \tag{4.24}$$

The internal magnetic field $\mathbf{b} = \mathbf{b}_R^{(N)} + \mathbf{b}_D^{(N)} = b_0^{(N)} \hat{\mathbf{b}}^{(N)}$ caused by the intrinsic Rashba and Dresselhaus spin-orbit couplings can be classified by the power of their momentum dependence N [66]. Thus, $\hat{\mathbf{b}}$ does not depend on the modulus of the momentum and the retarded component of the Green function according to Eqs. (4.12)-(4.16) can be shown as

$$g^R = \sigma^0 - c\hat{\mathbf{b}}^{(N)} \cdot \boldsymbol{\sigma}, \qquad c = \frac{N b_0^{(N)}}{2\epsilon_F}, \tag{4.25}$$

with $N = 1$ or $N = 3$ for, respectively, the linear or cubic spin-orbit couplings. When both linear and cubic spin-orbit couplings are present, the magnetic field becomes $\mathbf{b} = \mathbf{b}^{(1)} + \mathbf{b}^{(3)}$.

Now we use the minimal substitution in the Eilenberger equation in the presence of a time-dependent exernal electric field as

$$\partial_{\mathbf{x}} \to \partial_{\mathbf{x}} - |e| E \, \hat{\mathbf{E}} \, \partial_\epsilon \tag{4.26}$$

where $|e|$ and E are the absolute values of the electron charge and the applied electric field, respectively; $\hat{\mathbf{E}} \equiv (\hat{E}_x, \hat{E}_y) = (\cos\phi, \sin\phi)$ with ϕ the angle of the field with respect to the x-axis.
Solving Eq. (4.18) for the system under the influence of a uniform time-dependent electric field $\mathbf{E} = E\hat{\mathbf{E}}$ as

$$M_0 g^K = (N_0 + N_1) \left\langle g^K \right\rangle + S_{\mathbf{E}}, \tag{4.27}$$

with

$$S_{\mathbf{E}} = \tilde{E} \begin{bmatrix} \hat{\mathbf{E}} \cdot \hat{\mathbf{p}} \\ \hat{\mathbf{E}} \cdot \hat{\mathbf{p}} \dfrac{N+1}{2} \dfrac{b_0}{E_F} \hat{b}_x - \dfrac{\hat{\mathbf{E}} \cdot \partial_{\mathbf{p}}}{v_F} b_x \\ \hat{\mathbf{E}} \cdot \hat{\mathbf{p}} \dfrac{N+1}{2} \dfrac{b_0}{E_F} \hat{b}_y - \dfrac{\hat{\mathbf{E}} \cdot \partial_{\mathbf{p}}}{v_F} b_y \\ 0 \end{bmatrix}. \tag{4.28}$$

we eventually get

$$g^K = M_0^{-1} S_{\mathbf{E}} + M_0^{-1}(N_0 + N_1)\left\langle g^K \right\rangle . \tag{4.29}$$

We can take the angular average of Eq. (4.29)

$$S^i = -\frac{n_0}{4}\int d\epsilon \left\langle g_i^K \right\rangle . \tag{4.30}$$

and rewrite the Eilenberger equation (4.29) and (4.27) as a linear system of the components g_0^K and g_i^K to finally obtain

$$\left(1 - \left\langle M_0^{-1}(N_0 + N_1)\right\rangle\right)\left\langle g^K \right\rangle = \left\langle M_0^{-1} S_{\mathbf{E}} \right\rangle . \tag{4.31}$$

In this equation we neglect the term N_1 to a leading order in b_0/ϵ_F, that allows to decouple charge from spin. Besides, there is a decoupling between g_z component from g_x and g_y. This allows to reduce our in-plane spin dynamics problem to a 2×2 matrix configuration.

4.1 Inverse spin-galvanic effect beyond the diffusive regime in the linear Rashba-Dresselhaus spin-orbit couplings

In this section we describe the computation of the inverse spin-galvanic effect in the presence of the linear Rashba and Dresselhaus spin-orbit couplings. In the diffusive regime the spin-orbit coupling is small compared to the disorder expansion $2\tau p\alpha_1 \ll 1$, $2\tau p\beta_1 \ll 1$, but we are going beyond the diffusive regime and the magnitude of spin orbit couplings becomes significant $2\tau p\alpha_1 \gg 1$, $2\tau p\beta_1 \gg 1$. So far the calculation was done only for the diffusive regime, hence we will now extend the theory with our contribution beyond diffusive regime.

The effective magnetic field in the presence of linear Rashba and Dresselhaus spin-orbit couplings is [60]

$$\mathbf{b}^{(1)} = p \begin{bmatrix} \alpha_1 \hat{p}_y + \beta_1 \hat{p}_x \\ -\alpha_1 \hat{p}_x - \beta_1 \hat{p}_y \\ 0 \end{bmatrix}, \tag{4.32}$$

where α_1 and β_1 are the magnitudes of the linear Rashba and Dresselhaus spin-orbit couplings, respectively, and $\mathbf{p} \equiv p\,(\hat{p}_x, \hat{p}_y)$. The multiplication product of the effective magnetic field components is

$$\hat{b}_{x/y}^2 = p^2 \left(\frac{\alpha_1^2 + \beta_1^2}{2} \pm \frac{\cos 2\phi}{2}(-\alpha_1^2 + \beta_1^2) + \alpha_1\,\beta_1\,\sin 2\phi \right), \tag{4.33}$$

$$\hat{b}_x\,\hat{b}_y = -p^2\,(\frac{\sin 2\phi}{2}\,(\alpha_1^2 + \beta_1^2) + \alpha_1\,\beta_1) \tag{4.34}$$

The terms of $S_{\mathbf{E}}$ proportional to the uniform electric field are computed using Eq. (4.28)

$$S_{\mathbf{E}} = \tilde{E} \begin{bmatrix} s_{11} & s_{12} \\ s_{21} & s_{22} \end{bmatrix} \begin{bmatrix} \hat{E}_x \\ \hat{E}_y \end{bmatrix} \tag{4.35}$$

with $\tilde{E} = -|e|E\,\tau\,v_F\,\partial_\epsilon g_{eq}$ and elements

$$\begin{aligned} s_{11} &= \hat{p}_x\,(\alpha_1\,\sin\phi + \beta_1\,\cos\phi) - \partial_{p_x}\,(\alpha_1\,p_y + \beta_1\,p_x), \\ s_{12} &= \hat{p}_y\,(\alpha_1\,\sin\phi + \beta_1\,\cos\phi) - \partial_{p_y}\,(\alpha_1\,p_y + \beta_1\,p_x), \\ s_{21} &= -\hat{p}_x\,(\alpha_1\,\cos\phi + \beta_1\,\sin\phi) + \partial_{p_x}\,(\alpha_1\,p_x + \beta_1\,p_y), \\ s_{22} &= -\hat{p}_y\,(\alpha_1\,\cos\phi + \beta_1\,\sin\phi) + \partial_{p_y}\,(\alpha_1\,p_x + \beta_1\,p_y). \end{aligned} \tag{4.36}$$

Now we can rewrite the previous equations as

$$\begin{aligned} s_{11} &= \alpha_1 \sin 2\phi + \beta_1 \cos 2\phi, \\ s_{12} &= -\alpha_1 \cos 2\phi + \beta_1 \sin 2\phi, \\ s_{21} &= -\alpha_1 \cos 2\phi - \beta_1 \sin 2\phi, \\ s_{22} &= -\alpha_1 \sin 2\phi + \beta_1 \cos 2\phi. \end{aligned} \tag{4.37}$$

Taking the angular average of Eq. (4.28) we have

$$\hat{\Gamma}\left\langle g^K \right\rangle = \left\langle M_0^{-1} S_{\mathbf{E}} \right\rangle, \tag{4.38}$$

where $\hat{\Gamma} = 1 - \left\langle M_0^{-1}(N_0 + N_1)\right\rangle$ includes both the spin relaxation and the frequency dependence effects. To solve this equation we need to compute the integrals that will be done in the next steps, Eqs. (4.46, 4.103). Under the uniform electric field we have

$$\left\langle M_0^{-1}(N_0 + N_1)\right\rangle = \frac{1}{L^3 + La^2(\alpha_1^2 + \beta_1^2)} \begin{bmatrix} M_{11} & M_{12} \\ M_{21} & M_{22} \end{bmatrix}, \tag{4.39}$$

where $a = 2\tau p_F$ and $L = 1 - i\tau\Omega$. Here, Ω comes from the Fourier transform with respect to time t in Eq. (4.19). Since we are working beyond the diffusive regime, let us rewrite the denominator from the previous equation as

$$\frac{1}{L^3 + La^2(\alpha_1^2 + \beta_1^2)} = \frac{1}{L^3 + L\,(\alpha_1^2 + \beta_1^2)\,a^2}\,\frac{1}{1 + \mathcal{C}\,\sin 2\phi},$$

with

$$\mathcal{C} = a^2 \frac{2\alpha_1\beta_1 L}{L^3 + La^2(\alpha_1^2 + \beta_1^2)}. \tag{4.40}$$

Then, the matrix elements in Eq.(4.39) can be computed as

$$M_{11} = M_{22} = \left[L^2 + \frac{a^2}{2}(\alpha_1^2 + \beta_1^2)\right] \frac{1}{\sqrt{1-\mathcal{C}^2}} - \frac{a^2\alpha_1\beta_1}{\mathcal{C}} \frac{1-\sqrt{1-\mathcal{C}^2}}{\sqrt{1-\mathcal{C}^2}}, \tag{4.41}$$

$$M_{12} = M_{21} = a^2 \frac{\alpha_1^2+\beta_1^2}{2\mathcal{C}} \frac{1-\sqrt{1-\mathcal{C}^2}}{\sqrt{1-\mathcal{C}^2}} - a^2 \frac{\alpha_1\beta_1}{\sqrt{1-\mathcal{C}^2}}. \tag{4.42}$$

We can evaluate numerically the integrals used for averaging over the momentum direction in the calculations beyond the diffusive regime. For the combination of linear Rashba and Dresselhaus spin-orbit coupling, one finds that

$$\left\langle \frac{1}{1+\mathcal{C}\sin 2\phi} \right\rangle = \frac{1}{\sqrt{1-\mathcal{C}^2}} \tag{4.43}$$

$$\left\langle \frac{\sin 2\phi}{1+\mathcal{C}\sin 2\phi} \right\rangle = \frac{1}{\mathcal{C}} \left(1 - \frac{1}{\sqrt{1-\mathcal{C}^2}}\right) \tag{4.44}$$

$$\left\langle \frac{\cos 2\phi}{1+\mathcal{C}\sin 2\phi} \right\rangle = \left\langle \frac{\sin 4\phi}{1+\mathcal{C}\sin 2\phi} \right\rangle = 0 \tag{4.45}$$

$$\left\langle \frac{\cos 4\phi}{1+\mathcal{C}\sin 2\phi} \right\rangle = \frac{1}{\sqrt{1-\mathcal{C}^2}} + \frac{2}{\mathcal{C}^2} \left(1 - \frac{1}{\sqrt{1-\mathcal{C}^2}}\right). \tag{4.46}$$

The parameters $a\,\alpha_1$ and $a\,\beta_1$ are dimensionless and, as we mentioned at the beginning of this chapter, depending on their values we can identify two regimes. The spin-orbit splitting and the disorder value are much smaller than the Fermi energy ϵ_F, as for example in the model with Rashba spin-orbit coupling it is assumed that

$$\epsilon_F \gg \frac{1}{\tau}, \qquad \epsilon_F \gg 2\alpha_1\, p_F. \tag{4.47}$$

So, we can rewrite $a\alpha_1$ in terms of the two small parameters α_1/v_F and $1/\epsilon_F\tau$ as

$$a\alpha_1 = 2\tau\alpha_1\, p_F = \frac{4\alpha_1}{v_F}\epsilon_F\,\tau. \tag{4.48}$$

Thus, depending on the relation between α_1/v_F and $1/\epsilon_F\tau$ and considering Eq. (4.47), one can have two different regimes: diffusive and beyond diffusive regimes. The diffusive regime corresponds to a high impurity concentration, i.e. $a\alpha_1 \ll 1$. The second, beyond diffusive regime is related to the condition $a\alpha_1 \gg 1$ and describes the system with the low concentration of impurities and with spin-relaxation time close to τ. In the next sections both these regims will be considered for the

different contribution of linear and cubic spin-orbit couplings. Until then, let us focus on a model with only linear Rashba and Dresselhaus spin-orbit couplings.

When we have a diffusive regime at $\mathcal{C}$, the terms with the higher-order Rashba and Dresselhaus spin-orbit couplings can be neglected due to

$$\frac{\sqrt{1+\mathcal{C}^2}-1}{\sqrt{1+\mathcal{C}^2}} \approx \frac{\mathcal{C}^2}{2} \ll 1. \tag{4.49}$$

and the second term in Eq. (4.41) and the first term in Eq. 4.42 vanish. Besides, $\mathcal{C}=0$ when or $\alpha_1=0$, or $\beta_2=0$. Now we can write a generalized Bloch equation for the spin density using Eq. (4.30) as

$$\hat{\Gamma}\mathbf{S} = \hat{W}\mathbf{E}, \tag{4.50}$$

where the matrix $\hat{W}$, describing the spin generation torque in the right hand side of the above equation, is given by $\langle M_0^{-1} S_{\mathbf{E}} \rangle$ and can be calculated as

$$\begin{aligned}
\langle M_0^{-1} S_{\mathbf{E}} \rangle_{11} &= p_F \left(L^2 + a^2\,\hat{b}_x^2\right)(\beta_1\,\cos 2\phi + \alpha_1\,\sin 2\phi) - a^2\,p_F\,\hat{b}_x\,\hat{b}_y\,(\alpha_1\,\cos 2\phi + \beta_1\,\sin 2\phi),\\
\langle M_0^{-1} S_{\mathbf{E}} \rangle_{21} &= a^2\,p_F\,\hat{b}_x\,\hat{b}_y\,(\beta_1\,\cos 2\phi + \alpha_1\,\sin 2\phi) - p_F\left(L^2 + a^2\,\hat{b}_x^2\right)(\alpha_1\,\cos 2\phi + \beta_1\,\sin 2\phi),\\
\langle M_0^{-1} S_{\mathbf{E}} \rangle_{12} &= p_F \left(L^2 + a^2\,\hat{b}_x^2\right)(-\alpha_1\,\cos 2\phi + \beta_1\,\sin 2\phi) + a^2\,p_F\,\hat{b}_x\,\hat{b}_y\,(-\alpha_1\,\sin 2\phi + \beta_1\,\cos 2\phi),\\
\langle M_0^{-1} S_{\mathbf{E}} \rangle_{22} &= a^2\,p_F\,\hat{b}_x\,\hat{b}_y(-\alpha_1\,\cos 2\phi + \beta_1\,\sin 2\phi) + p_F\left(L^2 + a^2\,\hat{b}_x^2\right)(-\alpha_1\,\sin 2\phi + \beta_1\,\cos 2\phi)
\end{aligned} \tag{4.51}$$

For the matrix $\hat{W}$ we can use Eq.(4.51) to get

$$\omega_{11} = \frac{1}{2\alpha_1\,\beta_1\,L}(\alpha_1^2-\beta_1^2)\left(\frac{\mathcal{C}}{\sqrt{1-\mathcal{C}^2}}\frac{-\beta_1\,p_F}{4} + \frac{\alpha_1\,p_F}{2}\left(-1+\frac{1}{\sqrt{1-\mathcal{C}^2}}\right)\right), \tag{4.52}$$

$$\omega_{21} = -\frac{1}{2\alpha_1\,\beta_1\,L}(\alpha_1^2-\beta_1^2)\left(\frac{\mathcal{C}}{\sqrt{1-\mathcal{C}^2}}\frac{\alpha_1\,p_F}{2} - \frac{\beta_1\,p_F}{2}\left(-1+\frac{1}{\sqrt{1-\mathcal{C}^2}}\right)\right), \tag{4.53}$$

$$\omega_{12} = -\omega_{21}, \tag{4.54}$$

$$\omega_{22} = -\omega_{11}, \tag{4.55}$$

where we used that the angular average for $\cos 2\phi$ and $\sin 4\phi$ are null. For simplicity let us write

$$\hat{W} = \frac{S_0}{2}\frac{\beta_1^2-\alpha_1^2}{L^3 + La^2(\alpha_1^2+\beta_1^2)}\begin{bmatrix}\omega_{11} & \omega_{12}\\ \omega_{21} & \omega_{22}\end{bmatrix}, \tag{4.56}$$

with $S_0 = -|e|\tau n_0 E$ and

$$\omega_{11} = -\omega_{22} = -\frac{\beta_1 a^2}{\sqrt{1-\mathcal{C}^2}} - \alpha_1\delta, \tag{4.57}$$

$$\omega_{12} = -\omega_{21} = \frac{\alpha_1 a^2}{\sqrt{1-\mathcal{C}^2}} + \beta_1\delta, \tag{4.58}$$

and

$$\delta = L^2 \frac{1}{(\alpha_1^2+\beta_1^2)\mathcal{C} - 2\alpha_1\beta_1} \frac{1-\sqrt{1-\mathcal{C}^2}}{\sqrt{1-\mathcal{C}^2}}. \tag{4.59}$$

The matrix $\hat{\Gamma}$ is responsible for the spin-relaxation torque, the resulting spin density $\mathbf{S}$ comes from the balance between the generation and relaxation torques. In the diffusive regime with $\mathcal{C} \ll 1$, the value of δ is very small that retrieves the Dyakonov-Perel spin relaxation. When $\alpha_1^2 = \beta_1^2$, the contributions from linear spin-orbit couplings are canceled and we have a pure gauge configuration without inverse spin-galvanic efect [67]. The contribution to the spin torque with δ and $\mathcal{C}$ dependence occurs when the interaction of the Rashba and Dresselhaus spin-orbit couplings is considered beyond the diffusive regime. The powers of L consider terms relevant at high frequencies.

4.2 Inverse spin galvanic effect in the linear Rashba model

In this section we consider the case of linear Rashba spin-orbit coupling and describe a numerical solution of the generalized Bloch equations (4.50) by varying the Rashba parameter α_1 and for Dresselhaus parameter $\beta_1 = 0$ in Eq. (4.50). To start, let us write the Bloch equations in the two-dimentional electron gas with Rashba model

$$\begin{bmatrix} S^x \\ S^y \end{bmatrix} = \frac{1}{2} \frac{S_0^\alpha \alpha_1^2 a^2 E}{L^3 - L^2 + (L-1/2)\, a^2\alpha_1^2} \begin{bmatrix} \hat{E}_y \\ \hat{E}_x \end{bmatrix}, \tag{4.60}$$

with $S_0^\alpha = -|e|n_0\tau\alpha_1$. In the static limit when the frequency Ω is zero and $L = 1$, the spin polarization would be

$$\begin{bmatrix} S^x \\ S^y \end{bmatrix} = S_0^\alpha E \begin{bmatrix} \hat{E}_y \\ \hat{E}_x \end{bmatrix}, \tag{4.61}$$

which is the result found by Edelstein [40]. In the case when the inverse spin-galvanic effect is frequency-dependent and $L = 1 - i\,\Omega\tau$, from Eq.(4.60) we have

that

$$-i\,\Omega\tau\,(1-i\,\Omega\tau\,)^2+(\frac{1}{2}-i\,\Omega\tau\,)\,a^2\alpha_1^2=0. \tag{4.62}$$

The real part of the spin density becomes zero when

$$\Omega\tau \quad = \quad \frac{a\alpha_1}{2}, \tag{4.63}$$

while the imaginary part is zero when

$$\Omega\tau \quad = \quad 0;\ \sqrt{1+a^2\alpha_1^2}. \tag{4.64}$$

This means that when one of the components is zero, whether real or imaginary, the second one will be dominant. The same works in the opposite case. Thus, inverse spin-galvanic effect is dependent on the field frequency $\Omega\tau$.

Now let us define the frequency-dependent spin-galvanic conductivity using Eq. (4.60) as

$$S^i(\Omega)=\chi_{EC}^{ij}(\Omega)\,E_j(\Omega), \qquad i,j=x,y. \tag{4.65}$$

The charge current and the spin density in Eq. (4.65) are odd under time reversal operation while the Onsager reciprocal relations intend the equality of the inverse spin-galvanic and spin-galvanic responses and their conductivities. In the following we will use the normalized absolute imaginary and real value of the conductivities as

$$\chi^{ij}=\frac{\chi_{SG}^{ij}(\Omega)}{\chi_{SG}^{ij}(\Omega_{\max})}, \tag{4.66}$$

to $\Omega_{\max}$ is the frequency at the maximum value of χ_{SG}^{ij}. The plots of the real and imaginary parts and absolute value of the normalized conductivity χ^{yx} as a function of frequency in units of S_0^α for different magnitudes of Rashba spin-orbit coupling are shown in Figure 4.1. As we can notice when the frequencies are quite high, the conductivity vanishes, according to Eqs. (4.63)-(4.64), and a significant conductivity oscillation appears at $\Omega\sim\alpha_1 p_F$ if one goes beyond the diffusive regime, that is the condition $\alpha_1\,p_F\,\tau\gtrsim 1$ is satisfied.

4.3 Inverse spin-galvanic effect in the linear Rashba-Dresselhaus spin-orbit coupling

In this section we compute the inverse spin-galvanic effect in the presence of linear Rashba and Dresselhaus spin-orbit couplings. We work here in the diffusive regime, i.e. $a\alpha_1\ll 1$ and $a\beta_1\ll 1$, which allows to neglect the terms with higher orders. The generalized Bloch equation has the same form as Eq. (4.50) with $\hat{\Gamma}$ and $\hat{W}$ given by

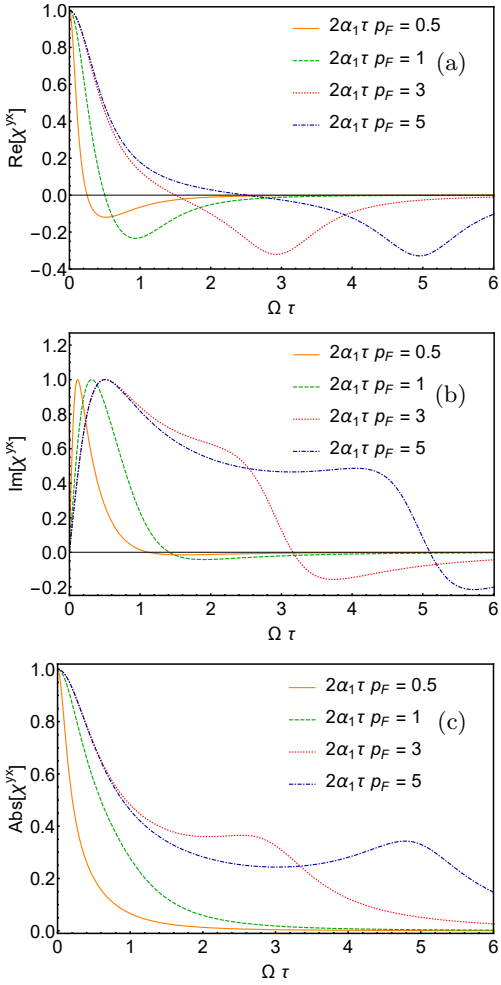

Figure 4.1. (a) Real part, (b) imaginary part and (c) absolute value of the normalized inverse spin-galvanic effect conductivity χ^{yx} as a function of the frequency $\Omega\tau$. In all plots: $2\alpha_1\tau p_F = 0.5$ (solid orange), and $2\alpha_1\tau p_F = 1$ (dashed green), and $2\alpha_1\tau p_F = 3$ (dotted red), and $2\alpha_1\tau p_F = 5$ (dot-dashed blue). Results are given in units of S_0^α.

$$\hat{\Gamma} = -i\Omega\tau + \frac{a^2}{2}\begin{bmatrix} \alpha_1^2+\beta_1^2 & 2\alpha_1\beta_1 \\ 2\alpha_1\beta_1 & \alpha_1^2+\beta_1^2 \end{bmatrix}, \tag{4.67}$$

$$\hat{W} = S_0\frac{a^2}{2}(\beta_1^2-\alpha_1^2)\begin{bmatrix} -\beta_1 & \alpha_1 \\ -\alpha_1 & \beta_1 \end{bmatrix}. \tag{4.68}$$

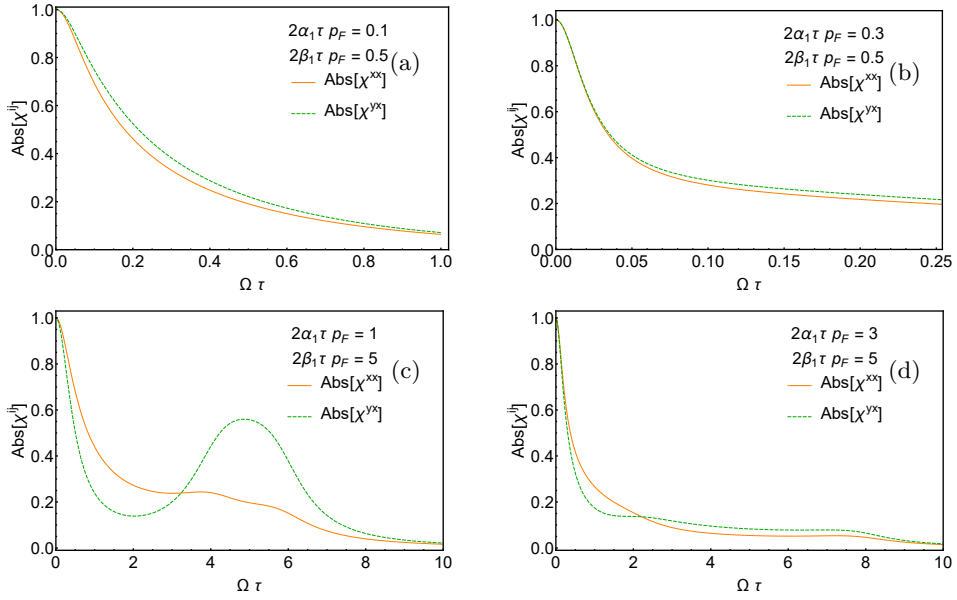

Figure 4.2. Absolute value of the normalized inverse spin-galvanic effect conductivity ($\chi^{ij} = \chi^{xx}$ (solid orange): χ^{yx}(dashed green)) as a function of frequency in the presence of linear Rashba and Dresselhaus spin-orbit couplings. From the left to the right: (a), (b) conductivity in diffusive regime and (c), (d) conductivity beyond the diffusive regime. The linear spin-orbit coupling coefficients from the top to the bottom: (a) $2\alpha_1\tau p_F = 0.1$ and $2\beta_1\tau p_F = 0.5$; (c) $2\alpha_1\tau p_F = 1$ and $2\beta_1\tau p_F = 5$; (b) $2\alpha_1\tau p_F = 0.3$ and $2\beta_1\tau p_F = 0.5$; (d) $2\alpha_1\tau p_F = 3$ and $2\beta_1\tau p_F = 5$. Results are given in units of S_0^α.

In the limit of spin helix regime, where Rashba and Dresselhaus spin-orbit couplings are comparable, we can write the spin polarization of Eq. (4.50) as

$$\begin{bmatrix} S^x(\Omega) \\ S^y(\Omega) \end{bmatrix} = S_0^{\alpha_1} \frac{a^2\Delta^2 E}{-2i\Omega\tau + a^2\Delta^2} \begin{bmatrix} \hat{E}_x + \hat{E}_y \\ -\hat{E}_x - \hat{E}_y \end{bmatrix}, \tag{4.69}$$

where $\Delta = \alpha_1 - \beta_1$, $|\Delta| \ll |\alpha_1|$ and $\Omega\tau \ll 1$. We notice that there is no effect for $\Delta = 0$, as expected, and the typical frequency scale is $\Omega \sim a^2\Delta^2/2\tau$.

In Figure 4.2(a-b), we plot the normalized conductivities, χ^{xx} and χ^{xy}, as a function of frequency for different values of α_1 and β_1 in the diffusive regime. The different scale in the frequency behavior from top to bottom is related to the difference between the two Rashba and Dresselhaus spin-orbit couplings, as shown in Eq. (4.69). In the diffusive regime, there is no finite-frequency peak in the conductivity, independent of the spin-orbit coupling details.

4.4 Inverse Spin-Galvanic Effect in the cubic Rashba-Dresselhaus Model

Now we take into account only the cubic Rashba-Dresselhaus spin-orbit coupling. Hence, the Hamiltonian will contain p-cubic terms in addition to the p-linear terms [68]. According to Refs. [59, 69], the effective Hamiltonian of the structural inverse asymmetry to the third order in the wave vector $\mathbf{p}$ reads

$$H_R^{(3)} = i\alpha_3 \begin{bmatrix} 0 & (p_x - ip_y)^3 \\ -(p_x + ip_y)^3 & 0 \end{bmatrix} \equiv \mathbf{b}_R^{(3)} \cdot \boldsymbol{\sigma} \tag{4.70}$$

with $\mathbf{b}_R^{(3)}$ being the effective internal magnetic field due to the cubic Rashba spin-orbit copling, which can also be written as

$$\mathbf{b}_R^{(3)} = \alpha_3 \begin{bmatrix} 3p_y\, p_x^2 - p_y^3 \\ 3p_x\, p_y^2 - p_x^3 \end{bmatrix} = \alpha_3 p^3 \begin{bmatrix} \sin 3\phi \\ -\cos 3\phi \end{bmatrix}. \tag{4.71}$$

Besides, there are terms occuring from the bulk of the material caused by the presence of Dresselhaus spin-orbit coupling [70]

$$H_D^{(3)} = -\beta_3 \begin{bmatrix} 0 & (p_x - ip_y)^3 \\ (p_x + ip_y)^3 & 0 \end{bmatrix} \equiv \mathbf{b}_D^{(3)} \cdot \boldsymbol{\sigma} \tag{4.72}$$

or by

$$\mathbf{b}_D^{(3)} = \beta_3 \begin{bmatrix} 3p_x\, p_y^2 - p_x^3 \\ -(3p_y\, p_x^2 - p_y^3) \end{bmatrix} = -\beta_3 p^3 \begin{bmatrix} \cos 3\phi \\ \sin 3\phi \end{bmatrix}. \tag{4.73}$$

The total effective internal magnetic field of the cubic Rashba-Dresselhaus spin-orbit coupling is given [60]

$$\begin{aligned} \mathbf{b}^{(3)} &= \mathbf{b}_R^{(3)} + \mathbf{b}_D^{(3)} = p^3 \begin{bmatrix} \alpha_3 \sin 3\phi - \beta_3 \cos 3\phi \\ -\alpha_3 \cos 3\phi - \beta_3 \sin 3\phi \end{bmatrix} \\ &\equiv b_0^{(3)} \hat{\mathbf{b}}^{(3)}. \end{aligned} \tag{4.74}$$

For the linear order in the external electric field, the source term $S_{\mathbf{E}}$ has the same form as in Eq. (4.35) with Eq. (4.37) replaced by

$$\begin{aligned} s_{11} &= p_F^2 \alpha_3 (2\sin 4\phi - \sin 2\phi) + p_F^2 \beta_3 (-2\cos 4\phi + \cos 2\phi), \\ s_{21} &= p_F^2 \alpha_3 (2\cos 4\phi + \cos 2\phi) + p_F^2 \beta_3 (-2\sin 4\phi + \sin 2\phi), \\ s_{12} &= -p_F^2 \alpha_3 (2\cos 4\phi + \cos 2\phi) - p_F^2 \beta_3 (2\sin 4\phi + \sin 2\phi), \\ s_{22} &= -p_F^2 \alpha_3 (2\sin 4\phi + \sin 2\phi) + p_F^2 \beta_3 (2\cos 4\phi + \cos 2\phi). \end{aligned} \tag{4.75}$$

By using Eqs. (4.22)-(4.28) we obtain for the generalized Bloch equation that

$$\hat{\Gamma} = \frac{L^2 + \frac{1}{2}a^2 p_F^4(\alpha_3^2 + \beta_3^2)}{L^3 + La^2 p_F^4(\alpha_3^2 + \beta_3^2)}\sigma_0, \tag{4.76}$$

$$\hat{\omega} = 0. \tag{4.77}$$

As we can see from Eq. (4.76) in the cubic Rashba and Dresselhaus spin-orbit coupling model the spin generation torque $\hat{W}\mathbf{E}$ vanishes, even though the spin relaxation rate $\hat{\Gamma}$ is non-zero. The latter contains the first harmonics of ϕ and hence, the $\mathbf{b}$ field with the third harmonics does not contribute, as it firstly noticed in Ref. [71].

4.5 Inverse spin galvanic effect in the linear and cubic Rashba model

In this section we compute the inverse spin-galvanic effect in the presence of linear and cubic Rashba spin-orbit couplings. From the previous section we know that in the presence of cubic Rashba-Dresselhaus spin-orbit couplings only the spin generation torque is zero. Let us then start with the internal magnetic field $\mathbf{b}$, which in this case reads

$$\mathbf{b}_{\mathcal{R}} = p \begin{bmatrix} \alpha_1 \sin\phi + \alpha_3\, p^2 \sin 3\phi \\ -\alpha_1 \cos\phi - \alpha_3\, p^2 \cos 3\phi \end{bmatrix}, \tag{4.78}$$

where α_1 and α_3 are the magnitudes of the linear and cubic Rashba spin-orbit couplings, respectively. According to Eq. (4.28) we can write the components of S_E as

$$S_{E_x} = \tilde{E} \begin{pmatrix} \hat{p}_x \\ \hat{p}_x \frac{N+1}{2} \frac{b_0}{E_F} \hat{b}_x - \frac{\partial_{p_x}}{v_F} b_x \\ \hat{p}_x \frac{N+1}{2} \frac{b_0}{E_F} \hat{b}_y - \frac{\partial_{p_x}}{v_F} b_y \\ 0 \end{pmatrix}, \tag{4.79}$$

$$S_{E_y} = \tilde{E} \begin{pmatrix} \hat{p}_y \\ \hat{p}_y \frac{N+1}{2} \frac{b_0}{E_F} \hat{b}_x - \frac{\partial_{p_y}}{v_F} b_x \\ \hat{p}_y \frac{N+1}{2} \frac{b_0}{E_F} \hat{b}_y - \frac{\partial_{p_y}}{v_F} b_y \\ 0 \end{pmatrix}.$$

Using the previous equations, the components of $S_{\mathbf{E}}$ are

$$
\begin{aligned}
s_{11} &= 2\,\hat{p}_x\,\alpha_1\,\sin\phi + \hat{p}_x\,4\,p_F^2\,\alpha_3\,\sin 3\phi - \partial_{p_x}\,(\alpha_1\,p_y + \alpha_3\,p_F^3\,\sin 3\phi), \\
s_{21} &= -2\,\hat{p}_x\,\alpha_1\,\cos\phi - \hat{p}_x\,4\,p_F^2\,\alpha_3\,\cos 3\phi + \partial_{p_x}\,(\alpha_1\,p_x + \alpha_3\,p_F^3\,\cos 3\phi), \\
s_{12} &= 2\,\hat{p}_y\,\alpha_1\,\sin\phi + \hat{p}_y\,4\,p_F^2\,\alpha_3\,\sin 3\phi - \partial_{p_y}\,(\alpha_1\,p_y + \alpha_3\,p_F^3\,\sin 3\phi), \\
s_{22} &= -2\,\hat{p}_y\,\alpha_1\,\cos\phi - \hat{p}_y\,4\,p_F^2\,\alpha_3\,\cos 3\phi + \partial_{p_y}\,(\alpha_1\,p_x + \alpha_3\,p_F^3\,\cos 3\phi).
\end{aligned} \tag{4.80}
$$

Notice that it was used $\cos 3\phi = -(3\,p_x\,p_y^2 + p_x^3)$ and $\sin 3\phi = 3\,p_y\,p_x^2 - p_y^3$. After a short computation the components become

$$
\begin{aligned}
s_{11} &= 2p_F^2\,\alpha_3 \sin 4\phi + (\alpha_1 - p_F^2\alpha_3)\sin 2\phi, \\
s_{21} &= -2p_F^2\,\alpha_3 \cos 4\phi + (-\alpha_1 + p_F^2\alpha_3)\cos 2\phi, \\
s_{12} &= -2p_F^2\,\alpha_3 \cos 4\phi - (\alpha_1 + p_F^2\alpha_3)\cos 2\phi, \\
s_{22} &= -2p_F^2\,\alpha_3 \sin 4\phi - (\alpha_1 + p_F^2\alpha_3)\sin 2\phi.
\end{aligned} \tag{4.81}
$$

Now let us calculate the product of the components of the effective magnetic field $\mathbf{b}$ as

$$
a^2\,b_x^2 = \frac{1}{2}\,(a_1^2 + a_3^2 + [2\,a_1a_3 - a_1^2]\,\cos 2\phi - 2\,a_1a_3\,\cos 4\phi - a_3^2\,\cos 6\phi), \tag{4.82}
$$

$$
a^2\,b_y^2 = \frac{1}{2}\,(a_1^2 + a_3^2 + [2\,a_1a_3 + a_1^2]\,\cos 2\phi + 2\,a_1a_3\,\cos 4\phi + a_3^2\,\cos 6\phi), \tag{4.83}
$$

$$
a^2\,b_xb_y = -\frac{1}{2}\,(a_1^2\,\sin 2\phi + a_3^2\,\sin 6\phi + 2\,a_1a_3\,\sin 4\phi), \tag{4.84}
$$

where $a_1 = a\,\alpha_1$ and $a_3 = a\,\alpha_3 p_F^2$

The inverse of the matrix in Eq. (4.22) is

$$
\hat{M}_0^{-1} = \frac{1}{L^3 + L\,(a_1^2 + a_3^2)}\,\frac{1}{1 + \mathcal{C}\,\cos 2\phi}\begin{pmatrix} L^2 + a^2\,b_x^2 & a^2\,b_xb_y \\ a^2\,b_xb_y & L^2 + a^2\,b_y^2 \end{pmatrix}. \tag{4.85}
$$

Since we are working beyond the diffusive regime we need to keep all the components.

By using Eqs. (4.22) and (4.23), the matrix $\langle M_0(N_0 + N_1)\rangle$ can be written as

$$
\langle M_0(N_0 + N_1)\rangle = \frac{1}{L^3 + L(a_1^2 + a_3^2)}\begin{bmatrix} M_{11} & 0 \\ 0 & M_{22} \end{bmatrix}, \tag{4.86}
$$

with $a_1 = a\alpha_1$ and $a_3 = ap_F^2\,\alpha_3$ and

$$
\begin{aligned}
M_{11} = {} & (L^2 + a^2\,b_x^2)\,\left(\cos 2\phi\,[\alpha_1 + \alpha_3\,p_F^2] + 2\,\alpha_3 p_F^2\,\cos 4\phi\right) \\
& + a^2\,b_xb_y\,(\sin 2\phi\,[\alpha_1 + \alpha_3\,p_F^2] + 2\,\alpha_3 p_F^2\,\sin 4\phi),
\end{aligned} \tag{4.87}
$$

$$
\begin{aligned}
M_{22} = {} & (L^2 + a^2\,b_y^2)\,\left(\cos 2\phi\,[\alpha_1 - \alpha_3\,p_F^2] + 2\,\alpha_3 p_F^2\,\cos 4\phi\right) \\
& + a^2\,b_xb_y\,(\sin 2\phi\,[\alpha_3\,p_F^2 - \alpha_1] - 2\,\alpha_3 p_F^2\,\sin 4\phi),
\end{aligned} \tag{4.88}
$$

which eventually become, after a short calculation,

$$\begin{aligned} M_{11} &= (L^2 + \frac{1}{2}(a_1^2 + a_3^2))A_0 \\ &+ \frac{1}{2}(-a_1^2 + 2a_1a_3)A_2 - a_1a_3A_4 - \frac{1}{2}a_3^2A_6, \end{aligned} \tag{4.89}$$

$$\begin{aligned} M_{22} &= (L^2 + \frac{1}{2}(a_1^2 + a_3^2))A_0 \\ &+ \frac{1}{2}(a_1^2 + 2a_1a_3)A_2 + a_1a_3A_4 + \frac{1}{2}a_3^2A_6, \end{aligned} \tag{4.90}$$

Here, all the coefficients A_n with $n = 0 \dots 6$ are

$$A_n = \left\langle \frac{\cos(n\phi)}{1 + \mathcal{D}\cos 2\phi} \right\rangle, \tag{4.91}$$

and

$$\mathcal{D} = \frac{2La_1a_3}{L^3 + L(a_1^2 + a_3^2)}. \tag{4.92}$$

They have been calculated numerically for further usage.

When $a_1 \ll 1$ and $a_3 \ll 1$, the diffusive regime occurs, and for this regime we have also $\mathcal{D} \ll 1$. In this case, all the integrals except the first one in Eqs. (4.89) and (4.90) can be neglected. Furthermore, we have that $\mathcal{D} = 0$ when either $a_1 = 0$ or $a_3 = 0$. Then, we can use Eqs. (4.22) and (4.28) to compute the matrix $\hat{W}$, it appears on the right hand side of Eq. (4.50) and can be written as

$$\hat{W} = \frac{S_0}{L^3 + L(a_1^2 + a_3^2)} \begin{bmatrix} 0 & w_{12} \\ w_{21} & 0 \end{bmatrix}, \tag{4.93}$$

with the components of the matrix as

$$\omega_{12} = \langle M_0^{-1}\, S_{E_y} \rangle_{11}, \tag{4.94}$$

$$\omega_{21} = \langle M_0^{-1}\, S_{E_x} \rangle_{22}. \tag{4.95}$$

By computing the angular average of the product between the inverse matrix M_0^{-1}, Eq. (4.85), and the matrix $S_{\mathbf{E}}$, Eq. (4.81), we find the components of the generation spin torque Eq. (4.93)

$$\begin{aligned} w_{12} &= \frac{\alpha_1}{2}\left(a_1^2 + 3a_3^2\right)A_0 \\ &+ \left[-L^2(\alpha_1 + p_F^2\alpha_3) + \frac{\alpha_1}{2}(a_1^2 + 2a_3^2 + 6a_1a_3) + 2\alpha_3p_F^2a_3^2\right]A_2 \\ &+ \frac{1}{4}\left(\alpha_1a_1^2 - \alpha_3p_F^2a_1^2 + 2\alpha_3p_F^2a_3^2\right)A_4 - \alpha_1a_3^2A_6, \end{aligned} \tag{4.96}$$

and

$$
\begin{aligned}
w_{21} &= \frac{\alpha_1}{2}\left(-a_1^2+3a_3^2\right)A_0 \\
&+\left[L^2(\alpha_1+p_F^2\alpha_3)+\frac{\alpha_1}{2}(a_1^2+a_3^2)-\frac{\alpha_3 p_F^2}{2}(3a_1^2+a_3^2)\right]A_2 \\
&+\frac{\alpha_3 p_F^2}{2}\left(4L^2+3a_1^2+a_3^2\right)A_4-\alpha_3 p_F^2 a_1 a_3 A_6. \qquad (4.97)
\end{aligned}
$$

In the presence of both the linear and cubic Rashba spin-orbit coupling, we have the following angular averages:

$$
\begin{aligned}
\left\langle \frac{\sin(2n\phi)}{1+\mathcal{D}\cos 2\phi}\right\rangle &= \left\langle \frac{\sin((2n+1)\phi)}{1+\mathcal{D}\cos 2\phi}\right\rangle = 0 && (4.98)\\
\left\langle \frac{\cos((2n+1)\phi)}{1+\mathcal{D}\cos 2\phi}\right\rangle &= 0, \quad n=0,1,2,\cdots && (4.99)\\
\left\langle \frac{1}{1+\mathcal{D}\cos 2\phi}\right\rangle &= \frac{-1}{\sqrt{1-\mathcal{D}^2}} && (4.100)\\
\left\langle \frac{\cos 2\phi}{1+\mathcal{D}\cos 2\phi}\right\rangle &= \frac{1}{\mathcal{D}}\left(1+\frac{1}{\sqrt{1-\mathcal{D}^2}}\right) && (4.101)\\
\left\langle \frac{\cos 4\phi}{1+\mathcal{D}\cos 2\phi}\right\rangle &= \frac{1}{\mathcal{D}^2}\left(-2-\frac{-2+\mathcal{D}^2}{\sqrt{1-\mathcal{D}^2}}\right) && (4.102)\\
\left\langle \frac{\cos(6\phi)}{1+\mathcal{D}\cos 2\phi}\right\rangle &= \frac{1}{\mathcal{D}^3}\left(4-\mathcal{D}^2+\frac{4-3\mathcal{D}^2}{\sqrt{1-\mathcal{D}^2}}\right) && (4.103)
\end{aligned}
$$

Notice that when the cubic Rashba spin-orbit coupling goes to zero ($\alpha_3 = 0$), Eq. (4.93, 4.96, 4.97) reproduces the result derived in Eq. (4.61). Furthermore, Eq. (4.96, 4.97) becomes zero when $\alpha_1 = 0$, independently of α_3. As a result, we found that when the linear and cubic Rashba spin-orbit couplings are present, the inverse spin-galvanic effect is changed due to few new terms in the spin relaxation and the spin generation torques.

4.6 The effects of the linear Rashba and Dresselhaus with the cubic Dresselhaus spin-orbit couplings

Here we take into account not only the linear Rashba-Dresselhaus coupling but also the cubic Dresselhaus spin-orbit coupling to evaluate the inverse spin-galvanic effect, and to compare our result with the experiment for InGaAs epilayers [31]. In this case we consider a diffusive regime. Starting again with the effective magnetic

field from the Hamiltonian in Eq.(4.1), taking into account terms for linear and cubic Rashba-Dresselhaus spin-orbit couplings, we write it as

$$\mathbf{b} = p \begin{bmatrix} \alpha_1 \sin\phi + \beta_1 \cos\phi - p^2 \beta_3 \cos 3\phi \\ -(\alpha_1 \cos\phi + \beta_1 \sin\phi + p^2 \beta_3 \sin 3\phi), \end{bmatrix} \tag{4.104}$$

where α_1, β_1 and β_3 are the above magnitudes of the linear Rashba and Dresselhaus and cubic Dresselhaus spin-orbit couplings, respectively. Then, as we did in the previous subsections, we find the product of the components of the magnetic field $\mathbf{b}$ and use them after to compute the matrix $\hat{W}$. The b_x^2, b_y^2 and $b_x b_y$ are

$$\begin{aligned} b_x^2 = {} & \frac{1}{2}\left(\alpha_1^2 + \beta_1^2 + \beta_3^2\, p^4\right) + \frac{\cos 2\phi}{2}\left(-\alpha_1^2 + \beta_1^2 - 2\,\beta_1\beta_3\, p^2\right) + \frac{\beta_3^2\, p^4}{2}\cos 6\phi \\ & + \sin 2\phi\, \alpha_1 \left(\beta_1 + \beta_3\, p^2\right) - \alpha_1\beta_3\, p^2 \sin 4\phi - \beta_1\beta_3\, p^2 \cos 4\phi, \end{aligned} \tag{4.105}$$

$$\begin{aligned} b_y^2 = {} & \frac{1}{2}\left(\alpha_1^2 + \beta_1^2 + \beta_3^2\, p^4\right) + \frac{\cos 2\phi}{2}\left(\alpha_1^2 - \beta_1^2 + 2\,\beta_1\beta_3\, p^2\right) - \frac{\beta_3^2\, p^4}{2}\cos 6\phi \\ & + \sin 2\phi\, \alpha_1 \left(\beta_1 + \beta_3\, p^2\right) + \alpha_1\beta_3\, p^2 \sin 4\phi - \beta_1\beta_3\, p^2 \cos 4\phi, \end{aligned} \tag{4.106}$$

$$b_x b_y = -\left(\frac{\sin 2\phi}{2}\left(\alpha_1^2 + \beta_1^2 + 2\,\beta_1\beta_3\, p^2\right) - \alpha_1\beta_3\, p^2 \cos 4\phi - \frac{\beta_3^2\, p^4}{2}\sin 6\phi + \alpha_1\beta_1\right). \tag{4.107}$$

According to Eq. (4.28) and using Eq. (4.50) we can write the components of S_E as

$$\begin{aligned} s_{11} &= 2\,\hat{p}_x\left(\alpha_1 \sin\phi + \beta_1 \cos\phi\right) - 4\hat{p}_x\, p_F^2\, \beta_3 \cos 3\phi - \partial_{p_x}\left(\alpha_1 \sin\phi + \beta_1 \cos\phi - \beta_3\, p_F^2 \cos 3\phi\right), \\ s_{21} &= 2\,\hat{p}_x\left(-\alpha_1 \cos\phi - \beta_1 \sin\phi\right) - 4\hat{p}_x\, p_F^2\, \beta_3 \sin 3\phi + \partial_{p_x}\left(\alpha_1 \cos\phi + \beta_1 \sin\phi + \beta_3\, p_F^2 \sin 3\phi\right), \\ s_{12} &= 2\,\hat{p}_y\left(\alpha_1 \sin\phi + \beta_1 \cos\phi\right) - 4\hat{p}_y\, p_F^2\, \beta_3 \cos 3\phi - \partial_{p_y}\left(\alpha_1 \sin\phi + \beta_1 \cos\phi - \beta_3\, p_F^2 \cos 3\phi\right), \\ s_{22} &= 2\,\hat{p}_y\left(-\alpha_1 \cos\phi - \beta_1 \sin\phi\right) - 4\hat{p}_y\, p_F^2\, \beta_3 \sin 3\phi + \partial_{p_y}\left(\alpha_1 \cos\phi + \beta_1 \sin\phi + \beta_3\, p_F^2 \sin 3\phi\right). \end{aligned} \tag{4.108}$$

After some calculation, the components of the matrix $S_{\mathbf{E}}$ become

$$\begin{aligned} s_{11} &= \alpha_1 \sin 2\phi + (\beta_1 + \beta_3 p_F^2)\cos 2\phi - 2\beta_3 p_F^2 \cos 4\phi \\ s_{21} &= -\alpha_1 \cos 2\phi - (\beta_1 - \beta_3 p_F^2)\sin 2\phi - 2\beta_3 p^2 \sin 4\phi \\ s_{12} &= -\alpha_1 \cos 2\phi + (\beta_1 - \beta_3 p_F^2)\sin 2\phi - 2\beta_3 p_F^2 \sin 4\phi \\ s_{22} &= -\alpha_1 \sin 2\phi + (\beta_1 + \beta_3 p_F^2)\cos 2\phi + 2\beta_3 p_F^2 \cos 4\phi. \end{aligned} \tag{4.109}$$

To evaluate the inverse spin-galvanic effect in the diffusive regime, we need to expand in Eq. (4.29) the denominator M_0^{-1} (with M_0 presented in Eq. (4.22)) in

terms of the spin-orbit field

$$M_0^{-1} = \frac{1}{L^3 + L\,(b_x^2 + b_y^2)\,a^2} \begin{bmatrix} L^2 + a^2\,\hat{b}_x^2 & a^2\hat{b}_x\hat{b}_y \\ a^2\hat{b}_x\hat{b}_y & L^2 + a^2\hat{b}_y^2 \end{bmatrix}, \tag{4.110}$$

For all the off-diagonal terms in the matrix M_0^{-1} we can neglect $b_x^2 + b_y^2$ in the denominator with respect to L, whereas for the diagonal terms one must expand the denominator, which becomes

$$\frac{1}{L^3 + L\,(b_x^2 + b_y^2)\,a^2} = \frac{1}{1 - 3i\,\Omega\,\tau + (b_x^2 + b_y^2)\,a^2} \approx 1 + 3i\,\Omega\,\tau - (b_x^2 + b_y^2)\,a^2, \tag{4.111}$$

where $L = 1 - i\,\Omega\tau$.

After this expansion, considering Eq.(4.111) we can rewrite Eq.(4.110) and the matrix M_0^{-1} as

$$M_0^{-1} \approx \begin{bmatrix} 1 + i\Omega\tau - a^2\hat{b}_y^2 & a^2\hat{b}_x\hat{b}_y \\ a^2\hat{b}_x\hat{b}_y & 1 + i\Omega\tau - a^2\hat{b}_x^2 \end{bmatrix}. \tag{4.112}$$

The left-hand side of Eq. (4.50) has a matrix $\hat{\Gamma}$ which, for the case of linear Rashba-Dresselhaus and cubic Dresselhaus spin-orbit coupling, can be written as

$$\hat{\Gamma} = 1 - \left\langle M_0^{-1} \right\rangle = a^2\alpha_1\beta_1\,p_F^2\,\sigma_x - (i\Omega\tau - \frac{a^2}{2}\,p_F^2\,[\alpha_1^2 + \beta_2^2 + \beta_3^2\,p_F^2]\,\sigma_0) \tag{4.113}$$

or simply as

$$\hat{\Gamma} = -i\Omega\tau + \hat{\Gamma}_1 + \hat{\Gamma}_3, \tag{4.114}$$

where the Dyakonov-Perel spin relaxation for the linear Rashba and Dresselhaus spin-orbit coupling ($\hat{\Gamma}_1$) and the cubic Dresselhaus spin-orbit coupling ($\hat{\Gamma}_3$) are given by

$$\hat{\Gamma}_1 = \frac{a^2}{2}\left[(\alpha_1^2 + \beta_1^2)\sigma^0 + 2\alpha_1\beta_1\sigma^x\right], \tag{4.115}$$

$$\hat{\Gamma}_3 = \frac{a^2}{2}\beta_3^2 p_F^4\sigma^0. \tag{4.116}$$

Hence, in the static limit where $\Omega = 0$ the Bloch equations in Eq. (4.50) can be rewritten as

$$(\hat{\Gamma}_1 + \hat{\Gamma}_3)\mathbf{S} = (\hat{\omega}^1 + \delta\hat{\omega}^{1,3})\mathbf{E}, \tag{4.117}$$

The right-hand side of Eq. (4.50) contains a product $\langle M_0^{-1} S_E \rangle$, which can be computed as a product of Eq.(4.112) at a static limit with $\Omega = 0$ and Eq.(4.109), and it becomes

$$\langle M_0^{-1} S_E \rangle = \frac{1}{L^3 + L(a_1^2 + a_3^2)} \begin{bmatrix} (1 - a^2\, b_y^2)\, s_{11} + a^2\, \hat{b}_x \hat{b}_y\, s_{21} & (1 - a^2\, b_y^2)\, s_{12} + a^2\, \hat{b}_x \hat{b}_y\, s_{22} \\ a^2\, \hat{b}_x \hat{b}_y\, s_{11} + (1 - a^2\, b_x^2)\, s_{21} & a^2\, \hat{b}_x \hat{b}_y\, s_{12} + (1 - a^2\, b_x^2)\, s_{22} \end{bmatrix} \tag{4.118}$$

or, after some manipulation,

$$\langle M_0^{-1} S_E \rangle = \frac{S_0 a^2}{2} p_F^2 \begin{bmatrix} 2\,\alpha_1^2\,\beta_3\,p_F^2 + \beta_1\,(\alpha_1^2 + 4\beta_3^2\,p_F^2 - \beta_1^2) & \alpha_1\,(\beta_1^2 - \alpha_1^2 - p_F^2\,(5\beta_3 + 2\beta_1\beta_3)) \\ \alpha_1\,(\alpha_1^2 - \beta_1^2 + p_F^2\,(5\beta_3 + 2\beta_1\beta_3)) & -2\,\alpha_1^2\,\beta_3\,p_F^2 - \beta_1\,(\alpha_1^2 + 4\beta_3^2\,p_F^2 - \beta_1^2) \end{bmatrix} \tag{4.119}$$

The right hand side of the Bloch equation can be rewriten with $\langle M_0^{-1} S_E \rangle$ like

$$\langle M_0^{-1} S_E \rangle \begin{bmatrix} E_x \\ E_y \end{bmatrix} = \begin{bmatrix} w_{11} & -w_{21} \\ w_{21} & -w_{11} \end{bmatrix} \begin{bmatrix} E_x \\ E_y \end{bmatrix} \tag{4.120}$$

where the indices correspond to the linear (1) and cubic parts (3) of the spin-orbit coupling and to their interplay $(1, 3)$. Then the matrices for the generation spin torque from Eq. (4.117) are

$$\hat{\omega}^1 = \frac{S_0 a^2}{2} (\alpha_1^2 - \beta_1^2) \begin{bmatrix} \beta_1 & -\alpha_1 \\ \alpha_1 & -\beta_1 \end{bmatrix}, \tag{4.121}$$

$$\hat{\omega}^{1,3} = \frac{S_0 a^2}{2} \begin{bmatrix} \tilde{\beta}_1 & -\tilde{\alpha}_1 \\ \tilde{\alpha}_1 & -\tilde{\beta}_1 \end{bmatrix}, \tag{4.122}$$

with

$$\tilde{\beta}_1 = 2 p_F^2 \beta_3 (2\beta_1 p_F^2 \beta_3 + \alpha_1^2), \tag{4.123}$$

$$\tilde{\alpha}_1 = \alpha_1 p_F^2 \beta_3 (5 p_F^2 \beta_3 + 2\beta_1). \tag{4.124}$$

The matrix $\hat{\omega}^1$ corresponds to the linear Rashba-Dresselhaus spin-orbit coupling, while $\hat{\omega}^{1,3}$ presents the interaction between the linear and cubic spin-orbit couplings.

The whole matrix $\hat{W}$ can be rewritten in terms of Pauli matrices as

$$\hat{W} = S_0\, a^2 \left(\frac{1}{2} (\beta_1\, p_F^2\, [\alpha_1^2 - \beta_1^2] + \tilde{\beta}_1)\, \sigma_z - \frac{i}{2}\, (\alpha_1\, p_F^2\, [\alpha_1^2 - \beta_1^2] + \tilde{\alpha}_1)\, \sigma_y \right) \tag{4.125}$$

or simply

$$\hat{W} = S_0 \frac{a^2}{2} \left(A\,\sigma_z - i\,B\,\sigma_y \right), \tag{4.126}$$

where the coefficients A, B are

$$\begin{aligned} A &= \beta_1\, p_F^2\, [\alpha_1^2 - \beta_1^2] + \tilde{\beta}_1, \\ B &= \alpha_1\, p_F^2\, [\alpha_1^2 - \beta_1^2] + \tilde{\alpha}_1 \end{aligned}$$

To calculate the inverse spin-galvanic effect from Eq. (4.117) we need to find the inverse matrix of the generation spin torque, $\hat{\Gamma}^{-1}$, using Eq. (4.113). The matrix $\hat{\Gamma}^{-1}$ is given by

$$\hat{\Gamma}^{-1} = \frac{2}{a^2} \frac{(\alpha_1^2 + \beta_1^2 + \beta_3^2\, p_F^4)\sigma^0 - 2\alpha_1\beta_1\sigma^x}{(\alpha_1^2 + \beta_1^2 + \beta_3^2\, p_F^4)^2 - 4\alpha_1^2\beta_1^2}. \tag{4.127}$$

Now we multiply the inverse matrix $\hat{\Gamma}^{-1}$ and the spin generation torque matrix $\hat{W}$ as

$$\begin{aligned} \hat{\Gamma}^{-1}\,\hat{W} = \frac{\tilde{E}}{4\,v_F\,p_F^2} & \frac{(-2\alpha_1\beta_1\sigma_x + (\alpha_1^2 + \beta_1^2 + \beta_3^2\, p_F^4)\sigma_0)}{(\alpha_1^2 + \beta_1^2 + \beta_3^2\, p_F^4) - 4\,(\alpha_1\beta_1)^2} \\ & \times \left([\tilde{\beta}_1 + 2\beta_1(\alpha_1^2 - \beta_1^2)\, p_F^2]\, \sigma_z - i\sigma_y\, [\tilde{\alpha}_1 + 2\alpha_1(\alpha_1^2 - \beta_1^2)\, p_F^2] \right) \end{aligned} \tag{4.128}$$

Finally, the spin polarization is defined by

$$\begin{aligned} \mathbf{S} = S_0 \Bigg(& \frac{-(\alpha_1 i\sigma^y + \beta_1\sigma^z)(\alpha_1^2 - \beta_1^2)^2}{(\alpha_1^2 + \beta_1^2 + \beta_3^2\, p_F^4)^2 - 4\alpha_1^2\beta_1^2} \\ & + \frac{2\beta_3 p^2\, (\xi i\sigma^y + 2\,\zeta\sigma^z)}{(\alpha_1^2 + \beta_1^2 + \beta_3^2\, p_F^4)^2 - 4\alpha_1^2\beta_1^2\sigma^z} \Bigg) \hat{\mathbf{E}}, \end{aligned} \tag{4.129}$$

where

$$\begin{aligned} \xi &= \alpha_1 \Big[\left(-\frac{1}{2}\beta_3\, p_F^2 + 2\beta_1 \right) (\alpha_1^2 - \beta_1^2) + \beta_3\, p_F^2 (3\beta_1^2 - 5\alpha_1^2) \\ &\quad -\beta_3^2\, p_F^4 (2\beta_1 + 5\beta_3\, p_F^2) \Big], \end{aligned} \tag{4.130}$$

$$\begin{aligned} \zeta &= (\alpha_1^2 - \beta_1^2) \left(\alpha_1^2 + \frac{1}{4}\beta_1\beta_3\, p_F^2 \right) + \beta_3\, p_F^2 \beta_1 (2\beta_1^2 - 3\alpha_1^2) \\ &\quad +\beta_3^2\, p_F^4 (\alpha_1^2 + 2\beta_1\beta_3\, p_F^2). \end{aligned} \tag{4.131}$$

In the equation for the spin polarization Eq. (4.129), the first term is responsible for the linear Rashba-Dresselhaus spin-orbit coupling, whereas the second one

represents not only the contribution of the cubic Dresselhaus spin-orbit coupling but also the interaction between the linear and cubic spin-orbit couplings.

At last, to compare our theoretical results with the ones experimentally measured in Ref. [31, 44], first we start by considering the simple case where there is only the linear spin-orbit coupling and $\beta_3 = 0$. So, Eq. (4.129) gives a result equivalent to Eqs. (4.67) and (4.68), and the spin polarization is given by

$$\begin{aligned} \mathbf{S} &= |e|\tau N_0(\beta_1\sigma^z + \alpha_1 i\sigma^y)\mathbf{E}, \\ &= \frac{N_0}{2}\mathbf{B}_{\rm int}, \end{aligned} \tag{4.132}$$

where $\mathbf{B}_{\rm int}$ is the spin-orbit field induced by the electric current.

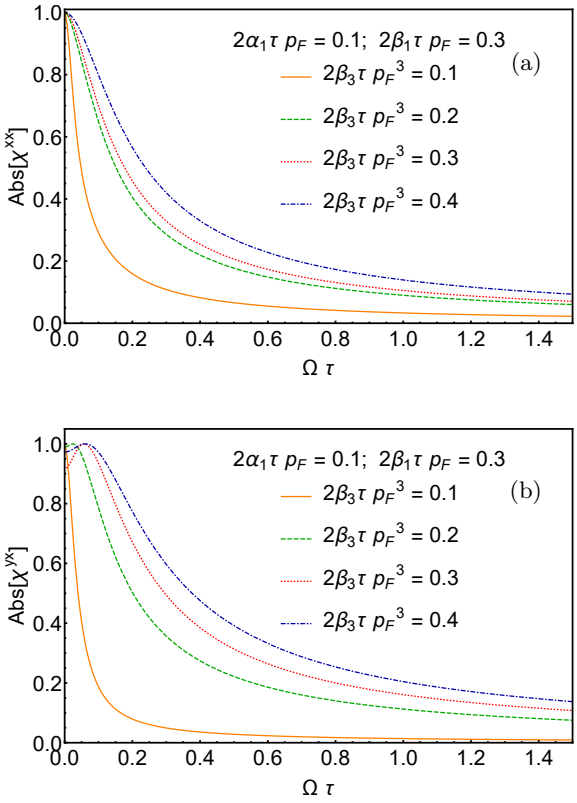

Figure 4.3. Absolute value of the normalized conductivity as a function of the frequency in diffusive regime. The components (a) χ^{xx} and (b) χ^{yx} are induced by the external electric field along x-direction. The linear spin-orbit coupling coefficients are fixed: $2\alpha_1\tau p_F = 0.1$, $2\beta_1\tau p_F = 0.3$. For (a), (b) $2\beta_3\tau p_F^3 = 0.1$ solid orange, $2\beta_3\tau p_F^3 = 0.2$ dashed green, $2\beta_3\tau p_F^3 = 0.3$ dotted red and $2\beta_3\tau p_F^3 = 0.4$ dot-dashed blue. Results are given in units of S_0^α.

In Figure 4.3 we plot the normalized conductivities, χ^{xx} and χ^{yx}, as a function of frequency for different values of the cubic Dresselhaus spin-orbit coupling $2\beta_3\tau p_F^3$ and fixed linear Rashba and Dresselhaus spin-orbit couplings, $2\alpha_1\tau p_F = 0.1$ and $2\beta_1\tau p_F = 0.3$ (values are dimensionless). As one can see from the plots, in the presence of the linear Rashba-Dresselhaus and cubic Dresselhaus spin-orbit couplings the conductivities χ^{xx} and χ^{yx} are the result of the interplay of these two mechanisms. The anisotropic feature of the spin polarization can be controlled by changing the strength of the cubic Dresselhaus spin-orbit coupling besides the present linear Rashba and Dresselhaus spin-orbit couplings.

Furthermore, we present the vector plot of the spin polarization $\mathbf{S}$ as a function of the electric field direction E for different values of the cubic Dresselhaus spin-orbit coupling while the linear couplings are fixed in Figure 4.4. The vector plot representation will help us to analyze the anisotropy of the inverse spin-galvanic effect. The black arrows within the empty circular sector correspond to the vector plot of the in-plane spin polarization (S^x, S^y) from Eq. (4.132) and the red arrows in the orange background correspond to the direction and the magnitude of the magnetic field B_{int}, where the value is represented by the background color, from low (light) to high (dark). Thus, in the two upper diagrams the inverse spin-galvanic effect is shown in the absence ($\beta_3 = 0$, top) and in the presence ($2\beta_3\tau p_F^3 = 0.1$, middle) of a weak cubic Dresselhaus spin orbit coupling. We can notice from Figure 4.4 that the largest magnitude of the inverse spin-galvanic effect arises for the electric field and the current along the crystallographic direction [1,1], which represents the effective linear spin-orbit coupling $\alpha_1 + \beta_1$. At the same time, the smallest effect appears for the field along the [1,-1] direction, that is responsible for the effective linear spin-orbit couplings $\alpha_1 - \beta_1$. Lastly, on the bottom plot of Figure 4.4 the inverse spin-galvanic effect is shown in the presence of a cubic Dresselhaus spin-orbit coupling with the strength greater than the linear coupling. We can see that the increase in β_3 ($2\beta_3\tau p_F^3 = 0.2$) significantly changes the anisotropy of the inverse spin-galvanic effect. It shows that the strongest polarization occurs for the spin along the [1,-1] direction and the smallest one appears for the field along [1,1] direction. Ultimately, the bottom figure explains the experimental result in Ref. [31, 44].

Summary and perspectives

In this chapter we described the model of quantum well in the presence of Rashba-Dresselhaus spin-orbit couplings, whether linear, cubic or both. To this purpose, we used the Keldysh formalism. First, we derived the kinetic Eilenberger equation from subtracted left-right Dyson equation. Then, by integrating the Keldysh component of quasi-classical Green's function we obtained the spin polarization. Specifically, for all the above countributions to the spin-orbit coupling we plotted the spin-galvanic conductivity. Finally, for the case of linear Rashba-Dresslhaus and cubic Dresselhaus terms we presented the vector diagram with varying cubic and fixed linear coefficients. A direct comparison with the experimental results in literature is also reported.

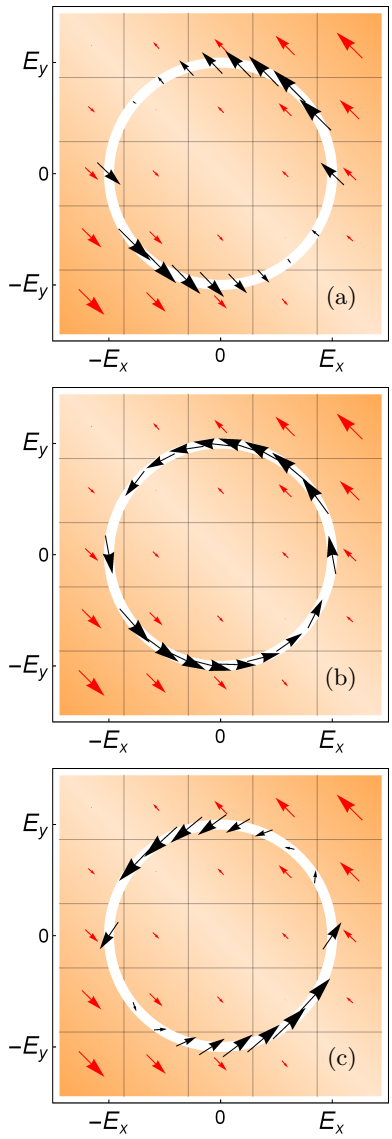

Figure 4.4. Black arrows correspond to the vector plot of the in-plane spin polarization (S^x, S^y). Red arrows correspond to the direction and the magnitude of the magnetic field B_{int}, where the greatest value is shown by the darkest color of the background. Results are given in units of S_0; E_x, E_y are the components of the electric field $\mathbf{E}$. Linear Rashba-Dresselhaus parameters are $2\alpha_1\tau p_F = 0.12$ and $2\beta_1\tau p_F = 0.125$. (a) Cubic Dresselhaus effect is absent for $2\beta_3\tau p_F^3 = 0$; (b) cubic Dresselhaus effect, $2\beta_3\tau p_F^3 = 0.05$, is comparable with the linear Rashba-Dresselhaus effects; (c) cubic Dresselhaus effect, $2\beta_3\tau p_F^3 = 0.2$, is greater than the linear Rashba-Dresselhaus effects.

Chapter 5

Synthetic spin-orbit coupling in cold gases

5.1 Gauge fields in ultracold atomic system

We focus on the gauge field engineered in ultracold neutral atomic systems. Here the description of the system is guided by effective gauge potentials that are generated within a configuration of atoms coupling to the lasers' fields. Laser induced gauge potentials in neutral atoms can imitate the action of an electron gas undergoing a magnetic field.

There are plenty of methods to create gauge potentials, some of them work better in Abelian or non-Abelian cases. The difference between them will be discussed below, for now let us concentrate on the main techniques realised or proposed. As we know, quantum atomic gases such as Bose-Einstein condensates [72] and degenerate Fermi gases [73], cannot be influenced by any external electromagnetic field being electrically neutral.

The coupling between spin and orbital angular momentum has been theoretically studied in Ref. [74]. Here, the authors generated it for Bose-Einstein condensates on a ring trap with fixed radius using Raman coupling through the two copropagating laser beams with higher-order Laguerre-Gauss. The coupling happens via a two-photon Raman process. The authors studied the ground state properties of such coupling on phase diagrams, showing strong effects of the transitions from non-degenerate ground states to multi-degenerate with a different strength of Raman coupling and with interactions. Besides, they propose a study of the coupling between spin and orbital angular momentum adding an external potential, gravitational potential and anisotropic trapping.

A theoretical study of a generalized scheme for Raman coupling in ultracold atoms mentioned above was proposed in [75]. There the authors address a general case using the resonance coupling when N atomic internal ground states couple to some additional excited state or sublevel of the atomic ground state, via N laser

beams, for generating Rashba-Dresselhaus spin-orbit coupling for spins larger than 1/2. In this case there are $N-1$ dark eigenstates. A particular case was considered with 4 laser beams and alkali-metal atoms.

Spin-orbit coupling in ultracold atomic systems was studied in Ref. [76] using homogeneus SU(N) non-Abelian model in square optical lattice. This model in the case $N = 3$ already gives a non-trivial state. Here, instead of the usual Pauli matrices in SU(2) systems, the authors applied Gell-Mann matrices for SU(3) systems. Furthermore, Ref. [77] contains a comprehensive collection of experimental schemes that have been implemented for studying spin-orbit coupling with ultracold atoms and optical lattices: the Raman scheme with an optical lattice with ^{86}Rb atoms and counter-propagating laser beams, the scheme of Raman assisting tunneling using atoms with the two internal states in a double-well potential, and schemes with Zeeman lattice and periodically driven lattice.

Experimental studies include ^{87}Rb Bose-Einstein condensate with a crossed dipole trap and two laser beams [78]. The coupling is created between the different spin states and laser field. Besides, they present the images of the vortices changing the detuning gradient. Their approach of optically generated magnetic fields avoids problems such as heating. In addition, the experimental and theoretical comparison of the results for Zitterbewegung in Bose-Einstein condensate was made in Ref. [79]. Other theoretical studies of synthetical spin-orbit coupling in real atomic Bose-Einstein condensates were proposed in Ref. [80] using four ground states. All four states are coupled cyclically at the same time by Raman transitions.

5.1.1 Berry's connection and the adiabatic principle

Gauge potentials can appear in cold atomic systems when the motion of the center of mass is coupled to atomic internal degrees of freedom or spin. The full time-dependent atomic Hamiltonian with state-independent trapping potential $V \equiv V(\mathbf{r},\ t)$ reads as follows

$$\hat{\tilde{H}}(\mathbf{r},\ t) = (\frac{\mathbf{p}^2}{2m} + V)\hat{I} + \hat{M}, \tag{5.1}$$

where $\mathbf{r}$ and $\mathbf{p} = -i\hbar\boldsymbol{\nabla}$ are respectively the atomic center of mass coordinate that denotes atomic position and the momentum operator, $\hat{I}$ is the identity operator acting on the internal atomic degrees of freedom and $\hat{M} = f(\mathbf{r},\ t)$ includes the Hamiltonian for the atomic internal motion and the atom-light interaction term. The diagonalization of the operator $\hat{M}$ gives a set of eigenstates, dressed states, and a set of eigenenergies dependent on $\mathbf{r}$ and t. We can expand any atomic state through a position dependent basis with a wave-function for the center of mass motion. The atomic basis states are connected through a position-dependent unitary transformation that diagonalises the operator $\hat{M}$

$$\hat{R}^{\dagger}\hat{M}(\mathbf{r},\ t)\hat{R} = \hat{\epsilon}, \tag{5.2}$$

where $\hat{\epsilon}$ is the set of eigenenergies. The final replacement of the original state vector with the transformed one gives a transformed Hamiltonian

$$\hat{H} = \hat{R}^\dagger \hat{\tilde{H}}(\mathbf{r}, t)\hat{R} - i\hbar \hat{R}^\dagger \partial_t \hat{R}. \tag{5.3}$$

It can be shown that Eq. (5.3) can be recast into

$$\hat{H} = \frac{(\mathbf{p} - \hat{\mathbf{A}})^2}{2m} + V + \hat{\epsilon} + \hat{\Phi} \tag{5.4}$$

by introducing the following quantities

$$\hat{\mathbf{A}} = i\hbar\, \hat{R}^\dagger \nabla \hat{R} = \sum_{n,m=1}^{N} |n\rangle \mathbf{A}_{nm} \langle m|, \qquad \mathbf{A}_{nm} = i\hbar \langle \eta_n | \boldsymbol{\nabla} | \eta_m \rangle, \tag{5.5}$$

$$\hat{\Phi} = i\hbar\, \hat{R}^\dagger \partial_t \hat{R} = \sum_{n,m=1}^{N} |n\rangle \Phi_{nm} \langle m|, \qquad \hat{\Phi}_{nm} = -i\hbar \langle \eta_n | \partial_t | \eta_m \rangle. \tag{5.6}$$

Here, the spatial dependence of the atomic dressed states causes the appearance of the vector operator $\hat{\mathbf{A}}$, and the time dependence - the scalar operator $\hat{\Phi}$. Referring to the adiabatic approximation, if a subset with $q \leq N$ number of dressed states is well distinct in energy from the other states, we can reduce the dynamic of the system by projecting it onto the cropped space of the internal states. To this purpose we act on our Hamiltonian $\hat{H}$ with the operator $\hat{P}^{(q)} = \hat{P}^{(q)} \hat{H} \hat{P}^{(q)}$ as

$$\hat{P}^{(q)} = \frac{(\mathbf{p} - \hat{\mathbf{A}}^{(q)})^2}{2m} + V_{tot}^{(q)}, \tag{5.7}$$

$$V_{tot}^{(q)} = V + \hat{\epsilon}^{(q)} + \hat{\Phi}^{(q)} + \hat{W}^{(q)}, \tag{5.8}$$

where the projections of the operators from the Hamiltonian $\hat{H}$ on the cropped subspace are $\hat{\epsilon}^{(q)}$, $\hat{\Phi}^{(q)}$ and $\hat{W}^{(q)}$, and the action of the operator $\hat{P}^{(q)}$ on the momentum $\mathbf{p}$ and potential V was skipped. An additional potential $\hat{W}^{(q)}$ arises from projecting $\mathbf{A}^2$ on the cropped subspace of the internal dressed states. This extra term can be justified as the kinetic energy of the atomic micro-trembling owing to off-resonance non-adiabatic transitions to the omitted dressed states

$$\hat{W}^{(q)} = \frac{1}{2m} \hat{P}^{(q)} \hat{\mathbf{A}} \left(\hat{I} - \hat{P}^{(q)} \right) \hat{\mathbf{A}} \hat{P}^{(q)}, \tag{5.9}$$

$$W_{nm} = \frac{1}{2m} \sum_{l=q+1}^{N} \mathbf{A}_{nl} \mathbf{A}_{lm}, \qquad n, m = 1, \ldots, q. \tag{5.10}$$

On one hand, the vector potential $\hat{\mathbf{A}}^{(q)}$ and the scalar potential $\hat{W}^{(q)}$ appear from spatial dependence of the atomic dressed states. On the other hand, the

potential $\hat{\Phi}^{(q)}$ occurs from their time dependence and describes the population transfer between the atomic levels caused by the time dependence of the external fields. In case the reduced subspace contains only one dressed state, $q = 1$, well separated in energy from the others, both the vector and the scalar potentials reduce to commuting vector and scalar fields. Only in this case the resulting synthetic electric and magnetic fields have the standard form $\mathbf{E} = -\boldsymbol{\nabla} V_{tot} - \partial_t \mathbf{A}$ and $\mathbf{B} = \boldsymbol{\nabla} \times \mathbf{A}$.

5.1.2 Abelian and non-Abelian cases

The vector and scalar potentials can lead to the common magnetic and electric fields. The problem in the quantum domain is that these two potentials are operators, and it is not always true that the scalar potential commutes with the Cartesian components of the vector potential. To this purpose, let us recollect the Heisenberg equation of motion operating the projected dynamics

$$\hat{\mathbf{v}} = -\frac{i}{\hbar}[\mathbf{r}, \hat{H}^{(q)}] = \frac{1}{m}(\mathbf{p} - \hat{\mathbf{A}}^{(q)}). \tag{5.11}$$

Here, the second derivative of the Heisenberg velocity, acceleration

$$\dot{\hat{\mathbf{v}}} = -\frac{1}{m}\partial_t \hat{\mathbf{A}}^{(q)} - \frac{im}{2\hbar}[\hat{\mathbf{v}}, \hat{v}^2] - \frac{i}{\hbar}[\hat{\mathbf{v}}, \hat{V}_{tot}^{(q)}], \tag{5.12}$$

then the Cartesian components of the acceleration are

$$\dot{\hat{v}}_k = -\frac{1}{m}\partial_t \hat{\mathcal{A}}_k^{(q)} - \frac{im}{2\hbar}\left(\hat{v}_l\left[\hat{v}_k, \hat{v}_l\right] + \left[\hat{v}_k, \hat{v}_l\right]\hat{v}_l\right) - \frac{i}{\hbar}\left[\hat{v}_k, \hat{V}_{\mathrm{tot}}^{(q)}\right]. \tag{5.13}$$

If we write the velocity commutators as $m^2\left[\hat{v}_k, \hat{v}_l\right] = i\hbar\hat{\mathcal{F}}_{kl}$ in terms of antsymmetric tensor

$$\hat{\mathcal{F}}_{kl} = \partial_k \hat{\mathcal{A}}_l^{(q)} - \partial_l \hat{\mathcal{A}}_k^{(q)} - \frac{i}{\hbar}\left[\hat{\mathcal{A}}_k^{(q)}, \hat{\mathcal{A}}_l^{(q)}\right], \tag{5.14}$$

the equation of motion becomes

$$m\dot{\hat{v}} = \frac{1}{2}(\hat{\mathbf{v}} \times \hat{\mathbf{B}}^{(q)} - \hat{\mathbf{B}}^{(q)} \times \hat{\mathbf{v}}) + \hat{\mathbf{E}}^{(q)}. \tag{5.15}$$

The vector operator

$$\hat{\mathbf{B}}^{(q)} = \nabla \times \hat{\mathbf{A}}^{(q)} - \frac{i}{\hbar}\hat{\mathbf{A}}^{(q)} \times \hat{\mathbf{A}}^{(q)}, \tag{5.16}$$

represents the artificial magnetic field (Berry curvature) providing the Lorenz force, with components $\hat{\mathbf{B}}_j^{(q)} = \frac{1}{2}\epsilon_{jkl}\hat{\mathcal{F}}_{kl}$. The Berry curvature is not zero only for the reduced dynamics of the atomic system, $q < N$, when some states vanish. The same is valid for the scalar potential W_{nm}.

When all the Cartesian components of the vector potential $\hat{\mathbf{A}}^{(q)}$ commute with each other, the vector potential is called Abelian. This situation happens when

$q = 1$. If some components do not commute for some j and l, $[\hat{A}_j^{(q)}, \hat{A}_l^{(q)}] \neq 0$, it is called non-Abelian gauge potential [81].

5.1.3 Raman induced spin-orbit coupling

In many experimental works, alkali atoms like ^{87}Rb and ^{40}K are used for generating spin-orbit coupling via Raman coupling. Raman induced spin-orbit coupling is generated by two counter-propagating laser beams along the $\hat{x}$ direction. Each laser beam is polarized: one is π polarized along the $\hat{z}$ direction and the other one is polarized linearly along the $\hat{y}$ direction. The spin quantization axes are set by a magnetic field along $\hat{z}$. Then, the atom will be affected by a two-photon process: first, by absorbing a π polarized (or linearly polarized, since it can be decomposed as $\sigma^{+/-}$ polarized beams) it gets excited to some intermediate excited state between $^2P_{1/2}$ and $^2P_{3/2}$, then it returns to the ground state of the spin system through emission of a $\sigma^{+/-}$ (or π).

Mathematically, the process is described by a rank-2 tensor and it can be decomposed in the sum of irreducible scalar, vector and tensor part. Experimental results showed that if we neglect the effect of fine structure splitting Δ_{FS} between $^2P_{1/2}$ and $^2P_{3/2}$, the scalar part is different from zero and this issue creates a spin-independent scalar potential. The vector and tensor parts are proportional to Δ_{FS}.

Usually one describes the motion of a single particle along $\hat{x}$ by the Hamiltonian $\hat{H}_0$, defining the two states of the vector term as two spin up and down.

$$\hat{H}_0 = \begin{pmatrix} \frac{k_x^2}{2m} + \frac{\delta}{2} & \frac{\Omega}{2} e^{2ik_0 x} \\ \frac{\Omega}{2} e^{-2ik_0 x} & \frac{k_x^2}{2m} - \frac{\delta}{2} \end{pmatrix}, \tag{5.17}$$

where $\Omega/2$ is the strength of Raman coupling and k_0 is the wave vector of the laser. Here the spin flipping process together with the momentum trasfer $2k_0$ along $\hat{x}$ direction is described by off-diagonal terms. Besides, it is assumed that the other spin states are far enough and do not resonate in our two-photon process. In particular we have $\delta = \omega_z - \delta\omega$, where ω_z is the Zeeman energy difference between our two spin states and $\delta\omega$ is the frequency difference between the two laser beams.

Following the standard procedure, we define a unitary transformation as $\phi = U\psi$, where the matrix U is

$$U = \begin{pmatrix} e^{-ik_0 x} & 0 \\ 0 & e^{ik_0 x} \end{pmatrix}. \tag{5.18}$$

The Hamiltonian $\hat{H}_0$ after diagonalization that is defined as $U\hat{H}_0 U^\dagger$, is

$$\hat{H}_0' = \begin{pmatrix} \frac{(k_x^2+k_0)^2}{2m} + \frac{\delta}{2} & \frac{\Omega}{2} \\ \frac{\Omega}{2} & \frac{(k_x^2+k_0)^2}{2m} - \frac{\delta}{2} \end{pmatrix} \tag{5.19}$$

or in the Pauli matrices representation

$$\hat{H}_0' = \frac{(k_x^2 + k_0\sigma_z)^2}{2m} + \frac{\delta}{2}\sigma_z + \frac{\Omega}{2}\sigma_x. \tag{5.20}$$

After a rotation of the spin axes along $\hat{y}$ by the angle $\frac{\pi}{2}$ in the way that $\sigma_x \to \sigma_z$ and $\sigma_z \to -\sigma_x$, the Hamiltonian becomes

$$\hat{H}_0'' = \frac{(k_x^2 - k_0\sigma_x)^2}{2m} - \frac{\delta}{2}\sigma_x + \frac{\Omega}{2}\sigma_z. \tag{5.21}$$

It looks like mixing of Rashba and Dresselhaus spin-orbit couplings with additional Zeeman field in the xz spin plane. The standard procedure used here will be shown in detail for our model in 5.2.

5.1.4 Rashba spin-orbit coupling

Rashba spin-orbit coupling with a single-particle Hamiltonian can be written as [82]

$$\hat{H}_0 = \frac{(k_x - k_0\sigma_x)^2}{2m} + \frac{(k_y - k_0\sigma_y)^2}{2m}. \tag{5.22}$$

Theoretical proposals about implementation of such a spin-orbit coupling experimentally can be devided intro three categories:

- *Dark-state scheme.* It is Lambda or tripod-scheme of laser coupling that is used to generate dark states. This kind of scheme is used for the experimental synthetic generation scheme for gauge potential in 2D Fermi gas in [51]. The dark states have a nontrivial spacial dependence and are considered as pseudospins. The operator of kinetic energy projected onto the subspace formed by the dark states, holds nontrivial abelian or non-abelian gauge field term. Usually the gauge fields created under such a configuration lead to the spin-orbit with the Hamiltonian mentioned above.

  The disadvantage of this scheme is that there is always a state with eigenenergy lower than a subspace of the dark states. This means that with time collisions between particles will lead to a decay to the lowest state, which sets a threshold for the system lifetime.

- *Generalized Raman scheme.* An example of such scheme was used in [52]. Comparing to the previous approach to generate a Rashba spin-orbit coupling, here one requires more laser beams. The main advantage is that the subspace for projection consists of the lowest energy and the collisional problem loses its relevance. It could seem a perfect option if it was not for the heating problem, which increases with the number of lasers.

- *Magnetic scheme.* This kind of scheme was proposed for avoiding the above heating problem. It was proposed to make a 2D and 3D Rashba-type spin-orbit coupling without using light in Ref. [83] with the method of pulsed

inhomogeneous magnetic fields that stamp appropriate phase gradients on the atoms. For 2D Rashba spin-orbit they used chip implementation and pulsed fields in two directions, while for 3D Rashba one more pulses should be added along the missing direction [83]. They found that for short pulses, the form of the interactions is not modified. The atomic spins point in the same direction of the magnetic field, which gives rise to an effective gauge potential. However, the strength of the gauge field depends on the size of the condensated atomic gas. Usually it is very weak.

5.2 System under investigation for our model

In this section it is shown in detail how to generate spin-orbit coupling synthetically for our original Hamiltonian following the method proposed in [9, 51]. We consider a cold atomic system with the external magnetic field which is described by the Hamiltonian

$$H(\mathbf{p}, t) = H_0 + H_{SO} + H_E + H_{ext}, \tag{5.23}$$

where $H_0 = \frac{1}{2m}[\mathbf{p} + e\mathbf{A}]^2$ with $\mathbf{A} = -E\,t\,\hat{\mathbf{x}}$ corresponds to the kinetic part, H_{SO} is the Rashba spin-orbit interacting term that is $H_{SO} = \alpha_1\,\sigma_x\,p_y - \alpha_2\,\sigma_y\,p_x$ with $p_{x,y}$ that are the in-plane components of the momentum operator and $\sigma_{x,y}$ - the Pauli matrices associated to the spin degree of freedom. Let us notice also, that the coupling constants $\alpha_1 = \alpha + \beta$, $\alpha_2 = \alpha - \beta$ correspond to the mixing of Rashba and Dresselhaus spin-orbit couplings. Besides, the presence of the electric field gives the Edelstein term $H_E = \alpha_2 eEt\,\sigma_y$. Furthermore, the last term corresponds to the Zeeman coupling with an external magnetic field $H_{ext} = -\mu_B \mathbf{B}\cdot\boldsymbol{\sigma}$. But before moving on let us show how to get a spin-orbit coupling term H_{SO}.

So, for the generation of synthetic Rashba coupling we consider a non-interacting ultracold atomic gas trapped by lasers in the xy-plane. The atoms with an internal three-level (tripod) scheme are coupled to the laser radiation with Rabi frequencies Ω_1 and Ω_2 [51]. In a general two-level case, the Rabi frequency quantifies the interaction between resonant laser radiation and atomic dipole moment, since it is related to the frequency of oscillation of the population in the excited level [84, 85]. In the tripod scheme the two lower atomic states $|1\rangle$ and $|2\rangle$ represent the hyperfine ground states (Zeeman splitting components) while the upper one $|0\rangle$ represents the excited state with laser detuning Δ. The two hyperfine states $|1\rangle$ and $|2\rangle$, taken as pseudo-spin states, are coupled to the excited state $|0\rangle$ through the transition $|1\rangle \to |0\rangle$, $|2\rangle \to |0\rangle$. And the single-particle Hamiltonian has the expression

$$H = H_0 + H_{int} + V(\mathbf{r}), \tag{5.24}$$

where $H_0 = \mathbf{p}^2/2m$ represents the kinetic part with momentum $\mathbf{p}$, $V(\mathbf{r})$ is the position-dependent trapping potential and H_{int} is the laser-atom interaction with laser detuning Δ to the excited state $|0\rangle$. The interation term of the Hamiltonian

has the form of a 3×3 matrix

$$H_{int} = \begin{pmatrix} \hbar\Delta & -\hbar\Omega_1 & -\hbar\Omega_2 \\ -\hbar\Omega_1^* & 0 & 0 \\ -\hbar\Omega_2^* & 0 & 0 \end{pmatrix}. \tag{5.25}$$

Following the model introduced in Ref. [51], the two Rabi frequencies can be written as $\Omega_1(\mathbf{r}) = \Omega_0 \cos\theta \; e^{i\Phi(\mathbf{r})}$ and $\Omega_2(\mathbf{r}) = \Omega_0 \sin\theta \; e^{i\Phi(\mathbf{r})}$ with position-dependent phase $\Phi(\mathbf{r}) = k_1 y$ and an angle 2θ between the two laser beams, with $\theta = k_2 x$. The diagonalization of the interacting part of the Hamiltonian gives eigenvalues $\lambda_1 = 0, \; \lambda_{2,3} = \frac{\hbar}{2}\,(\Delta \pm \sqrt{\Delta^2 + 4\Omega_0^2})$ while the eigenvectors would be $V_i = (a,\, b,\, c)$ for $i = 1 \ldots 3$. To find the first eigenvector that corresponds to λ_1 we solve the system

$$\begin{cases} \Delta\,|a\rangle - \Omega_1\,|b\rangle - \Omega_2\,|c\rangle = 0, \\ -\Omega_1^*\,|a\rangle = 0 \end{cases} \tag{5.26}$$

Assuming that the first component of the eigenvector is $|a\rangle = 0$ we get

$$\begin{aligned} -\Omega_1\,|b\rangle - \Omega_2\,|c\rangle &= 0, \\ -\cos\theta|b\rangle - \sin\theta|c\rangle &= 0. \end{aligned}$$

Solving the last equation, the eigenvector for λ_1 is $|V_1\rangle = \sin\theta|b\rangle - \cos\theta\,|c\rangle$. Using λ_2 the system of equations for $|V_2\rangle$ is

$$\begin{cases} (\Delta - \frac{1}{2}(\Delta + \sqrt{\Delta^2 + 4\Omega_0^2}))|a\rangle - \Omega_0\, e^{i\Phi}(\cos\theta\,|b\rangle + \sin\theta\,|c\rangle) = 0, \\ -\Omega_0\,\cos\theta\, e^{-i\Phi}\,|a\rangle - \frac{1}{2}(\Delta + \sqrt{\Delta^2 + 4\Omega_0^2})\,|b\rangle = 0 \end{cases} \tag{5.27}$$

Let us set the components of the eigenvector as

$$|V_2\rangle = \begin{pmatrix} -|c_1| \\ e^{-i\Phi}\cos\theta\;|c_2| \\ e^{-i\Phi}\sin\theta\;|c_2| \end{pmatrix}.$$

The remaining equation to solve is

$$|c_1| = |c_2|\frac{\Delta + \sqrt{\Delta^2 + 4\Omega_0^2}}{2\Omega_0}.$$

Then, to ensure the normalization we can choose $|c1|$ and $|c_2|$ functions of the parameter α as $|c_1| = \cos\alpha$ and $|c_2| = \sin\alpha$. Thus, the eigenvector corresponding to the eigenvalue λ_2 would be $|V_2\rangle = -\cos\alpha\,|a\rangle + e^{-i\Phi}\cos\theta\sin\alpha\,|b\rangle + e^{-i\Phi}\sin\theta\sin\alpha\,|c\rangle$. Finally, the equations for the last eigenvalue λ_3 are

$$\begin{cases} (\Delta - \frac{1}{2}(\Delta - \sqrt{\Delta^2 + 4\Omega_0^2}))\,|a\rangle - e^{i\Phi}(\cos\theta\,|b\rangle + \sin\theta\,|c\rangle) = 0 \\ -\Omega_0\,\cos\theta\, e^{-i\Phi}\,|a\rangle - \frac{1}{2}(\Delta - \sqrt{\Delta^2 + 4\Omega_0^2})\,|b\rangle = 0. \end{cases} \tag{5.28}$$

and we choose the components of the eigenvector $|V_3\rangle$ as

$$|V_3\rangle = \begin{pmatrix} e^{i\Phi}\ |d_1| \\ \cos\theta\ |d_2| \\ \sin\theta\ |d_2| \end{pmatrix}.$$

The remaining equation to solve is

$$|d_2| = |d_1| \frac{\Delta + \sqrt{\Delta^2 + 4\Omega_0^2}}{2\Omega_0}.$$

Here we can write $|d_1|$ and $|d_2|$ as $|d_1| = \sin\alpha$ and $|d_2| = \cos\alpha$, considering the ortogonality condition. Thus, we get the eigenvector corresponding to the eigenvalue λ_3 as $|V_3\rangle = e^{i\Phi}\sin\alpha\,|a\rangle + \cos\theta\cos\alpha\,|b\rangle + \sin\theta\cos\alpha\,|c\rangle$ and the matrix of eigenvectors becomes

$$U = \begin{pmatrix} 0 & \sin\theta & -\cos\theta \\ -\cos\alpha & e^{-i\Phi}\cos\theta\sin\alpha & e^{-i\Phi}\sin\theta\sin\alpha \\ e^{i\Phi}\sin\alpha & \cos\theta\cos\alpha & \sin\theta\cos\alpha \end{pmatrix}$$

where

$$\cot\alpha = \frac{\Delta + \sqrt{\Delta^2 + 4\Omega_0}}{2\Omega_0}.$$

By assuming $\Delta^2 \gg \Omega_0^2$, we can decompose the previous expession as

$$\tan\alpha = \frac{2\,\Omega_0}{\Delta} \frac{1}{1 + \sqrt{1 + 4\,\frac{\Omega_0^2}{\Delta^2}}} \simeq \frac{\Omega_0}{\Delta}$$

The degenerate dark states are $|V_1\rangle$ and $|V_3\rangle$, which correspond to the lower energy levels, and the state $|V_2\rangle$, which is the atomic non-degenerate bright state related to the higher energy level. In this case, the laser-dressed up and down states yield a synthetic spin-half system, so that we define the two pseudo-spin states as $\uparrow = |V_1\rangle$, $\downarrow = |V_3\rangle$, stable under atomic spontaneous emission and almost degenerate in case of large detuning.

The projection of the Hamiltonian onto the subspace of the two dark states manifold $|V_1, V_3\rangle$ gives the additional term due to the non-abelian gauge potential $\tilde{A}$. To this aim, we apply the unitary transformation U on the Hamiltonian (5.24) as it was mentioned in Chapter 5

$$\tilde{H} = U^\dagger\, H\, U, \tag{5.29}$$

where the Hamiltonian $\tilde{H}$ is diagonalized and becomes

$$\tilde{H} = U^\dagger\, H_0\, U + H_{int}^{diag} + U^\dagger\, V(\mathbf{r})\, U,$$

with $H_{int}^{diag} = U^\dagger H_{int} U$. Let us now see in detail the first component $U^\dagger H_0 U$ of the new Hamiltonian

$$U^\dagger \mathbf{p}^2 U = (U^\dagger \mathbf{p})(U\mathbf{p}) + (U^\dagger \mathbf{p})(\mathbf{p} U) + U^\dagger U\mathbf{p}^2 + U^\dagger (\mathbf{p} U)\mathbf{p} + U^\dagger (\mathbf{p}^2 U).$$

Since we know that $\operatorname{div} A = 0$, it decomposes as

$$U^\dagger (\mathbf{p} U)\mathbf{p} = -U^\dagger \mathbf{p}^2 U - (\mathbf{p} U^\dagger)(\mathbf{p} U).$$

Thus, the previous equation becomes

$$\begin{aligned} U^\dagger \mathbf{p}^2 U &= (U^\dagger \mathbf{p})(U\mathbf{p}) + (U^\dagger \mathbf{p})(\mathbf{p} U) + U^\dagger U\mathbf{p}^2 - (\mathbf{p} U^\dagger)(\mathbf{p} U) \\ &= \mathbf{p}^2 - 2i\hbar U^\dagger \nabla U\mathbf{p} + \hbar^2 (U^\dagger \nabla U)(U^\dagger \nabla U) \end{aligned}$$

Hereby, the new Hamiltonian after diagonalization reads

$$\tilde{H} = \frac{p^2}{2m} - \frac{\vec{\mathbf{A}} \cdot \vec{\mathbf{p}}}{m} + \frac{A^2}{2m} + H_{int}^{diag} + \tilde{V}(\mathbf{r}), \tag{5.30}$$

or

$$\tilde{H} = \frac{1}{2m}(-i\hbar\nabla - \tilde{\mathbf{A}})^2 + \lambda \hat{I} + \tilde{V}(\mathbf{r}) \tag{5.31}$$

where $\tilde{A} = \sum_\sigma A_\sigma = i\hbar \langle V_\sigma | \nabla | V_\sigma \rangle$, where V_σ is the eigenvector corresponding to $\sigma = 1..3$, $\hat{I}$ is the identity matrix, λ is the eigenvalues matrix and $\tilde{V}(\mathbf{r}) = U^\dagger V(\mathbf{r}) U$. The two lower eigenstates $|V_1\rangle$ and $|V_3\rangle$ are well separated from the upper one $|V_2\rangle$, so that we can neglect the latter due to the adiabatic condition. This observation implies that we can reduce our problem to a 2×2 configuration, taking into account only terms $\tilde{H}_{ij}$, $i = (1, 3)$ and $j = (1, 3)$. In this way, by projecting the Hamiltonian (5.24) onto the subspace $|V_1, V_3\rangle$ we obtain the components of the vector potential as

$$\begin{aligned} \tilde{A}_{11} &= i \langle V_1 | \boldsymbol{\nabla} | V_1 \rangle = 0, \\ \tilde{A}_{13} &= i \langle V_1 | \boldsymbol{\nabla} | V_3 \rangle = -ik_2 \cos\alpha \, \mathbf{e_x}, \\ \tilde{A}_{31} &= i \langle V_3 | \boldsymbol{\nabla} | V_1 \rangle = k_2 \cos\alpha \, \mathbf{e_x}, \\ \tilde{A}_{33} &= i \langle V_3 | \boldsymbol{\nabla} | V_3 \rangle = -k_1 \sin^2\alpha \, \mathbf{e_y}, \end{aligned}$$

and the 2×2 matrix of the vector potential is

$$\tilde{\mathbf{A}} = \begin{pmatrix} 0 & -ik_2 \cos\alpha \, \mathbf{e_x} \\ ik_2 \cos\alpha \, \mathbf{e_x} & -k_1 \sin^2\alpha \, \mathbf{e_y} \end{pmatrix}. \tag{5.32}$$

The values of $\sin^2\alpha$ and $\cos\alpha$ with $\alpha = \arctan\frac{\Omega_0}{\Delta}$ are

$$\sin\alpha = \frac{\frac{\Omega_0}{\Delta}}{\sqrt{1+(\frac{\Omega_0}{\Delta})^2}} \simeq \frac{\Omega_0}{\Delta}\left(1-\frac{\Omega_0^2}{2\Delta^2}+\dots\right) \approx \frac{\Omega_0}{\Delta}, \tag{5.33}$$

$$\cos\alpha = \frac{1}{\sqrt{1+(\frac{\Omega_0}{\Delta})^2}} \simeq 1-\frac{1}{2}\frac{\Omega_0^2}{\Delta^2}+\dots \approx 1. \tag{5.34}$$

From this configuration, by rotating around the y-axis of an angle $\theta = \frac{\pi}{2}$, the rotational matrix is

$$R^y_\theta = \begin{pmatrix} \cos\frac{\theta}{2} & \sin\frac{\theta}{2} \\ -\sin\frac{\theta}{2} & \cos\frac{\theta}{2} \end{pmatrix}$$

The rotation does not influence the momentum but the vector potential, so that the first term of the projected Hamiltonian

$$\tilde{H}' = (R^y_{\pi/2})^{-1}\,\tilde{H}\,R^y_{\pi/2}$$

becomes

$$(R^y_{\pi/2})^{-1}\,(\mathbf{p}-\tilde{\mathbf{A}})^2\,R^y_{\pi/2} = \mathbf{p}^2 - 2\tilde{\mathbf{A}}'\cdot\mathbf{p} + (\tilde{\mathbf{A}}')^2, \tag{5.35}$$

where $\tilde{\mathbf{A}}'$ is

$$\tilde{\mathbf{A}}' = (R^y_{\pi/2})^{-1}\,\tilde{\mathbf{A}}\,R^y_{\pi/2}. \tag{5.36}$$

Now, using the rotation matrix R^y_θ for $\theta = \pi/2$ and the matrix of the projected vector potential $\tilde{\mathbf{A}}$ from Eq. (5.32) we have

$$\tilde{\mathbf{A}}' = \frac{1}{2}\begin{pmatrix} 1 & 1 \\ -1 & 1 \end{pmatrix}\begin{pmatrix} 0 & -ik_2\cos\alpha\,\mathbf{e_x} \\ ik_2\cos\alpha\,\mathbf{e_x} & -k_1\sin^2\alpha\,\mathbf{e_y} \end{pmatrix}\begin{pmatrix} 1 & -1 \\ 1 & 1 \end{pmatrix} =$$
$$= \frac{1}{2}\begin{pmatrix} -k_1\sin^2\alpha\,\mathbf{e_y} & -2ik_2\cos\alpha\,\mathbf{e_x} - k_1\sin^2\alpha\,\mathbf{e_y} \\ 2ik_2\cos\alpha\,\mathbf{e_x} - k_1\sin^2\alpha\,\mathbf{e_y} & -k_1\sin^2\alpha\,\mathbf{e_y} \end{pmatrix}.$$

We can rewrite the gauge potential $\tilde{\mathbf{A}}'$ in terms of Pauli matrices as

$$\tilde{\mathbf{A}}' = -\frac{k_1}{2}\sin^2\alpha\,\hat{I}\,\mathbf{e_y} + k_2\cos\alpha\,\sigma_y\,\mathbf{e_x} - \frac{k_1}{2}\sin^2\alpha\,\sigma_x\,\mathbf{e_y},$$

or, using the expressions (5.33 - 5.34)

$$\tilde{\mathbf{A}}' = -\frac{k_1}{2}\frac{\Omega_0^2}{\Delta^2}\,\hat{I}\,\mathbf{e_y} + k_2\,\sigma_y\,\mathbf{e_x} - \frac{k_1}{2}\frac{\Omega_0^2}{\Delta^2}\sigma_x\,\mathbf{e_y}. \tag{5.37}$$

Other components of the projected Hamiltonian are

$$-\frac{\mathbf{A}'\cdot\mathbf{p}}{m} = \alpha_1\, p_y\sigma_x - \alpha_2\, p_x\sigma_y + \alpha_1\hat{I}p_y, \tag{5.38}$$

$$(\tilde{\mathbf{A}}')^2 = m\,(\alpha_1^2 + \frac{\alpha_2^2}{2})\,\hat{I}. \tag{5.39}$$

As we can see, Eq. (5.38) contains the Rashba spin-orbit interaction term

$$H_{SO} = \alpha_1\, p_y\,\sigma_x - \alpha_2\, p_x\,\sigma_y \tag{5.40}$$

with $\alpha_1 = \frac{\hbar\, k_1\,\Omega_0^2}{2m\Delta_0^2}$ and $\alpha_2 = \frac{\hbar\, k_2}{m}$. We see that this last operation leads us to the spin-orbit part as in the Hamiltonian in Eq. (5.23).

Let us then focus on the Hamiltonian of Eq. (5.23). As we know, the rotations of the pseudo-spin axes does not change the real ones. Let us choose the rotation matrix as $\hat{P} = \frac{1}{\sqrt{2}}(\sigma_z + \sigma_y)$ and apply it onto $H(\mathbf{p}, t)$ as

$$H(\mathbf{p},t)'' = \hat{P}^\dagger\, H(\mathbf{p},t)\,\hat{P} = H_0 + \hat{P}^\dagger\,(H_{SO} + H_E + H_{ext})\,\hat{P},$$

where

$$H''_{int+ext} = \hat{P}^\dagger\,(\alpha_1\,\sigma_x\,p_y - \alpha_2\,\sigma_y\,p_x + \alpha_2 eEt\,\sigma_y - \mu_B\mathbf{B}\cdot\boldsymbol{\sigma})\,\hat{P}, \tag{5.41}$$

where $\boldsymbol{\sigma} = (\sigma_x,\, \sigma_y,\, \sigma_z)$. The Hamiltonian $H''_{int+ext} = \hat{P}^\dagger\, H_{int+ext}\,\hat{P}$ with $H_{int+ext} = H_{SO} + H_E + H_{ext}$. Basically, the influence of the rotation $\hat{P}$ onto the pseudo-spin axes is

$$\begin{aligned}\sigma_x &\to -\sigma_x,\\ \sigma_y &\to \sigma_z,\\ \sigma_z &\to -\sigma_y.\end{aligned}$$

Then

$$H''_{int+ext} = -\alpha_1\,\sigma_x\,p_y - \alpha_2\,\sigma_z\,p_x + \alpha_2 eEt\,\sigma_z + \mu_B\,(B_x\,\sigma_x - B_y\,\sigma_z - B_z\,\sigma_y), \tag{5.42}$$

or in matrix form

$$H''_{int+ext} = \begin{pmatrix} -\alpha_2\, p\,\cos\theta + \alpha_2\, eEt - \mu B_y & -\alpha_1\, p\,\sin\theta + \mu(B_x + iB_z) \\ -\alpha_1\, p\,\sin\theta + \mu(B_x - iB_z) & \alpha_2\, p\,\cos\theta - \alpha_2\, eEt + \mu B_y \end{pmatrix}. \tag{5.43}$$

This Hamiltonian has the same form as the one of the Landau-Zener model (Chapter 6).

Let us now look at the effect of two different Rashba coefficients, namely $\alpha_1 \neq \alpha_2$. Without any external fields, the eigenvalues of the spin-orbit contribution to the Hamiltonian have the following expression

$$E_{1,2} = \frac{p^2}{2m} \mp \sqrt{\alpha_1^2 p_y^2 + \alpha_2^2 p_x^2} \tag{5.44}$$

where $p_x = p\cos\theta$ and $p_y = p\sin\theta$. The fact that the two coefficients are different breaks the circular symmetry of the constant energy contour of the pure Rashba spin-orbit coupling. Specifically, the magnitude of the momentum becomes a function of θ, the angle between the x axis and $\hat{\mathbf{p}}$, which gives an elongated shape to the contours:

$$p_{1,2}(\theta, p_0) = \sqrt{m^2\alpha^2(\theta) + p_0^2} \pm m\alpha(\theta) \tag{5.45}$$

where $\alpha(\theta) = \sqrt{\alpha_1^2\sin^2(\theta) + \alpha_2^2\cos^2(\theta)}$ and $p_0^2/2m$ define, respectively, the energy of the contour and the Fermi momentum without spin-orbit coupling.

The effect of this asymmetry for the spin polarization dynamics is described by the Schrödinger equation for the Hamiltonian in Eq. 5.23. Given a Fermi momentum $p_0 = p_F$, since levels with $p < p_2(\theta, p_F)$ have both spin states occupied they do not contribute to the spin dynamics. For this reason, we will focus only on the states with momentum $p_2(\theta, p_F) < p < p_1(\theta, p_F)$. The interacting and free parts of the Hamiltonian are described by a 2×2 matrix, with the y axis as the quantization direction for spin [9, 86].

The Fermi surface with anisotropic spin-orbit coupling is shown in Figure 5.1. The two ellipses correspond to the lower-energy momentum $p_1(\theta, p_F)$, and to the higher-energy momentum $p_2(\theta, p_F)$ from Eq.(5.45) with the fixed spin-orbit parameters as $m\,\alpha_2 = 0.1\,p_F$, and $\alpha_1/\alpha_2 = 1/4$. Notice that all the states below $p_2(\theta, p_F)$ are fully occupied that is shown with the dark blue region within the ellipse. Hence, we consider only the region with the light blue colour. As a consequence, the helicity of the spin eigenstates does not point anymore perpendicular to the momentum.

This expression is related to the Landau-Zener problem [87, 88, 89], where the difference of the energies between two coupled levels changes linearly in time. The term $\alpha_2\, eEt$ enters as an effective magnetic field and is called Edelstein field [9]. The two energy scales of interest are $p^2/2m$, the kinetic energy, and eEL_{SOC}, the voltage present over the spin-orbit length $L_{SOC} = \hbar(2m\alpha_2)^{-1}$. In the present anisotropic spin-orbit coupling, its length points in the same direction as the applied field. In the following, for simplicity, we will choose units such that $\hbar = 1$ and we will introduce an adiabaticity parameter γ_p, which is

$$\gamma_p = \frac{eEL_{SOC}}{p^2/2m} = \gamma_0\frac{p_0^2}{p^2}, \tag{5.46}$$

where $\gamma_0 = \frac{eE}{\alpha_2 p_0^2}$. The γ_p controls how fast the spin system reacts to an applied electric field. Using the natural units of energy $\alpha_2 p\sqrt{\gamma_p}$, we also define the following dimensionless quantities

$$\begin{aligned} \tau &= \alpha_2 p\sqrt{\gamma_p}\, t, & \tau_p &= \frac{\cos\theta}{\sqrt{\gamma_p}}, \\ \Delta_p &= \frac{\sin\theta}{\sqrt{\gamma_p}}\frac{\alpha_1}{\alpha_2}, & \xi_{x,y,z} &= \frac{\mu_B B_{x,y,z}}{\alpha_2\, p\,\sqrt{\gamma_p}}. \end{aligned} \tag{5.47}$$

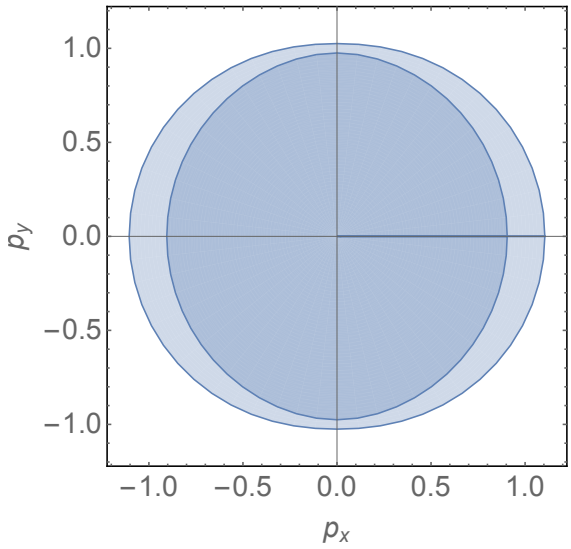

Figure 5.1. Fermi surfaces with anisotropic spin-orbit coupling, that are associated to the lower-energy momentum $p_1(\theta, p_F)$, and to the higher-energy momentum $p_2(\theta, p_F)$, are shown as a function of the momentum components in units of p_F. The parameters are $m\,\alpha_2 = 0.1\,p_F$, and $\alpha_1/\alpha_2 = 1/4$. States below $p_2(\theta, p_F)$ are fully occupied - dark blue region within the circle, thus it is considered only the region with the light blue colour.

These new quantities contain the momentum p, that is a function of θ in our anisotropic case. This makes the principle difference between our model and the two-dimensional electron gas model in [9], where the momentum p in Eq. (5.47) was a constant Fermi momentum p_F and the model was studied for the homogenious case in the absence of magnetic field. By inserting these definitions, the Hamiltonian takes the new form

$$H_p(\tau) = \begin{pmatrix} \tau - \tau_p - \xi_y & -\Delta_p + \xi_x + i\xi_z \\ -\Delta_p + \xi_x - i\xi_z & -(\tau - \tau_p - \xi_y) \end{pmatrix}. \tag{5.48}$$

The solution of the Schrödinger equation with the above Hamiltonian will be derived in Chapter 6.

Summary and perspectives

In this chapter we reported a general description of the methods for artificial generation of spin-orbit coupling in ultracold atomic systems. We presented a brief mathematical derivation of how this can be achieved through diagonalization of Hamiltonian and using the adiabatic principle. Besides, we considered the two symmetries in the Abelian and non-Abelian cases. Finally, we have described the three main schemes for inducing spin-orbit coupling through laser interactions.

Furthermore, we propose how to generate spin-orbit coupling synthetically in the system we investigated, namely using the internal tripod configuration in electrically neutral atoms and two lasers with Rabi frequencies. Using the adiabatic condition we projected the Hamiltonian onto the subspace of the two lower eigenvectors, neglecting the upper one. One of the terms that appear after this operation is the vector potential, which contains the asymmetric Rashba spin-orbit coupling and, hence, it is responsible for the asymmetry in the Fermi surfaces.

Chapter 6

Solution for the anisotropic spin-orbit coupling in cold gases

6.1 Landau-Zener problem

The Landau-Zener model [87, 89], known as a standard representation of a two-level system in quantum physics, describes the probability of transition between two quantum states. This model is used in quantum optics, solid-state physics, atomic collisions, nuclear physics.

The two quantum states are coupled by an external field with a constant amplitude and a time-dependent frequency. The last one experiences the resonance with the frequency of the transition. The level crossing in the diabatic basis can be seen as an avoided crossing in the adiabatic basis, where diabatic is called the basis formed of the two bare states (eigenstates in the absence of interaction) and adiabatic stands for the basis containing the two eigenstates of the Hamiltonian in the presence of interaction.

The Schrödinger equation of a coherently driven two-state quantum system is [90]

$$i\frac{d}{dt}\begin{bmatrix} c_1(t) \\ c_2(t) \end{bmatrix} = \begin{bmatrix} -\Delta(t) & \Omega(t) \\ \Omega(t) & \Delta(t) \end{bmatrix} \begin{bmatrix} c_1(t) \\ c_2(t) \end{bmatrix}, \tag{6.1}$$

where $c_1(t)$ and $c_2(t)$ are the probabilities amplitude of quantum states ψ_1 and ψ_2. The coupling between the two states $\Omega(t)$ and $\Delta(t)$ is a half of the difference between the system transition frequency and the field frequency. In the Landau-Zener model these functions are

$$\Omega(t) = const, \qquad \Delta(t) = \beta^2 t, \tag{6.2}$$

where β and Ω have a dimension of frequency, they are real and positive the same as β^2. The coupling $\Omega(t)$ is assumed to start at $t \to -\infty$ and be arriving to $t \to +\infty$. The dimensionless time τ and coupling ω are

$$\tau = \beta t, \qquad \omega = \frac{\Omega}{\beta}. \tag{6.3}$$

It was shown that the transitional probability $P_d(\tau) = |\, c_2(\tau)|^2$ at the diabatic basis from the initial state ψ_1 to the state ψ_2 at time τ

$$P_d(\tau) = \frac{\omega^2}{2} e^{-\pi\omega^4/4}\, |D_{-1+i\frac{\omega^2}{2}}(\tau\sqrt{2}e^{3i\pi/4})|^2, \tag{6.4}$$

where $D_\nu(z)$ with $\nu = -1 + i\omega^2/2$ is the parabolic cylinder function [91].

The Hamiltonian of the model that we study in Eq. (5.48) has a form similar to the one of Landau-Zener in Eq. (6.1). This feature will be used in the next steps.

6.2 Solution in our model

We will now look for the solution of the time-dependent Schrödinger equation with the Hamiltonian in Eq. 5.48, in the shape of a spinor with the amplitudes $U(\tau - \tau_p - \xi_y)$ and $V(\tau - \tau_p - \xi_y)$

$$\Psi(\tau) = U(\tau - \tau_p - \xi_y)\,|\uparrow\rangle + V(\tau - \tau_p - \xi_y)\,|\downarrow\rangle. \tag{6.5}$$

Using these quantities, the Schrödinger equation becomes

$$\begin{cases} i\dot{U}(\tau) = \tau U(\tau) - \tilde{\Delta}_p\, V(\tau), \\ i\dot{V}(\tau) = -\tau V(\tau) - \tilde{\Delta}_p^*\, U(\tau), \end{cases} \tag{6.6}$$

where $\tilde{\Delta}_p = \Delta_p - (\xi_x + i\xi_z)$. Rescaling the time variable τ as $z = \sqrt{2}e^{-i\frac{3\pi}{4}}\tau$ we obtain the system of equations

$$\begin{cases} \dot{U}(z) + \frac{z}{2}\, U(z) - \frac{1}{\sqrt{2}}\, e^{-i\frac{3\pi}{4}}\, \tilde{\Delta}\, V(z) = 0, \\ \dot{V}(z) - \frac{z}{2}\, V(z) + \frac{1}{\sqrt{2}}\, e^{i\frac{\pi}{4}}\, \tilde{\Delta}^*\, U(z) = 0, \end{cases}$$

which, by introducing the parameters

$$\nu_+ = \frac{\tilde{\Delta}_p}{\sqrt{2}}\, e^{-i\frac{3\pi}{4}},$$
$$\nu_- = \frac{\tilde{\Delta}_p^*}{\sqrt{2}}\, e^{i\frac{\pi}{4}},$$
$$\nu = \nu_+\nu_- = -\frac{i}{2}\,|\tilde{\Delta}_p|^2,$$

take the new form

$$\begin{cases} \dot{U}(z) + \dfrac{z}{2}U(z) - \nu_+ V(z) = 0, \\ \dot{V}(z) - \dfrac{z}{2}V(z) + \nu_- U(z) = 0. \end{cases} \tag{6.7}$$

The solutions to the above non-linear system of differential equations can be found in terms of parabolic cylinder functions by choosing

$$\begin{aligned} U(z) &= D(\nu, z), \\ V(z) &= \nu_- D(\nu - 1, z), \end{aligned} \tag{6.8}$$

which represent the anisotropic extension to the solutions originally found in Ref. [9]. In the normalized form, two mutually orthogonal solutions can be written as

$$\begin{aligned} U^{(1)}(\tau) &= e^{-\pi|\tilde{\Delta}_p|^2/8} D(\nu, z), \\ V^{(1)}(\tau) &= e^{-\pi|\tilde{\Delta}_p|^2/8} \nu_- D(\nu - 1, z), \\ U^{(2)}(\tau) &= -[V^{(1)}(\tau)]^*, \\ V^{(2)}(\tau) &= [U^{(1)}(\tau)]^*. \end{aligned} \tag{6.9}$$

By solving the Hamiltonian at $\tau = 0$, and by defining $\tilde{\tau}_p = \tau_p + \xi_y$, we impose on the general solution the initial conditions

$$\begin{aligned} U(-\tilde{\tau}_p) = U_0 &\equiv \sqrt{\frac{1}{2}\left(1 + \frac{\tilde{\tau}_p}{\sqrt{\tilde{\tau}_p^2 + |\tilde{\Delta}_p|^2}}\right)}, \\ V(-\tilde{\tau}_p) = V_0 &\equiv e^{-i\mathrm{Arg}(\tilde{\Delta}_p)} \sqrt{\frac{1}{2}\left(1 - \frac{\tilde{\tau}_p}{\sqrt{\tilde{\tau}_p^2 + |\tilde{\Delta}_p|^2}}\right)}, \end{aligned} \tag{6.10}$$

described by a linear combination of the two independent solutions with the coefficients A_p and B_p (6.9)

$$U(\tau - \tau_p - \xi_y) = A_p\, U^{(1)}(\tau - \tau_p - \xi_y) + B_p\, U^{(2)}(\tau - \tau_p - \xi_y), \tag{6.11}$$
$$V(\tau - \tau_p - \xi_y) = A_p\, V^{(1)}(\tau - \tau_p - \xi_y) + B_p\, V^{(2)}(\tau - \tau_p - \xi_y). \tag{6.12}$$

To find these coefficients we can use Eq. (6.11, 6.12) at time $\tau = 0$, so that

$$\begin{cases} U_0 = A_p\, U^{(1)}(-\tilde{\tau}_p) + B_p\, U^{(2)}(-\tilde{\tau}_p), \\ V_0 = A_p\, V^{(1)}(-\tilde{\tau}_p) + B_p\, V^{(2)}(-\tilde{\tau}_p), \end{cases} \tag{6.13}$$

or, using Eq. (6.9),

$$\begin{cases} U_0 = A_p\, U^{(1)}(-\tilde{\tau}_p) - B_p\, [V^{(1)}(-\tilde{\tau}_p)]^*, \\ V_0 = A_p\, V^{(1)}(-\tilde{\tau}_p) + B_p\, [U^{(1)}(-\tilde{\tau}_p)]^* \end{cases} \tag{6.14}$$

which give the coefficients

$$\begin{aligned} A_p &= U_0 [U^{(1)}(-\tilde{\tau}_p)]^* + V_0 [V^{(1)}(-\tilde{\tau}_p)]^* \\ B_p &= V_0\, U^{(1)}(-\tilde{\tau}_p) - U_0\, V^{(1)}(-\tilde{\tau}_p). \end{aligned} \tag{6.15}$$

The full solution can be obtained by combining Eqs. (6.5, 6.9 - 6.12, 6.15). The main difference from the solution of G. Vignale and I. Tokatly [9] is its dependence on the momentum, since we are focusing on the anisotropic case with two different Rashba coefficients α_1 and α_2. We note that the dimensionless time variable τ is proportional to α_2, only one of the Rashba coefficients, differently from Ref. [9] where $\tau \propto \alpha$. Besides, the external magnetic field $\mathbf{B}$ modifies the initial conditions and the detuning $\tilde{\Delta}_p$ through the dimensionless components ξ_x, ξ_y, ξ_z.

6.3 Spin polarization

The spin polarization and the analytical solution of the system are given respectively by $S^y = \Psi^\dagger \sigma_y \Psi$ and Eq. (6.6), for a spin quantization axis along the y direction [86]. Thus, for a given magnitude of the momentum in Eq.(5.45), and for $\theta = \frac{\pi}{2}$, the spin along the y direction reads $S^y_{\mathbf{p}}(\tau, p, \theta) = |U(\tau - \tau_p + \xi_z)|^2 - \frac{1}{2}$. The numerical computation of $S^y_{\mathbf{p}}$ as a function of the dimensionless time τ in different regimes is shown in Figure 6.1.

In the adiabatic regime (Figure 6.1a) when $\gamma_0 = 0.1$ the spin polarization component $S^y_{\mathbf{p}}$ relaxes slowly, depending on the relative value of α_1 and α_2, which also dictate the frequency of the oscillations. In the quasi-adiabatic or non-adiabatic regimes (Figure 6.1b) with, respectively, $\gamma_0 = 1$ and $\gamma_0 = 10$, relaxation occurs instead more rapidly, with the same qualitative differences due to the different α_1 and α_2.

We now turn our attention to the total spin polarization. Differently from the analysis of Vignale and Tokatly [9], who kept the momentum from Eq. (5.45) fixed at the Fermi level, assuming that the difference between p_1 and p_2 is small, we do not fix the momentum in our computation. In other words, the anisotropic case that we consider has the additional variable p. We consider the integration within the asymmetric region limited by the energies $E_1(p(\theta, p_F))$ and $E_2(p(\theta, p_F))$, and

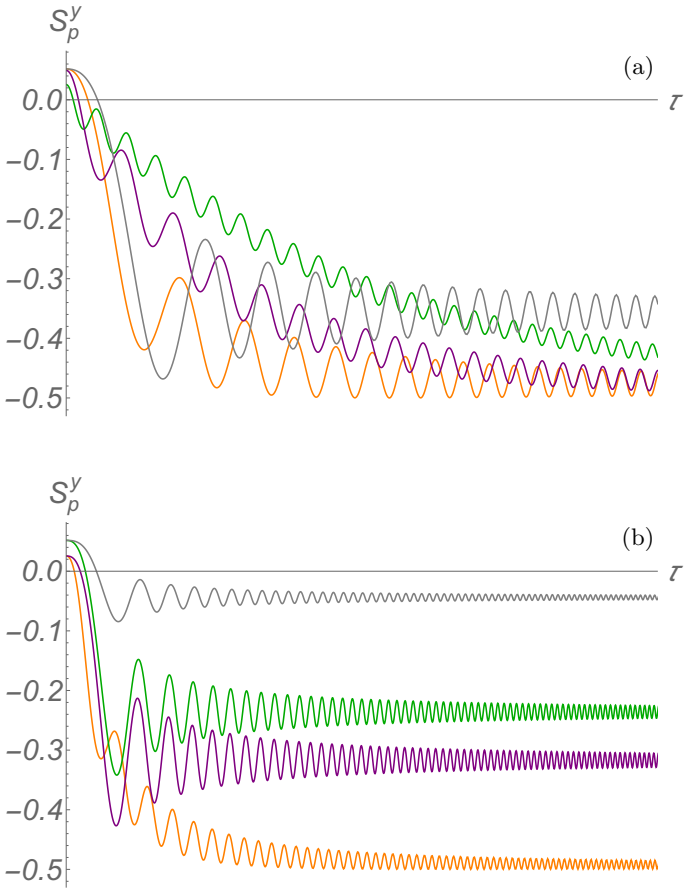

Figure 6.1. Spin polarization component $S^y_{\mathbf{p}}$ in different regimes. Spin polarization y-component as a function of dimensionless time τ from the solutions of Eq.6.6 at fixed momentum p_F and $\theta = \frac{\pi}{2}$. The z-component of magnetic field is $B_z = 0.3$. (a) Spin polarization $S^y_{\mathbf{p}}$ in adiabatic regime with $\gamma_0 = 0.1$. The varying Rashba coefficients (α_1, α_2) are: orange (1, 2), green (2, 1), purple (1.05, 0.95) and gray (1, 4). (b) Spin polarization $S^y_{\mathbf{p}}$ in quasiadiabatic regime ($\gamma_0 = 1$) for orange and green, in non-adiabatic regime ($\gamma_0 = 10$) for purple an gray. The Rashba coefficients (α_1, α_2) are: for orange and purple (2, 1); for green and gray (1, 2).

the Fermi level lays in this region. Thus, the total spin polarization must be integrated as

$$S^y(\tau) = \sum_{s=1,2} \int \frac{d^2p}{(2\pi)^2} \, (-1)^{s-1} \, S^y_{\mathbf{p}}(\tau) \Theta \left(\frac{p_F^2}{2m} - E_s(\mathbf{p}) \right) \tag{6.16}$$

where $\Theta\left(\frac{p_F^2}{2m} - E_s(\mathbf{p})\right)$ is the Heaviside step function. This means that the total spin polarization can be computed by integrating $S^y_{\mathbf{p}}$ over all the angles and averaging over the momentum $p(\theta, p_0)$ as

$$S^y(\tau) = \int_0^{2\pi} \frac{d\theta}{2\pi} \int_{p_2(\theta,p_0)}^{p_1(\theta,p_0)} \frac{p\, dp}{2\pi}\, S^y_{\mathbf{p}}(\tau, p, \theta). \tag{6.17}$$

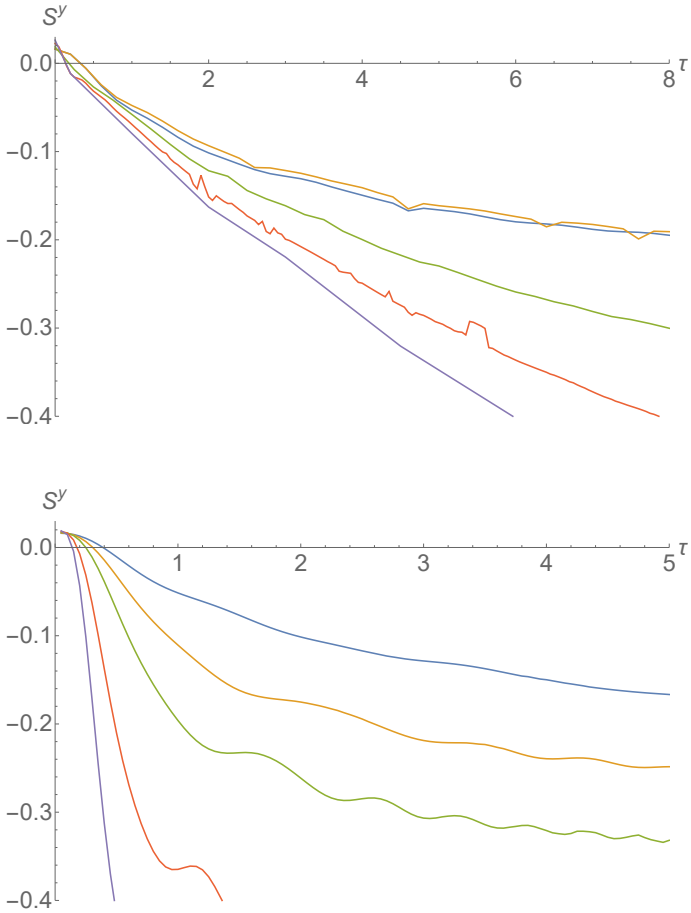

Figure 6.2. Total spin polarization $S^y(\tau)$ in the adiabatic regime ($\gamma_0 = 0.1$) as a function of the dimensionless time τ for a cold atomic system in the presence of spin-orbit coupling. The upper figure corresponds to $\alpha_1 > \alpha_2$, and from the upper to the lower curve Rashba coefficients are (α_1, α_2): blue (1.00001, 0.99999), orange (1.05, 0.95), green (2, 1), red (3, 1) and purple (4, 1). The bottom figure corresponds to $\alpha_1 < \alpha_2$, and from the upper to the lower curve Rashba coefficients are (α_1, α_2): blue (0.99, 1.01), orange (1, 1.5), green (1, 2), red (1, 3) and purple (1, 4). The external magnetic field is $\mathbf{B} = (0.1, 0.2, 0.3)$.

Figure 6.2 reports the total spin polarization S^y for the two ratios of Rashba coefficients $\alpha_1 > \alpha_2$ (Figure 6.2 upper) and $\alpha_1 < \alpha_2$ (Figure 6.2 bottom) in the adiabatic regime $\gamma_0 = 0.1$. To evaluate Eq.(6.16) we consider $m = 1$, $p_F = 2$ and $\mathbf{B}$=(0.1, 0.2, 0.3). The blue and orange curves in the upper plot of Figure 6.2, corresponding to the case $\alpha_1 \simeq \alpha_2$, reach a steady condition early, meaning that the spin direction follows that induced by the electric field. Besides, it confirms the theoretical prediction of the spin polarization for two-dimensional electron gas with Rashba spin-orbit and inverse spin-galvanic effect [9]. The purple, red and green curves are the total spin polarizations for ($\alpha_1 = 4$, $\alpha_2 = 1$), ($\alpha_1 = 3$, $\alpha_2 = 1$), and ($\alpha_1 = 2$, $\alpha_2 = 1$), respectively: they respond very slowly to the influence of an external electric field E, hence the steady state of the atomic spin takes longer to build up, again depending on the ratio of Rashba coefficients. From the second plot in Figure 6.2 we observe that all curves respond faster than in the case $\alpha_1 < \alpha_2$, since saturation occurs in shorter times: only the blue ($\alpha_1 = 0.99$, $\alpha_2 = 1.01$), orange ($\alpha_1 = 1$, $\alpha_2 = 1.5$) and green ($\alpha_1 = 1$, $\alpha_2 = 2$) curves have a longer build-up time.

6.4 Approximate solution

Now let us consider the adiabatic approximation and compare it to the exact solutions in the adiabatic regime of weak electric field E. Note that we calculate the spin polarization $S^y_{\mathbf{p},add}$ with respect to the lower eigenstate of the system, which means that for all times the system under adiabatical process of the external electric field remains in the instantaneous lower eigenstate. This approach allows to retrieve the evolution considering time τ as a parameter in the calculations. To this purpose, we solve the system of Eqs. (6.6) taking into account only the eigenvalue for the lowest state. The component of the approximated spin polarization in the adiabatic regime can be found from

$$\begin{pmatrix} \tau - \tilde{\tau}_p - \lambda & -\Delta_p + \xi_x + i\xi_z \\ -\Delta_p + \xi_x - i\xi_z & -(\tau - \tilde{\tau}_p) - \lambda \end{pmatrix} \begin{pmatrix} U \\ V \end{pmatrix} = 0. \tag{6.18}$$

From the system of equations we find that

$$U^2 = 1 - \frac{\left(\tau - \tilde{\tau}_p + \sqrt{|\tilde{\Delta}_p|^2 + \tilde{\tau}_p^2}\right)^2}{|\tilde{\Delta}_p|^2 + \left(\tau - \tilde{\tau}_p + \sqrt{|\tilde{\Delta}_p|^2 + \tilde{\tau}_p^2}\right)^2} \tag{6.19}$$

and $S^y_{\mathbf{p},ad} = U^2 - \frac{1}{2}$, so that

$$S^y_{\mathbf{p},ad} = \frac{1}{2} \frac{|\tilde{\Delta}_p|^2 - \left(\tau - \tilde{\tau}_p + \sqrt{|\tilde{\Delta}_p|^2 + \tilde{\tau}_p^2}\right)^2}{|\tilde{\Delta}_p|^2 + \left(\tau - \tilde{\tau}_p + \sqrt{|\tilde{\Delta}_p|^2 + \tilde{\tau}_p^2}\right)^2}. \tag{6.20}$$

Figure 6.3 shows the evolution of total spin polarization for a cold atomic system together with that in two-dimensional electron gas (blue) with $\mathbf{B} = 0$ and $\alpha_1 = \alpha_2$ with $k = \frac{\alpha_1}{\alpha_2}$, retrieved by integrating numerically over the angles and averaging over the momentum p as in Eq.(6.17) with the substitution of $S^y_{\mathbf{p}}(\tau, p, \theta)$ with its adiabatic expression $S^y_{\mathbf{p},ad}$.

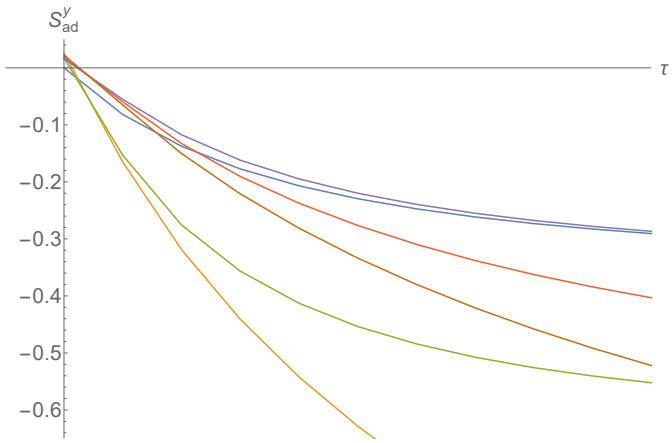

Figure 6.3. The approximated total spin polarization $S^y_{ad}(\tau)$ is shown as a function of the dimensionless time τ. The adiabatic parameter is fixed at $\gamma_0 = 0.1$, the external magnetic field $\mathbf{B} = (0.1, 0.2, 0.3)$. The ratios of Rashba coefficients $k = \frac{\alpha_1}{\alpha_2}$ are: purple ($k = 0.98$), red ($k = 2$), orange ($k = 3$), green ($k = 0.5$) and yellow ($k = 4$) curves. The blue curve is taken at $\mathbf{B} = 0$ and $\alpha_1 = \alpha_2$, which corresponds to the characteristic result for a two-dimensional electron gas.

As we can see from Figure 6.3 the blue curve for large times coincides with the purple one ($k = 0.98$), while for short times the presence of magnetic field $\mathbf{B} = (0.1, 0.2, 0.3)$ caused by Rashba spin-orbit coupling effect makes the latter lay higher than the one for the two-dimensional electron gas. The green curve ($k = 0.5$) saturates quite fast for short times, even slightly faster than the one for two-dimentional electron gas, which means that the Edelstein field is more significant than the Rashba field. The red ($k = 2$), orange ($k = 3$) and yellow curve ($k = 4$) decrease more slowly and their saturation occurs much later than for the purple and green curves, showing that in this condition the Rashba field still prevails.

The results obtained from the adiabatic approximation qualitatively coincide with the results calculated from the exact solution, and have the identical subsiding behavior in both small and large ratio of spin-orbit coupling parameters k. The artificial pseudospin states in cold atoms with Rashba spin-orbit coupling show a longer lifetime, highlighting their better tunability compared with two-dimentional electron gas.

Summary and perspectives

In this chapter we described the Landau-Zener model, whose Hamiltonian has an expression similar to the one of our model. By solving analytically our time-dependent Schrödinger equation we found the exact solutions in terms of cylinder parabolic functions. Integrating the component over both momentum and angle we have found the total spin polarization, which we plotted for different Rashba coefficients α_1, α_2. Results show that when $\alpha_1 > \alpha_2$ the spin polarized state responds very slowly to the external perturbations compared to the two-dimentional electron gas. Finally, we presented an adiabatic approximated solution for the total spin polarization, which has qualitatively similar behaviour to the exact one we retrieved.

Our results can be used for generating spin polarized states with given parameters in theory and experiments, controlling them by means of external perturbations.

Conclusions

In the thesis we studied the inverse-spin galvanic effect, one of the most interesting effects in spintronics. This phenomenon occurs under the influence of an external electric field onto the symmetric spin distribution of the splitted energy sub-bands, and as a result the asymmetry produces a non-equilibrium spin-polarization. By Onsager reciprocal relation, also the opposite effect, the spin-galvanic effect, can occur as a charge current due to non-equilibrium spin polarization. Both effects are possible if we restrict the symmetry conditions, so that the polar and axial vectors, i.e. the charge current and spin polarization, are coupled. In solid-state systems with symmetry broken the degeneracy of the energy sub-bands is lifted due to Rashba spin-orbit coupling in the absence of the external perturbations. While Rashba spin-orbit coupling is the surface effect, Dresselhaus spin-orbit coupling comes from the bulk of the material. Theoretically the effects that generate a spin current are well studied in solid-states materials as heterostructures, an example being the two-dimensional electron gas with linear Rashba spin-orbit coupling. In particular, from the theory we expect that with large spin-orbit magnetic fields the inverse spin-galvanic effect is large as well. However, experimental investigations carried out for $InGaAs$ epilayers have shown that the spin polarization increases when the effective magnetic field decreases along the crystallographic axes.

In addition to solid-state systems, also ultracold atoms are promising candidates for studying spin current effects. As a counterweight to the solid state case, systems based on ultracold atoms are "clean": free of disorder and not affected by external electromagnetic fields, being them electrically neutral. Nevertheless, the spin-orbit coupling in such systems can be generated artificially with the laser beams due to the Raman process.

As a first step during my research project, I have carefully reviewed the experimental result and found the missing part in the theory that explains the mismatch with the experimental results. To this purpose, I added a spin-orbit coupling cubic in momentum besides the linear one in a quantum well system. Then, using the real-time formalism we have derived the kinetic Eilenberger equation from the subtracted left-right Dyson equation by introducing the Wigner coordinates and making a Fourier transform. The Keldysh component of quasi-classical Green's function from the quantum kinetic equation has been computed as spin polarization. We have described the model with the separate contributions of linear

and cubic Rashba-Dresselhaus spin-orbit couplings within diffusive and beyond-diffusive regimes, respectively corresponding to small or large spin-orbit coupling with respect to the disorder. For all the cases considered, we plotted the spin-galvanic conductivity as a function of the frequency. Besides, we showed that, in the presence of only cubic Rashba and Dresselhaus spin-orbit couplings, the spin generation torque vanishes and the inverse spin-galvanic effect indeed does not show up. Finally, we have constructed the vector diagrams of the in-plane spin polarization and spin-orbit magnetic field versus electric current with the fixed linear Rashba-Dresselhaus and varying cubic Dresselhaus spin-orbit couplings. In particular, the vector diagram built for the case where the cubic Dresselhaus contribution is greater than the linear Rashba-Dresselhaus spin-orbit couplings shows that the smallest magnetic field and the greatest spin polarization coexist along the crystallographic axis [1, -1], and vice versa along [1, 1]. This result qualitatively coincides with the experimental measurements.

As for my second contribution, I have investigated the ultracold atomic system in the presence of Rashba spin-orbit coupling. The latter effect, arising from the gauge potential, was generated artificially through an internal tripod scheme and two lasers with Rabi frequencies. Unlike two-dimentional electron systems, the presence of synthetic spin-orbit coupling leads to a twofold value for the Rashba coefficients. Hence, the Fermi surface becomes now asymmetric, entailing that the magnitude of the momentum has an angular dependence. To study this aspect, I solved analytically the time-dependent Schrödinger equation in terms of spinors and parabolic cylinder functions. Then, the spin polarization has been estimated numerically by averaging over the directions of the momentum and angles, and for different values of the two Rashba coefficients in the adiabatic regime. Results have shown that the spin polarized states respond much more slowly when the Rashba coeffiecients satisfy $\alpha_1 > \alpha_2$. Finally, I derived the adiabatic approximation of spin polarization for weak electric fields, and I numerically compared it with the above-mentioned exact solution, showing that both qualitatively exhibit the same behavior.

The obtained results provide a complete picture of the tunability for the spin relaxation times in quantum wells and cold atomic system with Rashba and Dresselhaus spin-orbit couplings. The result can be used for spin polarization control, for instance by choosing the most efficient values of the Rashba and Dresselhaus parameters by externally-driven fields, and can guide further investigations on spin current manipulations.

Bibliography

[1] I. K. Kominis, T. W. Kornack, J. C. Allred, and M.V. Romalis. «A subfemtotesla multichannel atomic magnetometer». In: *Nature* 422.6932 (2003), p. 596 (cit. on p. 1).

[2] M. N. Baibich, J. M. Broto, A. Fert, F. Van Dau, F. Petroff, P. Etienne, G. Creuzet, A. Friederich, and J. Chazelas. «Giant magnetoresistance of (001)Fe/(001)Cr magnetic superlattices». In: *Phys. Rev. Lett.* 61.21 (1988), p. 2472 (cit. on p. 1).

[3] G. Binasch, P. Grünberg, F. Saurenbach, and W. Zinn. «Enhanced magnetoresistance in layered magnetic structures with antiferromagnetic interlayer exchange». In: *Phys. Rev. B* 39.7 (1989), p. 4828 (cit. on p. 1).

[4] J. C. Slonczewski. «Current-driven excitation of magnetic multilayers». In: *Journal of Magnetism and Magnetic Materials* 159.1 (1996), pp. L1–L7 (cit. on p. 1).

[5] R. Raimondi and P. Schwab. «Spin-Hall effect in a disordered two-dimensional electron system». In: *Phys. Rev. B* 71.3 (2005), p. 033311 (cit. on pp. 1, 3).

[6] J. Borge, C. Gorini, G. Vignale, and R. Raimondi. «Spin Hall and Edelstein effects in metallic films: from two to three dimensions». In: *Phys. Rev. B* 89 (2014) (cit. on pp. 1, 4, 21).

[7] J. Sinova, D. Culcer, Q. Niu, N. A. Sinitsyn, T. Jungwirth, and A. H. MacDonald. «Universal intrinsic spin Hall effect». In: *Phys. Rev. Lett.* 92.12 (2004), p. 126603 (cit. on pp. 1, 3).

[8] R. Raimondi, C. Gorini, and S. Tolle. «Spin–charge coupling effects in a two–dimensional electron gas». In: *WSPC Proceedings*. Rzeszow School. Rzeszow, Poland, 2016 (cit. on pp. 1, 21).

[9] G. Vignale and I. V. Tokatly. «Theory of the nonlinear Rashba–Edelstein effect: the clean electron gas limit». In: *Phys. Rev. B* 93.3 (2016), p. 035310 (cit. on pp. 1, 4, 11, 61, 67, 68, 73, 74, 77).

[10] Ka Shen, G. Vignale, and R. Raimondi. «Microscopic theory of the inverse Edelstein effect». In: *Phys. Rev. Lett.* 112.9 (2014), p. 096601 (cit. on pp. 1, 21).

[11] C. L. Kane and E. J. Mele. «Quantum spin Hall effect in graphene». In: *Physical Review Letters* 95.22 (2005), p. 226801 (cit. on p. 1).

[12] W. Heisenberg. «Über den Bau der Atomkerne». In: *Zeitschrift für Physik* 77.1-2 (1932), pp. 1–11 (cit. on p. 2).

[13] G. W. Semenoff. «Condensed-matter simulation of a three-dimensional anomaly». In: *Phys. Rev. Lett.* 53.26 (1984), p. 2449 (cit. on p. 2).

[14] C. Tőke, P. E. Lammert, V. H. Crespi, and J. K. Jain. «Fractional quantum Hall effect in graphene». In: *Physical Review B* 74.23 (2006), p. 235417 (cit. on p. 2).

[15] J. N. Ginocchio and A. Leviatan. «On the relativistic foundations of pseudospin symmetry in nuclei». In: *Physics Letters B* 425.1-2 (1998), pp. 1–5 (cit. on p. 2).

[16] D.H. Santamore and E. Timmermans. «Pseudospin and spin–spin interactions in ultracold alkali atoms». In: *New Journal of Physics* 13.2 (2011), p. 023043 (cit. on p. 2).

[17] M. I. D'yakonov and V. I. Perel. «Possibility of orienting electron spins with current». In: *Soviet Journal of Exp. and Theor. Phys. Lett.* 13 (1971), p. 467 (cit. on p. 3).

[18] S. Murakami, N. Nagaosa, and S.-C. Zhang. «Dissipationless quantum spin current at room temperature». In: *Science* 301.5638 (2003), pp. 1348–1351 (cit. on p. 3).

[19] E. I. Rashba. «Properties of semiconductors with an extremum loop. 1. Cyclotron and combinational resonance in a magnetic field perpendicular to the plane of the loop». In: *Sov. Phys. Solid State* 2 (1960), pp. 1109–1122 (cit. on p. 3).

[20] Y. A. Bychkov and E. I. Rashba. «Properties of a 2D electron gas with lifted spectral degeneracy». In: *JETP Lett.* 39.2 (1984), p. 78 (cit. on pp. 3, 6, 13).

[21] S. Datta and B. Das. «Electronic analog of the electro-optic modulator». In: *Appl. Phys. Lett.* 56.7 (1990), pp. 665–667 (cit. on p. 3).

[22] Y. H. Park, H.-J. Kim, J. Chang, S. H. Han, J. Eom, H.-J. Choi, and H. C. Koo. «Separation of Rashba and Dresselhaus spin-orbit interactions using crystal direction dependent transport measurements». In: *Appl. Phys. Lett.* 103.25 (2013), p. 252407 (cit. on p. 3).

[23] J. Nitta, T. Akazaki, H. Takayanagi, and T. Enoki. «Gate Control of Spin-Orbit Interaction in an Inverted $In_{0.53}Ga_{0.47}As/In_{0.52}Al_{0.48}As$ Heterostructure». In: *Phys. Rev. Lett.* 78.7 (1997), p. 1335 (cit. on p. 3).

[24] S. LaShell, B. A. McDougall, and E. Jensen. «Spin splitting of an Au(111) surface state band observed with angle resolved photoelectron spectroscopy». In: *Phys. Rev. Lett.* 77.16 (1996), p. 3419 (cit. on p. 3).

[25] H. Zhang, C.-X. Liu, X.-L. Qi, X. Dai, Z. Fang, and S.-C. Zhang. «Topological insulators in Bi_2Se_3, Bi_2Te_3 and Sb_2Te_3 with a single Dirac cone on the surface». In: *Nature physics* 5.6 (2009), pp. 438–442 (cit. on p. 3).

[26] M. Z. Hasan and C. L. Kane. «Colloquium: topological insulators». In: *Reviews of Modern Physics* 82.4 (2010), p. 3045 (cit. on p. 3).

[27] C. Beenakker. «Search for Majorana fermions in superconductors». In: *arXiv:1112.1950* (2011) (cit. on p. 3).

[28] E. L. Ivchenko and G. E. Pikus. «New photogalvanic effect in gyrotropic crystals». In: *Soviet Journal of Experimental and Theoretical Physics Letters* 27 (June 1978), p. 604 (cit. on pp. 3, 9).

[29] K. Shen, G. Vignale, and R. Raimondi. «Microscopic theory of the inverse Edelstein effect». In: *Phys. Rev. Lett.* 112.9 (2014), p. 096601 (cit. on p. 4).

[30] A. G. Aronov and Y. B. Lyanda-Geller. In: *JETP Lett.* 50 (1989), p. 431 (cit. on pp. 4, 9, 29).

[31] B. M. Norman, C. J. Trowbridge, D. D. Awschalom, and V. Sih. «Current-induced spin polarization in anisotropic spin-orbit fields». In: *Phys. Rev. Lett.* 112.056601 (2014) (cit. on pp. 4, 9, 10, 29, 46, 51, 52).

[32] S. Datta and B. Das. «Electronic analog of the electro-optic modulator». In: *Appl. Phys. Lett.* 56.7 (1990), p. 665 (cit. on p. 5).

[33] S. A. Wolf, D. D. Awschalom, R. A. Buhrman, J. M. Daughton, S. Von Molnar, M. L. Roukes, A. Y. Chtchelkanova, and D. M. Treger. «Spintronics: a spin-based electronics vision for the future». In: *Science* 294.5546 (2001), pp. 1488–1495 (cit. on p. 5).

[34] J.-I. Ohe, M. Yamamoto, T. Ohtsuki, and J. Nitta. «Mesoscopic Stern-Gerlach spin filter by nonuniform spin-orbit interaction». In: *Physical Review B* 72.4 (2005), p. 041308 (cit. on p. 5).

[35] V. Shah and M. V. Romalis. «Spin-exchange relaxation-free magnetometry using elliptically polarized light». In: *Physical Review A* 80.1 (2009), p. 013416 (cit. on p. 5).

[36] A. Manchon, H. C. Koo, J. Nitta, S. M. Frolov, and R. A. Duine. «New Perspectives for Rashba Spin-Orbit Coupling». In: *Nature Materials* 14 (2015), pp. 871–882. DOI: 10.1038/nmat4360 (cit. on p. 6).

[37] H. A. Kramers. «Théorie générale de la rotation paramagnétique dans les cristaux». In: *Proc. Amsterdam Acad.* 33 (1930), pp. 959–972 (cit. on p. 6).

[38] S. D. Ganichev, E. L. Ivchenko, V. V. Bel'Kov, S. A. Tarasenko, M. Sollinger, D. Weiss, W. Wegscheider, and W. Prettl. «Spin-galvanic effect». In: *Nature* 417.6885 (2002), p. 153 (cit. on pp. 7, 9).

[39] S. D. Ganichev and L. E. Golub. «Interplay of Rashba/Dresselhaus spin splittings probed by photogalvanic spectroscopy – A review». In: *Physica Status Solidi (B)* 251.9 (2014), pp. 1801–1823 (cit. on p. 8).

[40] V. M. Edelstein. «Spin polarization of conduction electrons induced by electric current in two-dimensional asymmetric electron systems». In: *Solid State Communications* 73.3 (1990), pp. 233–235 (cit. on pp. 9, 29, 38).

[41] L. E. Vorob'ev, E. L. Ivchenko, G. E. Pikus, I. I. Farbshtein, V. A. Shalygin, and A. V. Shturbin. «Optical activity in tellurium induced by a current». In: *Soviet Journal of Experimental and Theoretical Physics Letters* 29 (1979), p. 441 (cit. on p. 9).

[42] S. D. Ganichev, E. L. Ivchenko, V. V. Bel'kov, S. A. Tarasenko, M. Sollinger, D. Schowalter, D. Weiss, W. Wegscheider, and W. Prettl. «Spin-galvanic effect in quantum wells». In: *Journal of Superconductivity* 16.2 (2003), pp. 369–372 (cit. on p. 9).

[43] J. C. R. Sánchez, L. Vila, G. Desfonds, S. Gambarelli, J. P. Attané, J. M. De Teresa, C. Magén, and A. Fert. «Spin-to-charge conversion using Rashba coupling at the interface between non-magnetic materials». In: *Nature Communications* 4 (2013), p. 2944 (cit. on p. 9).

[44] M. Luengo-Kovac, S. Huang, D. Del Gaudio, J. Occena, R. S. Goldman, R. Raimondi, and V. Sih. «Current-induced spin polarization in InGaAs and GaAs epilayers with varying doping densities». In: *Physical Review B* 96.19 (2017), p. 195206 (cit. on pp. 9, 29, 51, 52).

[45] C. Gorini, P. Schwab, R. Raimondi, and A. L. Shelankov. «Non-Abelian gauge fields in the gradient expansion: generalized Boltzmann and Eilenberger equations». In: *Phys. Rev. B* 82.19 (2010), p. 195316 (cit. on pp. 9, 21).

[46] Y.-J. Lin, R. L. Compton, K. Jimenez-Garcia1, J. V. Porto, and I. B. Spielman. «Synthetic magnetic fields for ultracold neutral atoms». In: *Nature* 462 (2009), pp. 628–632 (cit. on p. 10).

[47] N. Goldman, G. Juzeliunas, P. Ohberg, and I. B. Spielman. «Light-induced gauge fields for ultracold atoms». In: *Reports on Progress in Physics*. Vol. 77. 12. IOP Publishing Ltd, 2014 (cit. on p. 10).

[48] J. Ruseckas, G. Juzeliūnas, P. Öhberg, and M. Fleischhauer. «Non-Abelian gauge potentials for ultracold atoms with degenerate dark states». In: *Phys. Rev. Lett.* 95.1 (2005), p. 010404 (cit. on p. 10).

[49] Y.-J. Lin, K. Jiménez-García, and I. B. Spielman. «Spin-orbit-coupled Bose-Einstein condensates». In: *Nature* 471.7336 (2011), pp. 83–86 (cit. on p. 10).

[50] S.-W. Su, S.-C. Gou, Q. Sun, L. Wen, W.-M. Liu, A.-C. Ji, J. Ruseckas, and G. Juzeliūnas. «Rashba-type spin-orbit coupling in bilayer Bose-Einstein condensates». In: *Phys. Rev. A* 93.5 (2016), p. 053630 (cit. on p. 10).

[51] X.-J. Liu, M. F. Borunda, X. Liu, and J. Sinova. «Effect of Induced Spin-Orbit Coupling for Atoms via Laser Fields». In: *Phys. Rev. Lett.* 102.046402 (2009) (cit. on pp. 10, 60–62).

[52] T. D. Stanescu, Z. Chuanwei, and V. Galitski. «Nonequilibrium Spin Dynamics in a Trapped Fermi Gas with Effective Spin-Orbit Interactions». In: *Phys. Rev. Lett.* 99.110403 (2007) (cit. on pp. 10, 60).

[53] V. Galitski and I. B. Spielman. «SpinâĂŞorbit coupling in quantum gases». In: *Nature* 494 (2013), pp. 49–54 (cit. on p. 10).

[54] X.-J. Liu, X. Liu, L. C. Kwek, and C. H. Oh. «Optically induced spin-Hall effect in atoms». In: *Physical Review Letters* 98.2 (2007), p. 026602 (cit. on p. 10).

[55] S.-L. Zhu, H. Fu, C.-J. Wu, S.-C. Zhang, and L.-M. Duan. «Spin Hall effects for cold atoms in a light-induced gauge potential». In: *Phys. Rev. Lett.* 97.24 (2006), p. 240401 (cit. on p. 10).

[56] J. C. Slater. *Quantum theory of atomic structure*. Tech. rep. 1960 (cit. on p. 14).

[57] J. J. Sakurai. *Advanced quantum mechanics*. Pearson Education India, 1967 (cit. on p. 14).

[58] Y. Vakarchuk. «Quantum mechanics». In: *L.: Lviv* (1998) (cit. on p. 14).

[59] R. Winkler. «Rashba spin splitting in two-dimensional electron and hole systems». In: *Physical Review B* 62.7 (2000), p. 4245 (cit. on pp. 16, 42).

[60] R. Winkler. *Spin-orbit coupling effects in two-dimensional electron and hole systems*. Vol. 191. Springer Science & Business Media, 2003 (cit. on pp. 16–19, 24, 34, 42).

[61] J.-M. Jancu, R. Scholz, E. A. de Andrada e Silva, and G. C. La Rocca. «Atomistic spin-orbit coupling and kâĹŹ p parameters in III-V semiconductors». In: *Physical Review B* 72.19 (2005), p. 193201 (cit. on p. 16).

[62] R. Raimondi, P. Schwab, C. Gorini, and G. Vignale. «Spin-orbit interaction in a two-dimensional electron gas: a SU(2) formulation». In: *Ann. Phys.* 524 (2012) (cit. on p. 21).

[63] J. Rammer. *Quantum field theory of non-equilibrium states*. Cambridge University Press, 2007 (cit. on pp. 21, 23, 26, 27).

[64] A. M. Sheikhabadi, I. Miatka, E. Y. Sherman, and R. Raimondi. «Theory of the inverse spin galvanic effect in quantum wells». In: *Physical Review B* 97.23 (2018), p. 235412 (cit. on p. 29).

[65] R. Raimondi, C. Gorini, P. Schwab, and M. Dzierzawa. «Quasiclassical approach to the spin Hall effect in the two-dimensional electron gas». In: *Physical Review B* 74.3 (2006), p. 035340 (cit. on p. 30).

[66] A. Khaetskii. «Intrinsic spin current for an arbitrary Hamiltonian and scattering potential». In: *Physical Review B* 73.11 (2006), p. 115323 (cit. on p. 33).

[67] I. V. Tokatly and E. Y. Sherman. «Gauge theory approach for diffusive and precessional spin dynamics in a two-dimensional electron gas». In: *Annals of Physics* 325.5 (2010), pp. 1104–1117 (cit. on p. 38).

[68] G. E. Pikus and A. N. Titkov. «Spin relaxation under optical orientation in semiconductors». In: *Optical Orientation* 8 (1984), pp. 73–131 (cit. on p. 42).

[69] K. Nomura, J. Wunderlich, J. Sinova, B. Kaestner, A. H. MacDonald, and T. Jungwirth. «Edge-spin accumulation in semiconductor two-dimensional hole gases». In: *Physical Review B* 72.24 (2005), p. 245330 (cit. on p. 42).

[70] W. Knap, C. Skierbiszewski, A. Zduniak, E. Litwin-Staszewska, D. Bertho, F. Kobbi, J. L. Robert, G. E. Pikus, F. G. Pikus, and S. V. et al. Iordanskii. «Weak antilocalization and spin precession in quantum wells». In: *Physical Review B* 53.7 (1996), p. 3912 (cit. on p. 42).

[71] S. Murakami. «Absence of vertex correction for the spin Hall effect in p-type semiconductors». In: *Physical Review B* 69.24 (2004), p. 241202 (cit. on p. 43).

[72] A. Griffin, D. W. Snoke, and S. Stringari. *Bose-Einstein condensation*. Cambridge University Press, 1996 (cit. on p. 55).

[73] B. DeMarco and D. S. Jin. «Onset of Fermi degeneracy in a trapped atomic gas». In: *Science* 285.5434 (1999), pp. 1703–1706 (cit. on p. 55).

[74] K. Sun, C. Qu, and C. Zhang. «Spin–orbital-angular-momentum coupling in Bose-Einstein condensates». In: *Physical Review A* 91.6 (2015), p. 063627 (cit. on p. 55).

[75] G. Juzeliūnas, J. Ruseckas, and J. Dalibard. «Generalized Rashba-Dresselhaus spin-orbit coupling for cold atoms». In: *Physical Review A* 81.5 (2010), p. 053403 (cit. on p. 55).

[76] R. Barnett, G. R. Boyd, and V. Galitski. «SU (3) spin-orbit coupling in systems of ultracold atoms». In: *Physical Review Letters* 109.23 (2012), p. 235308 (cit. on p. 56).

[77] S. Zhang, W. S. Cole, A. Paramekanti, and N. Trivedi. «Spin-orbit coupling in optical lattices». In: *Annual Review of Cold Atoms and Molecules*. World Scientific, 2015, pp. 135–179 (cit. on p. 56).

[78] Y.-J. Lin, R. L. Compton, K. Jimenez-Garcia, J. V. Porto, and I. B. Spielman. «Synthetic magnetic fields for ultracold neutral atoms». In: *Nature* 462.7273 (2009), p. 628 (cit. on p. 56).

[79] C. Qu, C. Hamner, M. Gong, C. Zhang, and P. Engels. «Observation of Zitterbewegung in a spin-orbit-coupled Bose-Einstein condensate». In: *Physical Review A* 88.2 (2013), p. 021604 (cit. on p. 56).

[80] S. W. Su, S. C. Gou, I. K. Liu, I. B. Spielman, L. Santos, A. Acus, A. Mekys, J. Ruseckas, and G. Juzeliūnas. «Position-dependent spin–orbit coupling for ultracold atoms». In: *New Journal of Physics* 17.3 (2015), p. 033045 (cit. on p. 56).

[81] N. Goldman, G. Juzeliūnas, P. Öhberg, and I. B. Spielman. «Light-induced gauge fields for ultracold atoms». In: *Reports on Progress in Physics* 77.12 (2014), p. 126401 (cit. on p. 59).

[82] H. Zhai. «Degenerate quantum gases with spin–orbit coupling: a review». In: *Reports on Progress in Physics* 78.2 (2015), p. 026001 (cit. on p. 60).

[83] B. M. Anderson, I. B. Spielman, and G. Juzeliūnas. «Magnetically generated spin-orbit coupling for ultracold atoms». In: *Physical Review Letters* 111.12 (2013), p. 125301 (cit. on pp. 60, 61).

[84] P. L. Knight and P. W. Milonni. «The Rabi frequency in optical spectra». In: *Physics Reports* 66.2 (1980), pp. 21–107 (cit. on p. 61).

[85] D. F. Walls and G. J. Milburn. *Quantum optics*. Springer Science & Business Media, 2007 (cit. on p. 61).

[86] This can be obtained from the original Hamiltonian via the replacement $\sigma_x \to -\sigma_x$, $\sigma_y \to \sigma_z$, $\sigma_z \to \sigma_y$. (cit. on pp. 67, 74).

[87] C. Zener. «Non-adiabatic crossing of Energy Levels». In: *Proc. R. Soc. Lond. A* 137 (1932), p. 696 (cit. on pp. 67, 71).

[88] E. Majorana. «Atomi orientati in campo magnetico variabile». In: *Il Nuovo Cimento (1924-1942)* 9.2 (1932), pp. 43–50 (cit. on p. 67).

[89] L. D. Landau. In: *Phys. Zs. Sowjet* 2 (1932), p. 46 (cit. on pp. 67, 71).

[90] N. V. Vitanov. «Transition times in the Landau-Zener model». In: *Physical Review A* 59.2 (1999), p. 988 (cit. on p. 71).

[91] H. Batman and A. Erdélyi. *Higher transcendental functions, vol. II*. McGraw-Hill, New York, 1953 (cit. on p. 72).